University of BLIDA 1 SAAD DAHLAB

Faculty of technology

Department of Civil Engineering

DOCTORAL THESIS

THE EFFECTS OF SEISMOLOGICAL PARAMETERS ON THE NONLINEAR BEHAVIOR OF STRUCTURES

by HAMMAL Sofiane

Examination panel

K. GRINE	*Professor*	U. Saad Dahlab Blida	President
B. MENADI	*Professor*	U. Saad Dahlab Blida	Examiner
M. HADID	*Professor*	E.N.S.T.P Kouba	Examiner
Y. ABED	*MCA*	U. Saad Dahlab Blida	Examiner
N. LAOUAMI	*Research Director*	C.G.S Alger	Thesis director
N. BOURAHLA	*Professor*	E.N.P El Harrach	Thesis co-director

Blida, Mai 2021

Abstract

The focus of this study is to analyze the effects of earthquake parameters on the ground motion characteristics and structural behavior. The intensity measures of the ground motion investigated are the peak ground acceleration, significant duration, and the mean period. These measures were strategically selected to take into account the main features of the ground motion, such as the amplitude of the motion, cumulative effect, and frequency content. As for the engineering demand measures investigated, the inelastic response spectra and hysteretic energy demand spectra are selected to evaluate the nonlinear behavior of structures. For each of the parameters considered, a predictive model is developed, tested, and finally used to perform a sensitivity analysis.

The strong motion database developed in this study includes 1104 records, collected from the Kiban Kyoshin Network (KiK-Net) from 10 events. The selected events have a depth less than 13km, a magnitude between 4.8 and 7.3 and an epicentral distance ranging between 15 to 200 km. The Artificial Neural Network ANN technique is used as an alternative to regression methods.

Compared to the existing attenuation models, in addition to the earthquake independent parameters used for attenuation relationships, a new aspect is considered in this dissertation called directionality. An analysis of the effect of directionality on the Peak Ground Acceleration (PGA) was performed, and it was found that their effect could cause an increase in the PGA that may reach up to 35%. Therefore, a radial angle parameter has been included in the input of the predictive model. The performance criteria used indicate that the predicted values of the intensity measures by the neural network are in good accordance with the observed ones. Finally, a sensitivity analysis for the earthquake parameters was performed in order to quantify the influence of each parameter on the intensity measures and structural behavior using the synaptic weights of the validated ANN.

The ANN model with only one hidden layer and a limited number of neurons, makes it easy to implement it in a spreadsheet or a simple computer program using the synaptic matrices and the bias vector, so that it can be routinely integrated in engineering applications and for Seismic Hazard Analysis studies.

Keywords: Seismological parameters, earthquake ground motion, Artificial Neural Networks, KiK-net network, Intensity Measures.

Résumé

Ce travail a pour objet d'analyser les effets des paramètres sismologiques sur les caractéristiques de mouvement du sol et le comportement structurel des batiments. Les mesures d'intensité du mouvement du sol étudié sont l'accélération maximale du sol, la durée significative et la période moyenne. Ces mesures ont été sélectionnées pour prendre en compte les principales caractéristiques du mouvement du sol, telles que l'amplitude du mouvement, l'effet cumulatif et le contenu fréquentiel. En ce qui concerne la réponse structurelle, les spectres de réponse inélastique et les spectres d'énergie hystérétique ont été sélectionnés pour évaluer le comportement non linéaire des structures. Pour chacun des paramètres considérés, un modèle prédictif est développé, testé et finalement utilisé pour réaliser une analyse de sensibilité.

La base de données de mouvement fort développée dans cette étude comprend 1104 enregistrements, collectés à partir du réseau Kiban Kyoshin (KiK-Net) à partir de 10 événements sismiques. Les séismes sélectionnés ont une profondeur inférieure à 13 km, une magnitude comprise entre 4,8 et 7,3 et une distance épicentrale comprise entre 15 et 200 km. La méthode basée sur les réseaux de neurones artificiels est utilisée comme alternative aux méthodes de régression statistiques.

Par rapport aux modèles d'atténuation existants, en plus des paramètres indépendants du séisme utilisés dans les équations d'atténuation, un nouvel aspect est considéré dans cette thèse appelé directionnalité. Une analyse de l'effet de la directionnalité sur le PGA a été réalisée, et il a été constaté que leur effet pouvait entraîner une augmentation du PGA pouvant atteindre 35%. Par conséquent, un nouveau paramètre nommé « angle radial » a été introduit dans l'entrée du modèle prédictif. Les critères de performance utilisés indiquent que les valeurs des mesures d'intensité prédites par le réseau neuronal sont en bon accord avec celles observées. Une analyse de sensibilité des paramètres sismiques a été réalisée afin de quantifier l'influence de chaque paramètre sur les mesures d'intensité et le comportement structurel à l'aide des poids synaptiques de l'ANN validé.

Le modèle ANN avec une seule couche cachée et un nombre limité de neurones, facilite sa mise en œuvre dans un tableur Excel ou un simple programme informatique en utilisant les matrices synaptiques et le vecteur de biais, de sorte qu'il puisse être systématiquement intégré dans les applications d'ingénierie et pour études des risques sismiques.

Mots clés: paramètres sismologiques, mouvement du sol, réseaux de neurones artificiels, réseau KiK-Net, mesures d'intensité.

ملخص

تهدف الأطروحة إلى تقييم تأثير المعلمات الزلزالية على السلوك الزلزالي للهياكل. من المعروف أن جميع أشكال التحميل الزلزالي المستخدمة في التصميم مشتقة في الأصل من سجلات الحركة الزلزالية الأرضية. ولذلك، فإن تأثير المعلمات الزلزالية على خصائص الحركة الأرضية الزلزالية تم تناولها في إطار بحثنا. وفقًا لبحوث سابقة، تم اقتراح مئات النماذج المعروفة باسم نماذج التنبؤ بالحركة الأرضية، أو علاقات التوهين. والتي تربط خصائص الحركة الزلزالية بمعلمات الزلازل. نظرًا لتعقيد ظاهرة النشاط الزلزالي والارتياب المتعلق بمعلمات الإدخال، تطور عدد نماذج تنبىء الحركة يستمر في الزيادة من سنة إلى أخرى. الا يومنا هذا لا تزال هناك حاجة الى دمج معملات زلزالية جديدة في تطوير نماذج التنبىء بحركة الزلزال.

في الجزء الأول من الأطروحة ، تمت معالجة توصيف الحركة الزلزالية، ومعايير قياس خصائص شدتها . في بحثنا معايير قياس الشدة التي تم فحصها هي ذروة تسارع الأرض ، والمدة المعبرة للزلزال ، ومتوسط التردد. معايير قياس الشدة الزلزالية تم اختيارها بشكل استراتيجي لمراعاة السمات الرئيسية لحركة الأرض مثل سعة الحركة الزلزالية والتأثير التراكمي وتردد الحركة الزلزالية. ملفات الحركة المستخدمة في هذه الدراسة تم حصول عليها من قاعدة البيانات العالمية المقدمة من المعهد الوطني الياباني لبحوث علوم الأرض والكوارث. استخدمت ملفات الحركة الزلزالية المحصل عليها لتطوير نموذج يربط بين خصائص الحركة الزلزالية والمعلمات الزلزالية. في هذه الدراسة استخدمت تقنية الشبكة العصبية الاصطناعية كبديل لطرق الانحدار لنجاعاتها في عديد من المجالات التقنية. تشير النتائج إلى أن القيم المتوقعة لمقاييس الشدة بواسطة الشبكة العصبية تتوافق مع القيم المرصودة. نتيجة لذلك، تم إجراء تحليل الحساسية للتحقيق في كيفية تأثير المدخلات المختلفة على خصائص الحركة الزلزالية ، وتبين من النتائج أن المعلمات الزلزالية لها تأثير متفاوت على خصائص الحركة الزلزالية. خصائص الحركة الزلزالية في حد ذاتها لا توفر أي معلومات عن الاستجابة الهيكلية للبنايات. لهذا في الجزء الثاني من الأطروحة تم التطرق الى العلاقة بين مقاييس الشدة التي تميز حركة الزلزالية ومعلمات الطلب الهندسي للبنايات والتي تمثل مقدار الاستجابة الهيكلية. تم الاعتماد في هذه المرحلة على أنظمة ذات درجة الحرية الواحدة المكافئة بذالك فإن مقاييس الطلب الهندسي التي تم فحصها هي أطياف الاستجابة غير المرنة وأطياف الطلب على الطاقة التخلقية. في اطار دراستنا تم إجراء التحليلات الديناميكية غير الخطية لأنظمة باستخدام نهج القوة الثابتة ، لفترات اهتزاز مختلفة عند مستويات قوة الخضوع المختلفة. أظهر أداء نماذج الشبكة العصبية توافقًا جيدًا بين القيم المتوقعة والمحسوبة لكل من خصائص الحركة الزلزالية و الاستجابة الهيكلية.

من منظور الجانب العملي نماذج الشبكة العصبية مع طبقة مخفية واحدة وعدد محدود من العقد يمكن من السهل تنفيذه في جدول بيانات أو برنامج كمبيوتر بسيط باستخدام المصفوفات متشابك وناقلات التحيز، بحيث يمكن أن تدرج بشكل متكامل في التطبيقات الهندسية ودراسات التحليل للمخاطر الزلزالية.

الكلمات المفتاحية:

المعلمات الزلزالية, سجلات الحركة الزلزالية, نماذج التنبؤ بالحركة الأرضية , الشبكات العصبونية الاصطناعية

Acknowledgments

Firstly, I thank Allah, the most high, for giving me the ability, strength, attitude, and motivation through this research to complete this thesis.

I am very pleased to express my sincerest gratitude to my supervisor Prof. Laouami Nasser for accepting me as a Ph.D. student at the civil engineering department.

I would like to thank and express my special gratitude to my Co-supervisor Prof. Bourahla Nouredine for working with me and giving me the focus and the motivation to accomplish this work.

I would like to extend my sincere thanks to all my colleagues, friends, and the staff at the civil engineering department, the University of Blida for their help to accomplish this work.

We wish to thank the National Research Institute for Earth Science and Disaster Prevention (NIED) in Japan for making the KiK-Net data available for the research community.

List of contents

List of figures

List of tables

List of abbreviations

GMPE	Ground Motion Prediction Equation
IM	Intensity Measure
PSHA	Probabilistic Seismic Hazard Analysis
PBEE	Performance Based Earthquake Engineering
ANN	Artificial Neural Network
FFBP	Feed-Forward-Back-Propagation
PGA	Peak Ground Acceleration
SD	Significant Duration
Tm	Mean Period
FFT	Fast Fourier Transform
Mw	Magnitude of earthquake
R	Epicentral distance
D	Hypocenter Depth
Vs30	Shear wave velocity in the top 30 m of soil
f800	Resonant Frequency
K-Net	Kyoshin seismograph network
KiK-Net	Kiban Kyoshin seismograph network
EDP	Engineering Demand Parameter
SDOF	Single-Degree-Of-Freedom
MDOF	Multi-Degree-Of-Freedom
EPP	Elastic Perfectly Plastic
CSM	Capacity Spectrum Method
Sd	Inelastic Response Spectra
Eh	Hysteretic Energy Spectra
Fy	Yielding Force
MSE	Mean Square Error
R	Correlation Coefficient
Pi	Percentage of Synaptic weight

NEHRP National Earthquake Hazards Reduction Program

Chapter I. INTRODUCTION

I.1. Background

One of the popular methodologies used to characterize the seismic behavior of civil structures is called Performance-Based Earthquake Engineering (PBEE). It is considered the most common approach used for evaluating seismic risk decision-making. The first step in this process is to analyze and evaluate the seismic hazard to obtain a good estimate of the earthquake's force. The complexity of the earthquake phenomena poses a challenge to identify, assess and control the seismic hazard level.

The ground motions recorded from previous earthquake are the basis of all forms of seismic loading. From a practical perspective the earthquake accelerogram is a key component that links the seismological parameters to the structural response (figure I.1). The scalar parameters characterizing the ground motion are called intensity measures (IMs), which are usually used in assessing the seismic demand for a given location. As the ground motion is complex and transiency excitation, a complete description of earthquake ground motion requires consideration of various features. Therefore, multiple parameters have been proposed in the literature to describe the ground motion records. The intensity measures can be categorized into three groups:

(1) Peak ground motion parameters, which are used to determine the peak amplitude of different measures such as the acceleration (PGA), the velocity (PGV), and the displacement (PGD). These parameters primarily influence the response of structural systems.

(2) Duration and cumulative parameters, these measures are used to assess the cumulative effects of ground motion, which correlate well with the energy imparted to structures. Well-known parameters such as the Intensity Arias (IA) and Significant Duration (SD) are widely used to take into account the cumulative effect.

(3) Frequency content, it is well known that the frequency of earthquake loading has a great impact on the seismic response of engineering systems. Several parameters derived from the Fourier Amplitude Spectrum (FAS) are proposed to characterize this last, such as the mean period (Tm), the average spectral period (Tavg), the smoothed spectral predominant period (To), and the predominant spectral period (Tp).

Investigating the relationship between the intensity measures and seismological independent parameters is increasingly becoming a vital factor in seismic hazard and risk analysis. The relationship form expressing a single intensity measure (e.g., PGA, PGV, etc.) in terms of seismological parameters (e.g., magnitude, source-to-site distance, and site condition, etc.) is called the Ground Motion Prediction Equation (GMPE) or attenuation relationship.

The attenuation equation not only helps to capture the effects of seismological parameters on the properties of ground motion, but it can also predict the hazard level for a given site so that earthquake-resistant buildings can be appropriately designed.

Most of the GMPEs developed in the literature relate the intensity measures of ground motion (e.g., Peak Ground Acceleration, PGA, significant duration, SD) to a set of explanatory variables describing earthquake source, path, and site condition. Douglas (2019) summarized 440 models published between 1964 and 2019 for the PGA. Compared to PGA, a limited number of predictive models have been published on the duration and frequency content. Kempton et Al. (2006) expressed the significant duration of earthquake ground motion as a function of magnitude, closest site-source distance, shear wave velocity, basin depth, and near-fault parameters [1]. Several recent studies have proposed Ground Motion Prediction Equations (GMPEs) expressing various duration definitions as a function of source, path, and site parameters [2-4]. Despite the fact that the frequency content of ground motion is an important aspect in earthquake engineering, the number of existing attenuation models for frequency content is limited. To date only a few empirical models have been developed. The generally used model is that of Rathje et al. (2004), which was an update of the previously developed model by Rathje et al. (1998) [5, 6]. Other models have been proposed for specific regions to predict the frequency content as a function of earthquake parameters, such as the United States, and Iran [7, 8].

On the other hand, there has been an increasing interest in developing GMPEs for engineering demand parameters with the purpose of capturing the influence of earthquake parameters on structural response measures (e.g., inelastic response spectra). In earthquake engineering, The inelastic response spectra have played a significant role [9]. The concept is especially convenient in modal analysis of structural systems, where the maximum response of a Multi Degree Of Freedom (MDOF) system can be efficiently approximated by a modal combination of the maximum responses of a series of Single Degree Of Freedom (SDOF) modal systems. Therefore, expressing the response spectra for a given site in terms of seismological parameters and structural properties has received increasing interest; a number of studies have been conducted to develop prediction models, which express the inelastic response spectra in terms of seismological parameters in the form of attenuation relationships [10].

Due to the ground motion complexity and the uncertainty related to earthquake parameters, the number of GMPEs continues to increase from year to year. Nonetheless, to date, there still a need to: (1) Incorporate new seismological parameters and examine their effects on the intensity measures of ground motion; (2) Use new data modelling tools (such as nonlinear regression, Fuzzy logic methods, Neural network methods) to capture and express the relationship between the earthquake parameters and the intensity measures of ground motion; (3) Extend and use new ground motion databases collected from different sources.

The seismograph network installed on the surface captures the ground motion during an earthquake; each station provides three components of the accelerogram (two in the main horizontal direction, EW and NS and one in the vertical direction). The ground motions vary in intensity as a function of the orientation of interest. Most of GMPEs predict the geometric mean of the intensity measures of two horizontal components of ground motion. In some cases, it may be of greater interest to know the maximum value, over all possible directions, of the intensity measures. Although a large number of prediction equations for intensity measures, the ground-motion directionality effect is rarely addressed. This study presents a simplified approach, which considers the directionality aspect in GMPE development by introducing new parameters called the radial angle epicenter-station as an explanatory variable.

I.2. Objectives and scope

The present dissertation, in the framework of PBEE methodologies, focuses on the interface between hazard analysis and structural responses and aims to analyze the effects of the seismological parameters on Intensity Measures and Engineering Demand Parameters by developing new Ground Motion Prediction Equations (GMPEs) expressing the Intensity Measures and Engineering Demand Parameters in terms of seismological parameters.

Compared to the existing attenuation models, in addition to the earthquake independent parameters used for attenuation relationships, a new aspect is considered in this dissertation called directionality. An analysis of the effect of directionality on the PGA was performed, and it was found that their effect could cause an increase in the PGA that may reach up to 35%.

In this work, a new approach is proposed to take into account the directionality effect by introducing a new parameter called radial angle as an explanatory variable.

A ground motion database collected from the Kiban Kyoshin seismograph network (KiK-NET) is compiled and prepared, including all the metadata such as event name, station, time, place, time step, etc. The intensity measures that characterize the main features of ground motion

(amplitude motion, duration, and frequency content) were selected and investigated. Consequently, Ground Motion Prediction Equations (attenuation relationships) have been developed and used to analyze the effects of seismological parameters based on sensitivity analysis. In the second stage, the engineering demand parameters that characterize structural response is addressed. For this purpose, a dataset is constructed based on dynamic time history analysis of SDOFs systems subjected to a series of ground motion records carefully selected. The dataset was then used to develop predictive models. These latter were used to investigate the effects of intensity measures and seismological parameters on the engineering demand parameters.

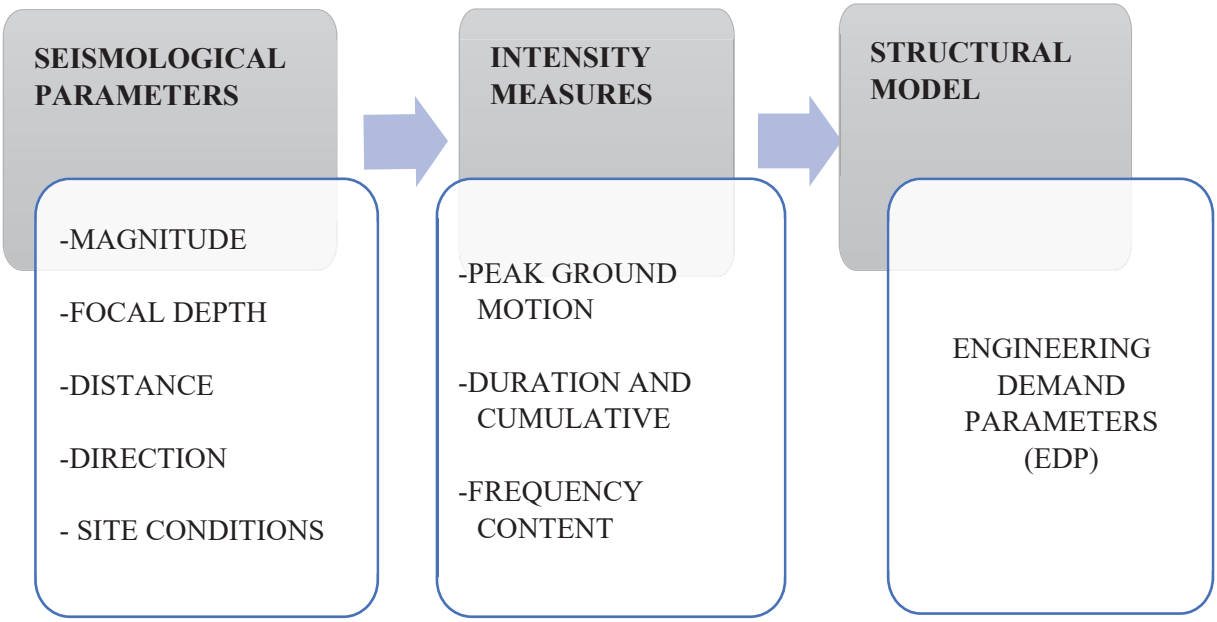

Figure I-1 Process of investigation

I.3. Thesis organization

This dissertation is organized into six chapters. The first chapter presents the background and motivation factors and sets the present study in its framework. An explanation of the role and the importance of the characterization of ground motions to understand the effects of the seismological parameters on structural responses is given. The second chapter presents a description of the seismological parameters and provides an overview of the intensity measures and engineering demand parameters and their corresponding empirical prediction relationships proposed in the literature. The third chapter is dedicated to the methodology adopted. A brief description of the database developed is given and a summary of the knowledge required to develop a prediction

model using the Artificial Neural Network is provided. Chapter 4 covers data modeling analysis for the intensity measures, including the formulating of the neural models using the Feed-Forward-Back-Propagation algorithm. This chapter consists of three sections, each of which concerns a single intensity measure. Chapter 5 covers data modeling analysis. This chapter concerns the Engineering Demand Parameters and has the same structure as chapter four. Chapter 6 offers a summary of the results and findings of this study.

Chapter II. Ground Motion prediction equations or « Attenuation models »

II.1. Introduction

During an earthquake, the ground shaking can cause severe damage to the structural and non-structural members, the seismic excitation applied in the low part of the structure produce force and displacement, which may exceed the structural capacity. One of the most popular approaches for characterizing seismic behavior of civil structures is called Performance-Based Earthquake Engineering. It is considered the modern approach to earthquake-resistant design currently being applied in seismic design and evaluation on various buildings and bridges. The PBEE goal is to design buildings that sustain a given level of seismic demand while maintaining the desired level of performance. The performance levels are classified as fully operational, operational, life safety, and near collapse, while hazard levels are classified as frequent, occasional, rare, and very rare events.

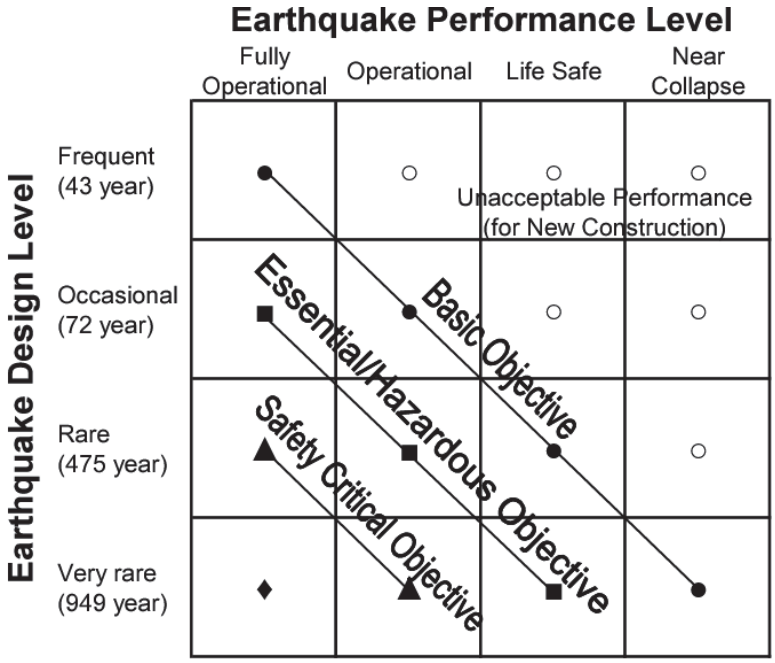

Figure II-1 Vision 2000 recommended seismic performance. Reproduced from Krawinkler (2005) [11]

As illustrated in Figure II-2, The Performance-based design can be summarized into four following main steps: hazard analysis, structural analysis, damage analysis, and loss analysis. The PBEE methodology begins with the estimation of one (or more) ground motion Intensity Measures

(IMs) that should capture the important characteristics of earthquake ground motion that influence the response of the structural and nonstructural components and building contents. The end result of hazard analysis is the Hazard Curve, which describes the variation of the selected IM versus its Mean Annual Frequency (MAF) of exceedance parameter using the attenuation relationship for a specific location of the building and its mechanical characteristics (e.g., first and second mode periods).

The second step is to define the Engineering Demand Parameters that characterize the building behavior. This step is accomplished by structural response simulations using the IMs and corresponding earthquake motions from step one. The EDPs are used along with component fragility functions to determine Damage Measures (DMs) specific to facility components. Lastly, given these DMs, a set of variables including operability, repair costs/duration and potential for casualties can be evaluated. Such performance measures are referred to as decision variables (DVs) since they serve to inform stakeholder decisions regarding future performance.

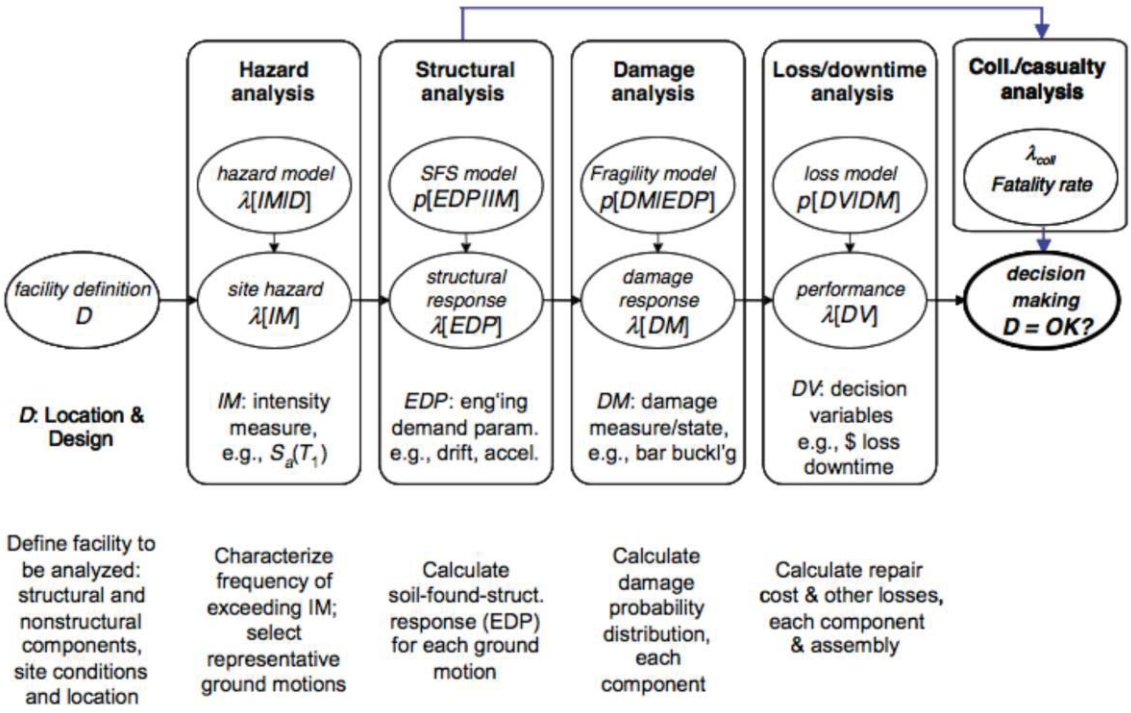

Figure II-2 Overview of PEER-PBEE methodology. Reproduced from Krawinkler (2005)[11].

Determining the level of hazard for the facility site is regarded as a critical component in PBEE methodologies. Forecasting a probable seismic demand for a given site is not an easy task since it combines multiple types of uncertainties related to the earthquake source, path, and site

conditions. A well-known approach called Probabilistic Seismic Hazard Analysis “PSHA” has been developed and widely used to quantify these uncertainties and combine them to estimate the probability of the parameters related to the ground shaking that may occur at a particular site over a given return period.

The outcomes of the Probabilistic Seismic Hazard Analysis (PSHA) process is used for a wide range of applications such as (1) Site-specific seismic demand analysis and design of earthquake-resistant structures and facilities; (2) Development of official seismic hazard maps which provide important information to help mitigate disasters; and (3) social and financial loss estimation. As shown in Figure II-3 the Probabilistic Seismic Hazard Analysis is composed of five following steps [12]:

1. Identification and characterization of all earthquake sources.

2. Characterization of the recurrence rate of various earthquake magnitudes expected to occur.

3. Description of the distribution of source-to-site distances corresponding to potential earthquakes.

4. Use the attenuation relationship to predict the resulting distribution of ground-motion intensity measures as a function of earthquake magnitude, distance, etc.

5. Combine uncertainties in earthquake size, location, and ground motion intensity based on the probability computations to determine the hazard curves.

The end results of probabilistic seismic hazard analysis are the seismic hazard curves, which show the mean annual rate of exceedance of a particular intensity measures of ground motion. The probabilistic seismic hazard analysis has been widely used for almost 50 years by governments and industry applications. Many types of research have been conducted to investigate each step. In this dissertation, the steps 4 of PSHA methodology regarding predicting the intensity measures of ground motion for a given earthquake parameters is addressed.

The attenuation relationships (GMPE's) are key components of PSHA methodology, which represents a tool commonly used to: give a prediction of the level of ground motion at a given site; evaluate the influence of seismological parameters on ground motion characteristics. By definition, the GMPE or “Attenuation model” is an equation typically developed from statistical analysis of earthquake motions to estimate the level of ground motion as a function of various variables characterizing the earthquake proprieties.

Up-to-date the availability of the ground motion database and the evolution of robust regression techniques have made dramatic progress in developing and updating the Empirical predictive relationships. In literature, many researchers have proposed GMPEs and investigated their performances. The attenuation relationship can be classified into two main categories

depending on the nature of the parameter to be addressed; the first group concerns the Intensity measures (IMs), which are parameters that describe quantitatively different features of ground motion records. The second group relates to the Earthquake Demand Parameters (EDP), which are structural response measures that can be used to assess seismic damage.

The present chapter includes an overview of the IMs and EDPs investigated in this study and provides a literature review of the prediction models.

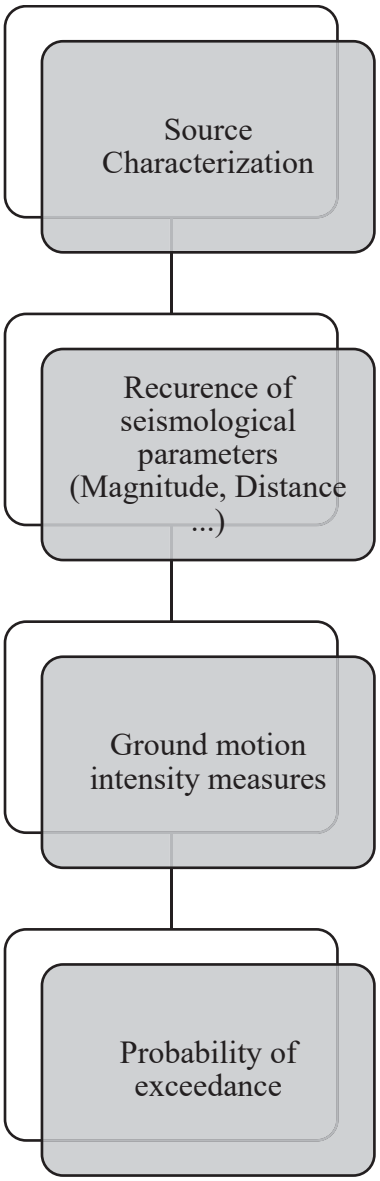

Figure II-3 Main steps of PSHA

II.2. The independent seismological parameters used

For practical purposes, earthquake information needs to be expressed in the form of specific physical parameters called seismological parameters or earthquake parameters. These parameters serve as an important tool for generalists and synthesizers in seismology since they are used as an initial starting basis to build practical theories. As illustrated in Figure II-4, the seismological parameters were divided into three categories:

- Source parameters (e.g., moment magnitude, mechanism of faulting);
- Path parameters (e.g., site-to-site distance, site-to-site orientation)
- Site parameters (e.g., shear-wave-velocity and site frequency).

The parameters used in this study are presented briefly in the following paragraphs.

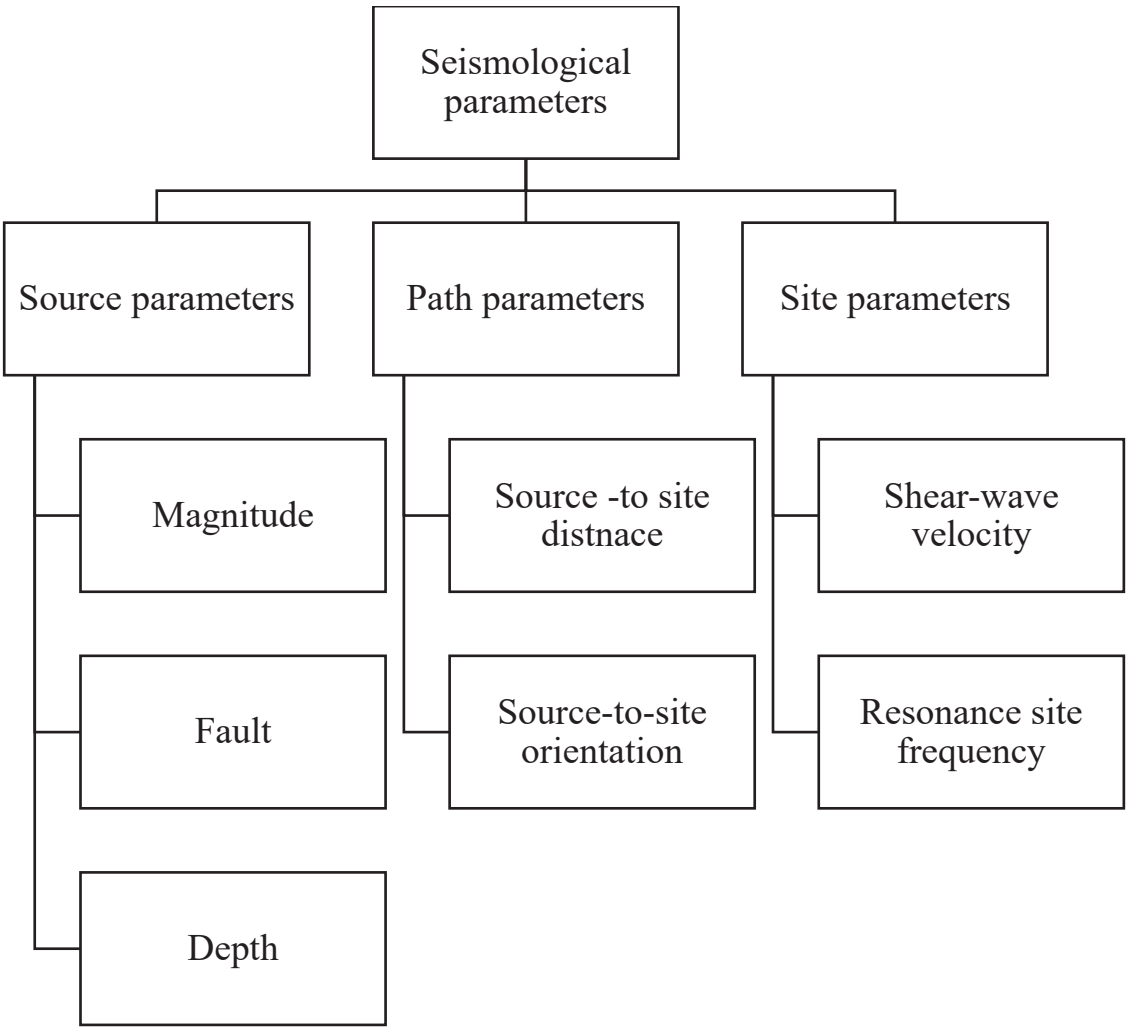

Figure II-4 Groups of seismological parameters

II.3. Source Parameters

Source parameters, which characterize the effects of earthquake size and characteristics of rupture, these parameters are constant for a given earthquake event, the fundamental source parameters used in this study are earthquake magnitude (M), the depth to the top of the fault rupture (d).

II.3.1. Moment Magnitude

In this study, the moment magnitude (Mw) was adopted as the magnitude measure. The moment magnitude has several advantages over other magnitude scales including that it ties the magnitude directly to earthquake source processes, it does not saturate for magnitudes greater than 6, and it is directly proportional to the area of the fault plane that ruptured times the average displacement along the rupture plane. The moment magnitude has been adopted by engineers and engineering seismologists worldwide as a unifying reliable magnitude measure [13, 14]. This measure is primarily linked to the characteristics of the fault rupture and the energy released during the earthquake. Katsumata (1996) proved that the average difference between M_{JMA} (Japan Meteorological A) and moment magnitude Mw is not significant, especially in the magnitude range from 5 to 7 [15].

II.3.2. Depth

The depth of focus from the epicenter, referred to as “Focal Depth”, is an important parameter in determining the damage potential of an earthquake. Most of the damaging earthquakes have shallow focus with focal depths less than about 70km.

II.4. Path Parameters

The path parameters are used to characterize the propagation and attenuation of the seismic energy from the earthquake source to the site of interest. Two parameters are used in this study: Source to site distance and source to site orientation.

II.4.1. Source-to-site distance

Source-to-site distance is a primary input parameter for evaluating the intensity measure parameters in risk and hazard analysis [16]. The distance measure is the basis for the assessment of the attenuation effect in seismic excitation. Multiple definitions of distance measures have been proposed in the literature. Douglas (2003) provides an extensive review of these definitions [17]. As illustrated in Figure II-5, various definitions of source-to-site distance are available in the literature. Typical distance measures employed in attenuation relationship investigations are based on either a point-source representation or an extended-source representation (fault plane). The epicentral distance (Repi) and hypocentral distance (Rhypo) are the point source-based measures, while the Joyner-Boore distance (Rjb, the shortest distance to the surface projection of a fault plane)

and rupture distance (Rrup, shortest distance to a fault plane) are the extended source-based measures.

This study uses the epicentral distance (R_{epi}) defined as the horizontal distance between the surface projection of the hypocenter and the site.

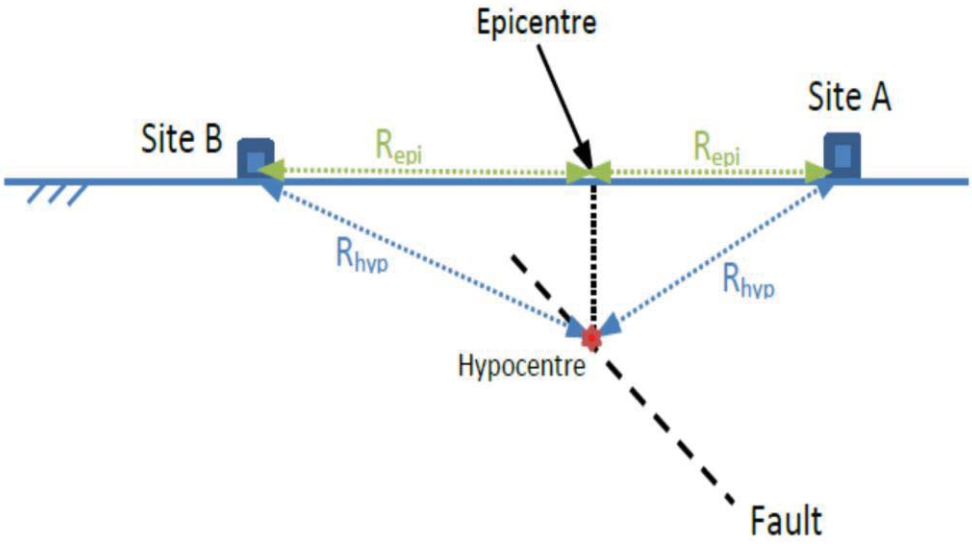

Figure II-5 Source-to-site distance definition

II.4.2. Source-to-site orientation

Source-to-site orientation is the angle formed between the orientation of the epicenter-station path and the direction of the component (see Figure II-7). This parameter is considered in this study following an analysis of the directionality effect which was found significant. The details of this analysis are presented in Chapter 4 section 2. Therefore, the source-to-site angle parameter is introduced as an input to take into account the directionality effect.

It should be noted that the metadata associated with ground motion records includes the coordinates (latitude/longitude) for each record and the seismic source, as presented in Figure II-6.

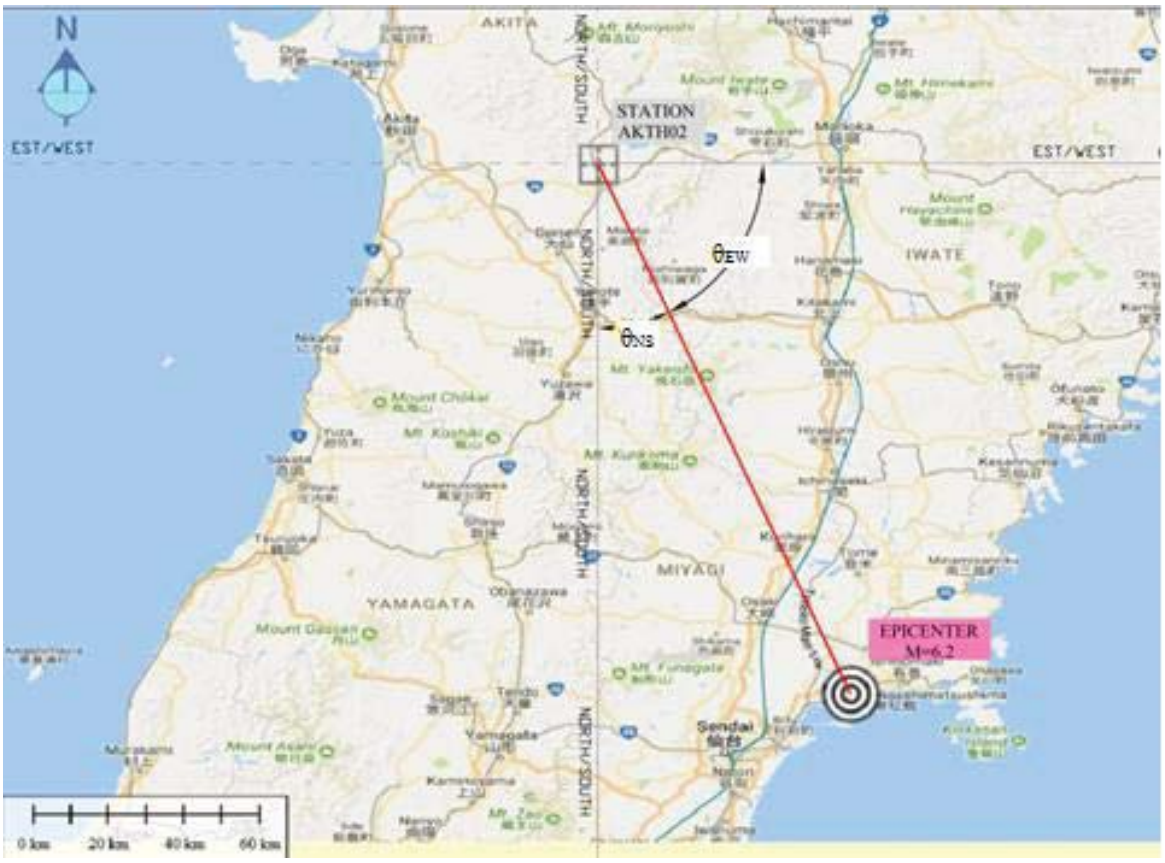

Figure II-6 Radial angle θ for two components of AKTH02 station during 26-07-2003 earthquake M=6.2.

II.5. Site Parameters

The geotechnical parameters are practically measured locally and used to investigate the influence of the local site condition on the intensity measures of ground motion. The Kyoshin database provides geotechnical information on the site of each KiK-Net station. This information includes a description of the lithology and the velocity profile for both S and P waves.

Local site effect is one of the most important aspects in earthquake engineering design and is often characterized by a set of simplified parameters, such as the site predominant period [18], the geological and geotechnical description of soil layers, and site period [19].

In the present study, two parameters were used to consider the site condition, the shear wave velocity (V_{s30}), and resonant site frequency (f_{800}).

II.5.1. Shear wave velocity

The average soil shear-wave velocity down to a depth of 30m (V_{S30}) is successfully used by many recent ground motion prediction equations (GMPE) to introduce the site effects [20-22]. The Vs30 is calculated using the following equation:

$$V_{s30} = \frac{30}{\sum_{i=1}^{n} \frac{h_i}{v_i}} \quad (1)$$

- h_i: thickness of i^{th} layer
- v_i: shear wave velocity

In this dissertation, the distribution of the site classes is performed according to NEHRP classification (see Table II-1) which is based on the shear wave velocity V_{s30} [23].

Table II-1 NEHRP Site Classification (BSSC, 2003)

Site Class	Vs30 (m/s)	General Description
S_A	>1500	Hard rock
S_B	760-1500	Rock with moderate weathering
S_C	360-760	Very dense soil and soft rock
S_D	180-360	Stiff soil
S_E	<1800	Soft clay soil

II.5.2. The resonant frequency

Besides V_{S30}, the resonant frequency f_{800} is also considered as a governing parameter to characterize the site effect on the intensity measures of the strong ground motion. The f_{800} for each site is calculated using the following equation:

$$f_{800} = \frac{\sum_{l=1}^{n} h_l \Big/ \sum_{l=1}^{n} (\frac{h_l}{v_{sl}})}{4.\, z_{800}} \quad (2)$$

- h_l : the thickness of the l^{th} layer
- V_{sl} : the shear velocity of the l^{th} layer.
- Z_{800}: the depth down to a velocity 800 m/s (reference site)

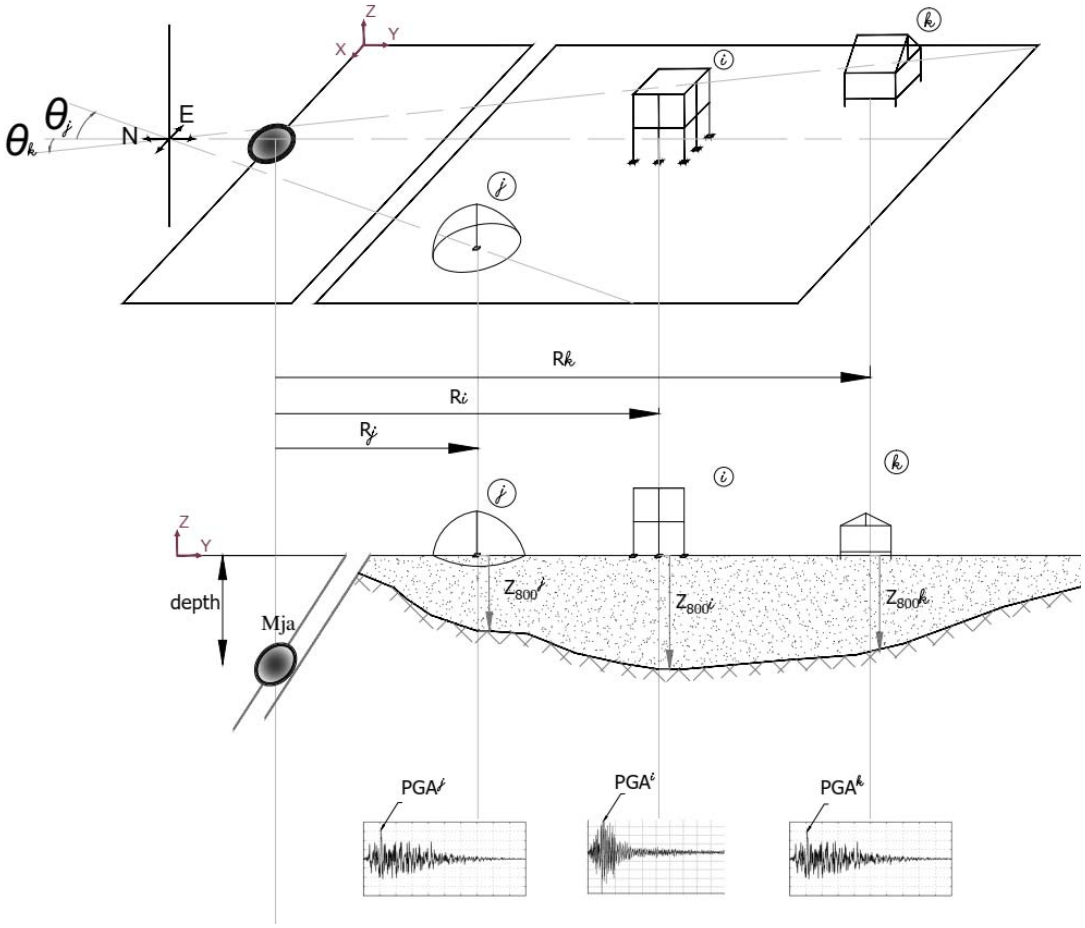

Figure II-7 Site seismic parameters.

II.6. Predictive models for Intensity measures (IMs)

The intensity measure of ground motion are parameters that describe quantitatively various aspects of the earthquake ground motion records. The characterization of earthquake strong motion is essential in risk assessment and earthquake-resistant design methodologies. It is considered as a link between seismic hazard analysis and seismic demand analysis. In earthquake engineering practice, various definitions of IMs were proposed and used with the aim of evaluating the potential damage of an earthquake motion.

As presented in Figure II-8, the intensity measures can be categorized into three groups:

(1) Peak ground motion parameters, which are used to determine the peak amplitude of different measures such as the acceleration (PGA), the velocity (PGV), and the displacement (PGD). These parameters primarily influence the response of structural systems.

(2) Duration and cumulative parameters, these measures are used to assess the cumulative effects of the ground motion which correlate well with the energy imparted to structures, well-

known parameters such as Intensity Arias (IA) and significant duration (SD) are widely used to take into account the cumulative effect.

(3) Frequency content, it is well known that the frequency of earthquake loading has a great impact on the seismic response of the engineering systems.

The intensity measures are intended to characterize the three aspects of ground motion, namely, the amplitude of motion, duration, and frequency content. In this dissertation, for each of the ground motion features, one parameter is investigated namely, respectively, PGA, Significant duration, and Mean period.

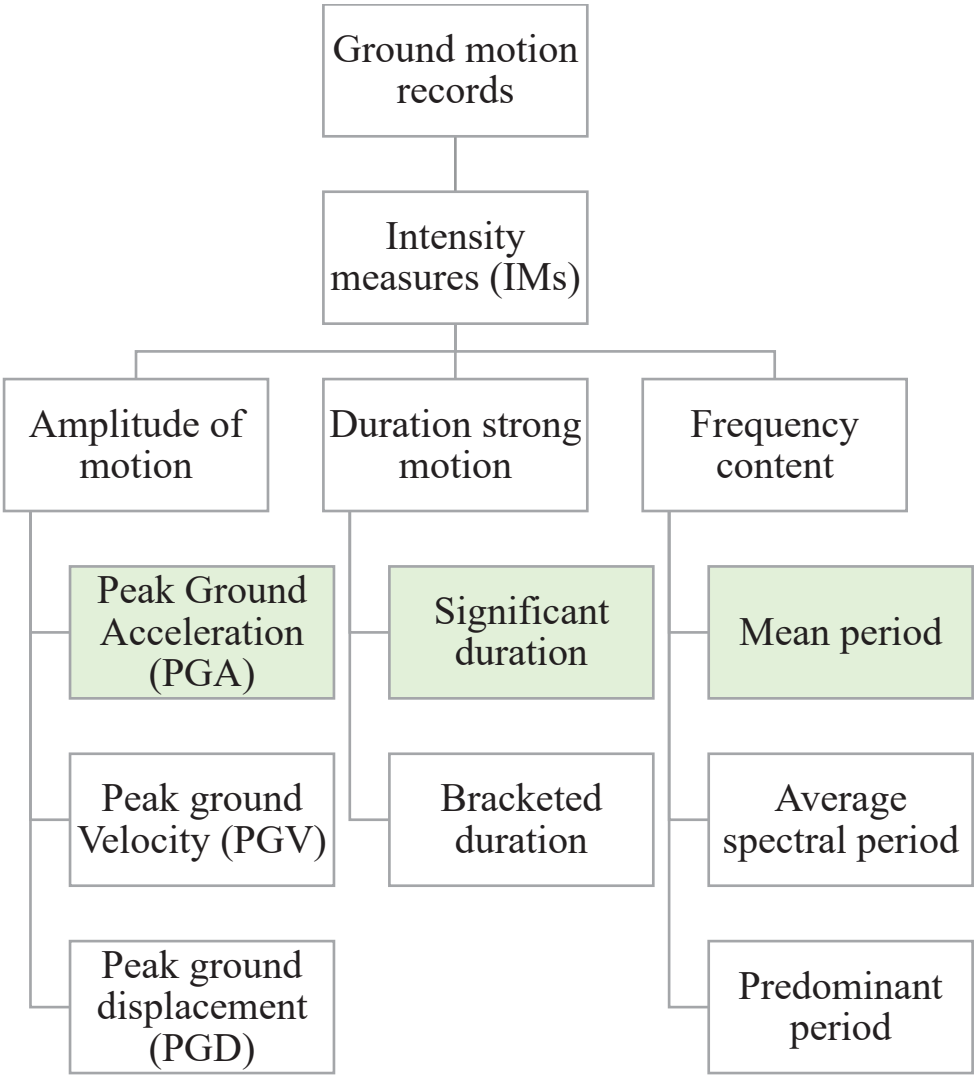

Figure II-8 Classification of Intensity measures parameters

II.6.1. GMPEs for the Peak ground acceleration (PGA)

Peak ground motion parameters influence the response of the structures and correlate well with the structural response during seismic excitation. The most commonly used parameter is the

Peak Ground Acceleration, which is equal to the maximum ground acceleration recorded on an accelerogram at a given site.

Until now, the GMPE has attracted considerable interest. Most of attenuation relationships developed are addressed to the PGA parameters, which are frequently presented as functions of seismological parameters. The early models were based on two parameters, source-to-site distance and the magnitude. Presently, advanced attenuation models are mainly considered the source to site distance, earthquake magnitude, geotechnical site condition, and faulting mechanism and stress drop, rupture propagation, directivity.[22, 24, 25]

The attenuation relationship for the PGA has undergone a revolutionary development, especially with the availability of data records and computational tools. for example, a brief comparison between the first attenuation model proposed by Esteva and Rosenblueth (1964) [26] and Abrahamson et al. (2014) [27]. The GMPE of Esteva and Rosenblueth (1964) was based on only 46 records and its three coefficients were estimated via standard least-squares regression. In contrast, the model of Abrahamson et al. (2014) is based on over 15 000 records from more than 300 earthquakes, and its roughly 40 coefficients were determined based on random-effects regression. As is common for early GMPEs, Esteva and Rosenblueth (1964) do not report the standard deviation (σ) of their equation, whereas Abrahamson et al. (2014) concentrate much of their effort on deriving a complex σ that models the different components of ground-motion variability.

Attenuation models for the PGA are currently published at the rate of more than one per month and, at the last count, A number of reviews of GMPEs have been made in the past, Douglas performed an extensive analysis of earlier empirical models and summarized 400 empirical equations for the prediction of PGA published between 1964 and 2019. Table II-2 summarizes some of the attenuation models proposed in the literature. Basically, the proposed attenuation models are strongly depend on the data records used which varied greatly with geographical regions [28]. Due to the increasing development of the GMPEs, Bommer suggested criteria to select the GMPE [29].

The typical forms of the attenuation models are expressed as follow:

$$\log(Y) = f_{source}(M) + f_{path}(R, M) + f_{site}(Vs30) + \varepsilon\sigma \quad (3)$$

While:

Y is the measure of ground-motion (PSA, PSV, or PGA, PGV, etc.).

f_{source} is a function that appropriately scales ground-motion with magnitude,

f_{path} is a function accounting for attenuation, and f_{site} is a function that accounts for local effects (e.g., amplification) at the recording site.

Table II-2 Typical attenuation relationships for PGA

Data source	Relationships	Reference
1970	$PGA = 1.254\, e^{0.8M}/(R+25)^2$	Esteva 1963 [30]
1994	$\ln PG = -3.512 + 0.904M - 1.328 \ln \sqrt{R^2 + [\,0.149\, e^{0.647M}]^2} + +[1.125 - 0.1121 lnR - 0.0957M]F + [0.440 - 0.171 lnR]S_{sr} + [0.405 - 0.222 lnR]S_{hr}$ F=0 for strike-slip and normal fault eathquake and 1 for reverse, reverse-oblique, and thrust fault earthquakes. Ssr=1 for soft rocka nd 0 for hard rock and alluvium Shr=1 for hard rock and 0 for soft rock and alluvium	Campbell and Bozoegnia[31]
1981	$\log PGA = -1.02 + 0.249M - log\sqrt{R^2 + 7.3^2} - 0.00255\sqrt{R^2 + 7.3^2}$	Joyner and Boore [32]
1997	$\ln PGA = b + 0.527(M - 6.0) - 0.778 \ln \sqrt{R^2 + (5.570)^2} - 0.371 \ln \frac{V_s}{1396}$ -where b=-0.313 for strike-slip earthquakes = -0.117 for reverse-slip eathquakes = -0.242 if mechanism is not specified	Boore [33]

II.6.2. GMPEs for Significant Duration of ground motion

In literature, more than 10 definitions characterize the seismic duration were proposed. Two classes can be distinguished: significant and bracketed duration.

II.6.2.1. Bracketed duration

Bracketed duration is defined as the time interval between the first and last exceedance of ground acceleration above or below a specified threshold value. [34]

The bracketed duration was initially used by Ambraseys and Sarma 1967 [35]. They selected a threshold of 0.03g. Page et al. (1972) [36] had slightly changed the initial definition by using a

threshold equal to 0.05g. The term “brackted duration” was first introduced by bolt 1973, he used the interval between the first and last excursion greater than or equal to 0.05 or 0.1g. [37]

Mcguire and Barhad [38] suggested bracketed duration based on various threshold values (e.g. 0.1g, 0.15g, and 0.2g). Figure II-9 illustrates as an example the calculation of the bracketed duration for a threshold acceleration of 0.05g.

The bracketed duration depends strongly on the absolute values of the acceleration, if the records are scaled to different levels of peak ground acceleration the duration value substantially changed. To overcome this shortcoming and eliminate the acceleration amplitude dependence. A new concept called fractional duration was proposed and used, which defines the threshold as a proportional of the peak acceleration. Since then, this concept has been used by several studies and is known as the normalized bracketed duration [39].

The main advantage of bracketed duration is the simplicity, while their disadvantage lies in the sensitivity to a small change in the threshold level.

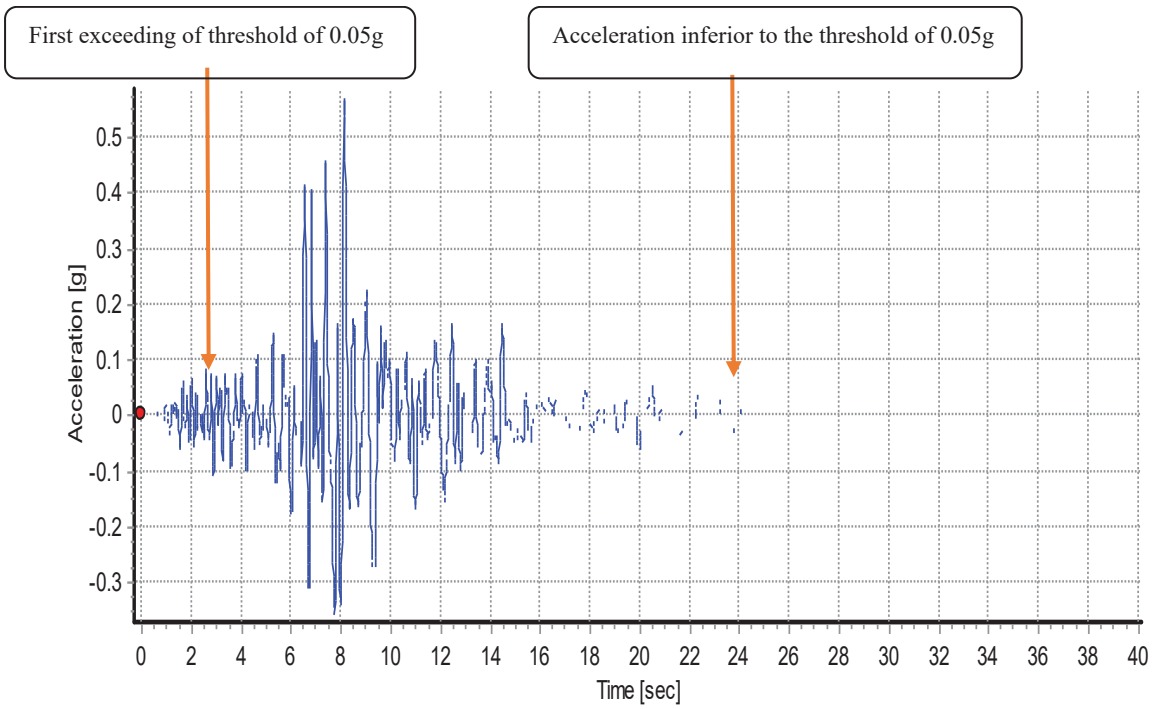

Figure II-9 Bracketed duration for The Northridge (USA) earthquake of January 17, 1994 record
Source: PEER Strong Motion Database

II.6.2.2. Significant duration

The “Significant Duration” refers to all definitions of ground motion duration that uses the energy content of an earthquake.

Most of the definitions of significant duration in the literature use Arias intensity, which is a measure of the energy content of the acceleration time history, by definition, the intensity of Arias equal to the integral of the square of the acceleration time history divided on (2xpi) value. Various approaches have been suggested to calculate the significant duration. Kempton and Stewart [1] have proposed a definition based on the square of the velocity time history while Trifunac and Brady [40] have used the squares of both the velocity and the displacement time history (2006, 1975, respectively).

The Arias intensity measure is a good representative parameter to evaluate the potential destructiveness of an earthquake [41]. Since it takes into account the characteristics of amplitude, frequency content, and duration of ground motion. Arias intensity appears to correlate well with several commonly used demand measures of structural performance and liquefaction [42, 43].

The total Arias intensity I_a is expressed as follow:

$$I_a = \frac{1}{2\pi g}\int_0^{t_{max}} a^2(t)dt \qquad (4)$$

Where:

- a(t) : ground motion time history
- t_{max}: duration time of accelerogram
- g : gravitational acceleration

Husid (1969) [44] defines the duration of strong shaking of an earthquake record as the time interval from 0% to 95 % of Arias intensity, whereas Trifunac (Trifunac and Brady 1975) used the time interval (SD595) between 5% and 95% of the Arias intensity which was more suitable. Similarly, (Somerville et *al.* 1997) [45] defined the significant duration as the time interval (SD575) between 5% and 75%. The last two significant duration definitions are investigated in the present study. The Trifunac and Brady definition of duration is illustrated in the Husid plot in Figure II.10.

In the present dissertation, the adopted significant duration is the one given by Trifunac and Brady (1975) which has been successfully used in previous researches. It represents the time interval t_{max} needed to reach a specific percentage of the total Arias intensity I_a.

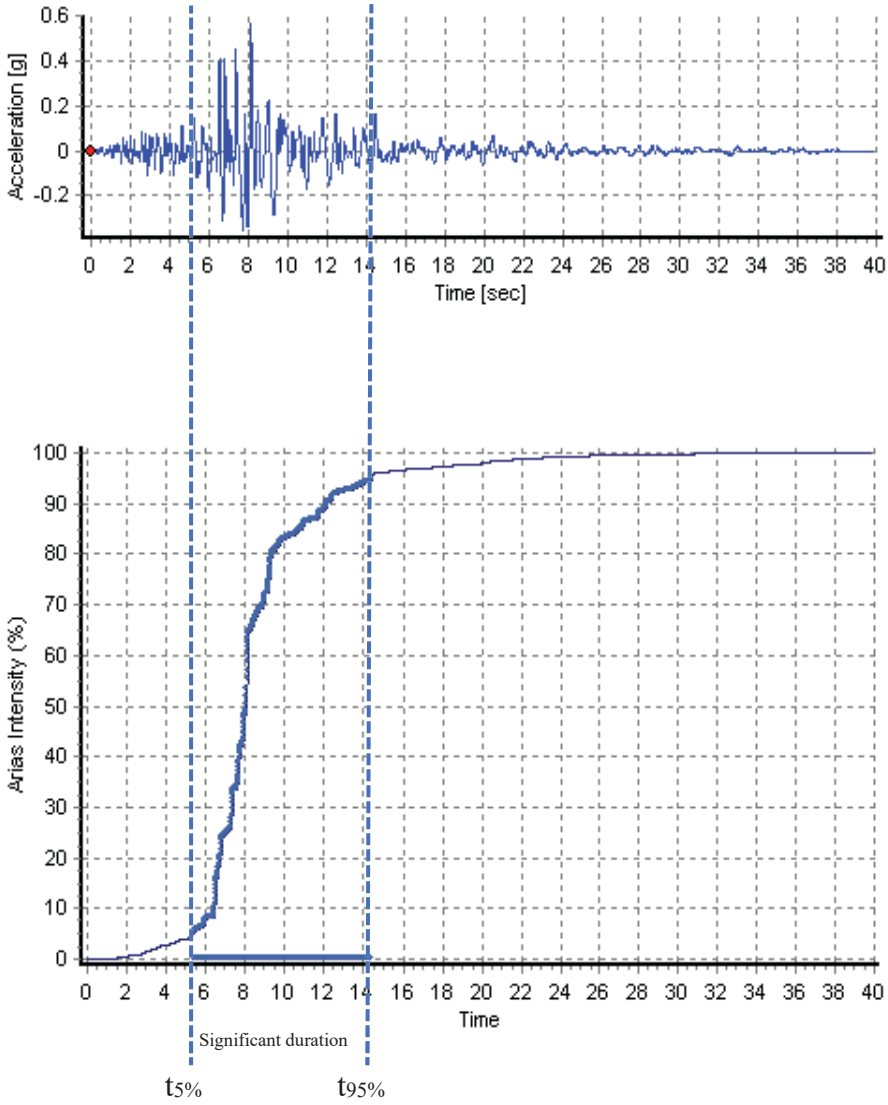

Figure II-10 Significant duration for The Northridge (USA) earthquake of January 17, 1994 record
Source: PEER Strong Motion Database

II.6.3. Significant duration relationships

Developing an attenuation relationship to estimate the significant duration of potential strong motion at any given site is challenging in seismic hazard analysis. Several recent studies have proposed predictive models to express various duration definitions based upon seismological consideration (Bommer et al. 2009 [2]; Afshari and Stewart 2016 [3], Hammal et al.2017 [46]).

Kempton and Stewart (2006) proposed an attenuation relationship that expresses the significant duration of earthquake ground motion as a function of magnitude, closest site-source distance, near-surface, shear wave velocity, basin depth, and near-fault parameters. Their ground

motion database used is collected from the worldwide strong ground motion records database, which records refer to the active tectonic regions such as USA (California) and Japan.

Lee and Green (2014) used the nonlinear-mixed effects regression technique to develop an empirical predictive relationship for a significant duration of horizontal strong ground motions in stable continental regions. Boore and Thompson (2014) [47] suggested an equation for path duration that can be used in the stochastic method.

Additionally, simple functional forms employing predictor seismological variables have been proposed by (Afshari and Stewart 2016; Du and Wang 2016) using Next Generation Attenuation-West2 (NGA-West2) database to predict the significant duration.

Nolasco et al. (2014) [48] used neural networks to determine the strong motion duration for the Mexican cities, even though based on a limited database.

Table II-3 summarizes some of the recent GMPEs for significant duration including the functional form. It can clearly be seen from this table that Abrahamson and Silva (1996) [49]and Kempton and Stewart (2006) [1] used a very similar functional form.

Table II-3 Empirical Models for Significant Duration

Investigators	Function form	Year
Triffunac and Brady [40]	$SD = a + ne^{CM}$	1975
Dobry et al.[50]	$SD = 10^{(aM-b)}$	1978
Abrahamson and Silva[49]	$\ln(SD) = \ln(6.38 * 10^{-8}(\left(\frac{\exp(b1 + b2(M - M*)}{10^{(1.5M+16.05)}}\right)^{\frac{-1}{3}})$	1996
Kempton and Stewart[1]	$\ln(SD) = \ln(6.38 * 10^{-8}(\left(\frac{\exp(b1 + b2(M - M*)}{10^{(1.5M+16.05)}}\right)^{\frac{-1}{3}})$	2006
Bommer et al. [2]	$\ln(SD) = C_0 + C_1 M_W$	2009

II.6.4. GMPEs for Frequency content

The frequency content of an earthquake ground motion is one of the key information to assess the severity of seismic action and is still often used as a parameter to describe strong ground motion. When the frequency content of an earthquake ground motion closely matches the natural period of geotechnical or structural systems (e.g., Soil deposit, Dam, Building, Bridge), the dynamic response is enhanced, larger force is exerted on the system, and significantly damage may occur.

A scalar representation of frequency is an essential parameter to compare the frequency content of different strong ground motions quickly and easily. A scalar frequency content parameter can be compared with the natural period of a dynamic system to evaluate the possibility of resonance conditions or an enhanced dynamic response. The existing parameters of frequency content are based on Fourier amplitude spectrum (FAS) which is a conversion of the motion from a time domain to a frequency domain through a Fourier transform. Figure II-11 illustrates an example of a typical Fourier amplitude spectrum for the S00E component of El Centro, the Imperial Valley earthquake of May 18, 1940. Four parameters have been proposed in the literature to characterize the frequency content of strong ground motions, which are (1) the mean period (Tm), (2) the average spectral period (Tavg), (3) the smoothed spectral predominant period (To), and (4) the predominant spectral period (Tp).

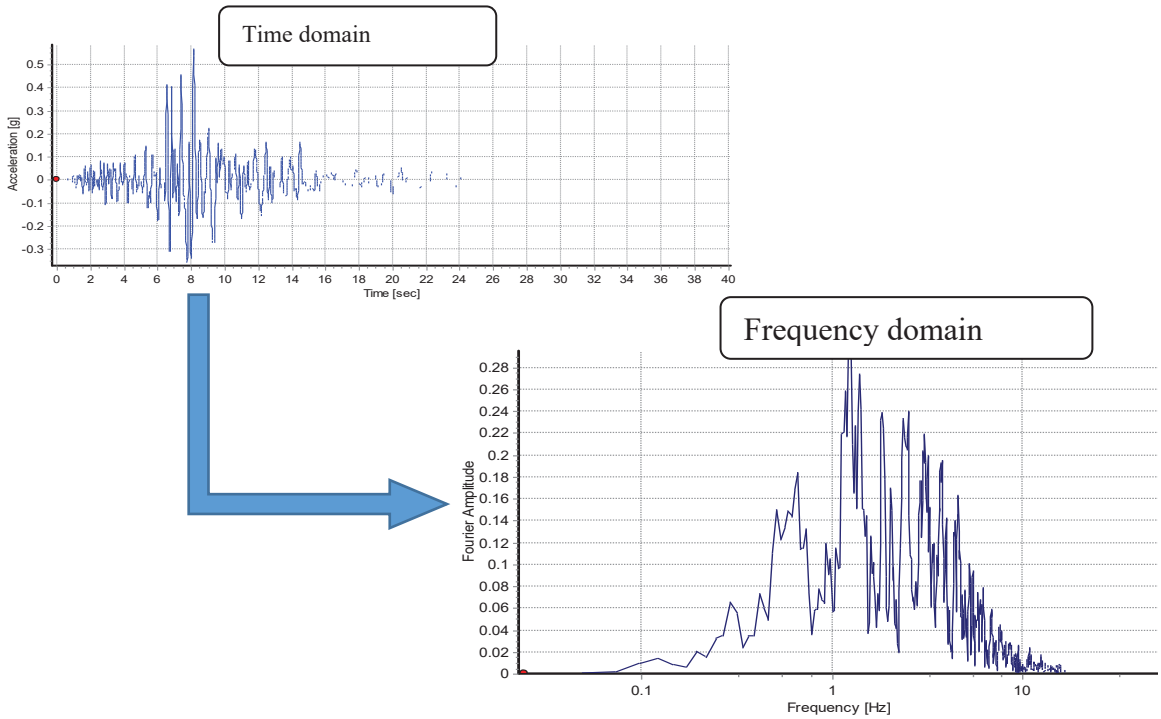

Figure II-11 Representation of Northridge record in frequency domain using Fourier amplitude spectrum (FAS)

In this dissertation, the adopted parameter is the mean period (Tm) which has been used and recommended in a number of past studies [6]. Several models have been proposed in literature to predict the frequency content; a predictive model is an empirical relationship that expresses the frequency content as a function of earthquake parameters.

The mean period (Tm) is a stable and reliable indicator of frequency content because it is based on all frequencies of engineering interest included in time history .The definition of the mean period initially proposed by ***Rathje et al*** is used, expressed mathematically as:

$$T_m = \frac{\sum C_i^2 \times \frac{1}{f_i}}{\sum {C_i}^2} \quad (5)$$

For 0.25 Hz <fi<20 Hz

fi : Discrete fast Fourier transform (FFT) rang 0.25-0.25Hz

Ci : Fourier Amplitude corresponding to the frequency fi

Although the mean period (Tm) is an important and widely used frequency content parameter in earthquake engineering, the number of attenuation relationships for Tm is limited. Only a few empirical models have been proposed to estimate the Tm.

The widely applicable model was proposed by Rathje et al (2004), which is updated to their previous own model developed in 1998. Rathje et al. (1998). [5] A limited number of research has proposed predictive models based on data from different regions, such as the western and central-east US [7] and Iran [8]. Table II-4 summarizes the existing prediction equation for Tm and the predictor variables used to predict the Tm. Noted that: Mw: moment magnitude; Rrup: closest distance from site to the rupture plane (km); Sc, Sd and Ss: indicators of site types; FD and Idir: indicators of the directivity effect; Vs30: time-average shear wave velocity of the upper 30 m (m/s); Z1: depth to the 1.0 km/s shear wave isosurface (km); Ztor: depth to the top of rupture (km).

Table II-4 Summary of the existing prediction equation forTm

Authors	Year	Predictor Variables	Range of application
Rathje et al [5]	1998	Mw, Rrup	5.2<Mw<7.3, R<200km
Rathje et at [6]	2004	Mw,Rrup,Sc,Sd,FD	4.9<Mw<7.6, R<200km
Lee [7]	2009	Mw,Rrup,Sa	4.5<Mw<7.6, R<200km
Yaghmari-Sabegh [8]	2015	Mw,Rtup,Sc,Sd	3.7<Mw<7.7, R<293km
Wenqui Du [51]	2019	Mw,Rrup,Vs30,Z1,Ztor,Idir	3.05<Mw<7.9, R<499.5km

II.6.5. Predictive models for Engineering Demand Parameters (EDP)

The reliable determination of engineering demand parameters (EDP) takes special consideration in current earthquake design and evaluation methodologies [52]. Although such engineering demand parameters can be calculated by means of sophisticated non-linear response history analyses, their application in the field of seismic assessment and evaluation of existing structures is still hindered by the considerable time, cost, and expertise required. Therefore, there is a need for simplified yet reliable methods for the estimation of structural seismic demands. Moreover, although in many cases structures do not behave as single-degree-of-freedom (SDOF) systems, various studies have shown that equivalent SDOF models can provide the basis for the estimation of global demands on building structures [53];

Equivalent single-degree-of-freedom (ESDOF) systems have made a significant contribution to many types of research in the field of earthquake and structural engineering [54-57]. The response of the multi-degree-of-freedom (MDOF) structure, including regular RC buildings, can be related to the response of an equivalent SDOF system, if the response is controlled by a single-mode, determined from a high enough modal participation factor. Different methods also make use of equivalent SDOF systems to predict damage in structures. Furthermore, recent recommendations are proposed to evaluate the maximum deformation in buildings based on such SDOF representation [58].

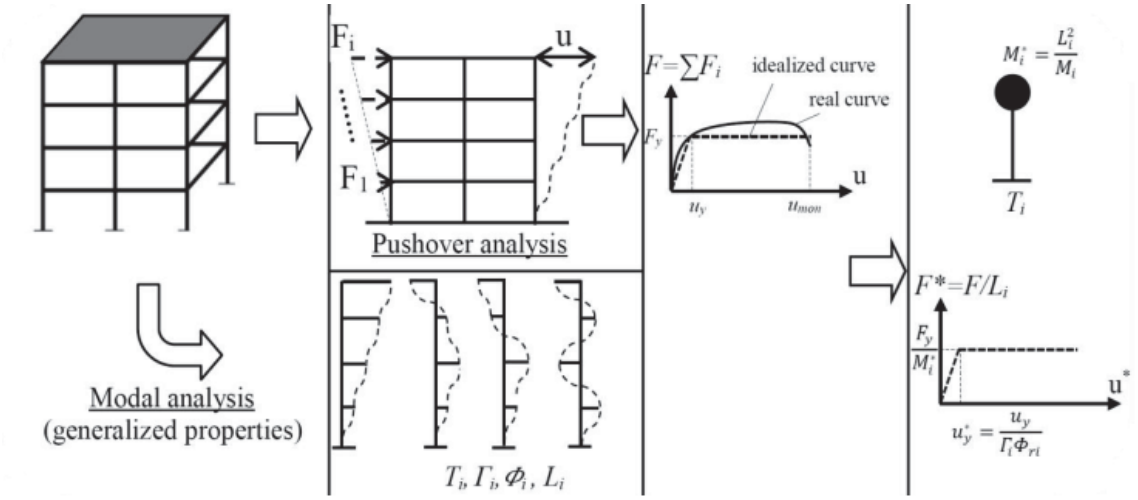

Figure II-12 Process of idealization of MDOF to Equivalent SDOF

Several studies agree with the application of a simplified nonlinear analysis procedure to base-isolated buildings [59-61]. The simplified nonlinear analysis procedure, which combines the nonlinear static (pushover) analysis of a Multi-Degree-Of-Freedom (MDOF) model with the

response spectrum analysis of an equivalent single-degree-of-freedom (SDOF) model, is widely applied to the traditional earthquake-resistant structures.

Numerous studies have used SDOF models to develop predictive relationships in terms of earthquake parameters and structural proprieties [62-65]. Some of these studies have focused on the estimation of strength ratios for systems of known ductility, distinguishing between stiff and soft soils and providing relationships that can be useful in the design of new structures to attain specified target ductility levels [64]. On the other hand, other studies have evaluated peak displacement demands for strength-defined structures and have provided relationships, which are useful for the seismic assessment of existing buildings. More recently, Bozorgnia et al. [65] performed a detailed investigation on inelastic deformations in SDOF systems based on predictive equations formulated on the basis of a large database including 3122 records. The attenuation relationship for EDP can be used to produce hazard curve and uniform hazard spectra.

The second part of this dissertation focuses on two engineering demand measures: **Inelastic Displacement** and **Hysteretic Energy**. Which are usually combined to evaluate the seismic damage.

II.7. Response spectrum

The structural damage can be related to seismic displacement demand and in particular to interstory drift ratios. Well-known methods such as the Capacity Spectrum Method (CSM) are based on superimposing the seismic capacity over the corresponding seismic demand for a given hazard level to determine the expected response of the structure. The capacity curve relies on the use of nonlinear static analysis (pushover method) while the seismic demand is a representation of the earthquake ground motion, generally it is obtained directly by time-history analyses of inelastic SDOF systems, or indirectly from elastic spectra [66].

Expressing the response spectra for a given site in terms of seismological parameters and structural properties has received much interest; a large number of studies have been conducted to develop the Ground Motion Prediction Equation (GMPE), which express the response spectra in terms of seismological parameters in the form of attenuation relationships [9, 10]. Two approaches have been proposed to estimate the inelastic seismic demand. In the first approach, the inelastic response is derived from the elastic one through a reduction coefficient, which has been criticized and many researchers contend that these reduction factors used in seismic code are highly simplified, and have shown that they depend on the natural period, local site condition, Magnitude and source to site distance [67]. To overcome this shortcoming, a second approach was proposed

which consists of developing Ground Motion Prediction Equations (GMPEs) of inelastic response spectra, without the need to resort first to elastic spectra.

II.8. Energy spectrum

The earthquake input energy imparted into structural systems can be classified into two groups, namely recoverable and irrecoverable (Figure II-13). Specifically, the elastic strain (Es) and kinetic energies (Ek) are stored components that vanish when the vibration of the system ceases, whereas the damping (E_d) and hysteretic energy (E_H) are dissipated throughout damping and inelastic deformations.

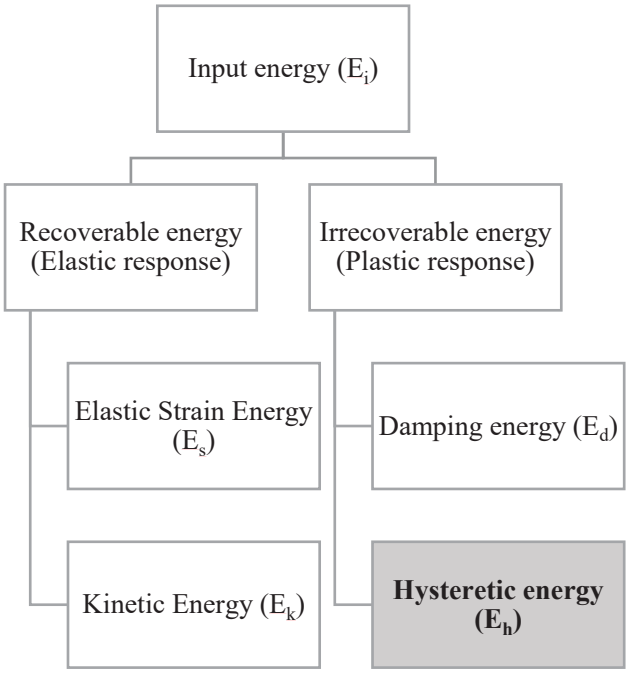

Figure II-13 Energy component

The dissipated energies are essential in the evaluation and design of the structures. From a practical perspective, several damage indices have been proposed to quantify the local and global structural damage of buildings, the most commonly used is called the Park-Ang index, which relies on two aspects, the maximum ductility and hysteretic energy dissipation demand imposed by the earthquake [68]. The hysteretic energy term is investigated in this dissertation, which is considered as the most important energy component contributing to structural damage.

In current practice, both conventional Force-Based Design (FBD) and Displacement-Based Design (DBD) can not appropriately consider the cumulative damage from numerous inelastic cycles [69, 70]. The Energy-based design (EBD) is attracting an increasing interest due to its ability to take into account both strength and displacement characteristics as well as hysteretic behavior of

the structure. Hounser [71] initially discussed the energy-based concept during the First Word Conference Engineering (1956). He reached the conclusion that safe design could be achieved if the cumulative elastic energy (energy supply) is greater than or equal to total input energy (energy demand). Akiyama (1985) has traced the evolution of the energy-based method in his groundbreaking study where he has concluded that the total input energy is generally controlled by the fundamental period and the total mass of the structure [72]. Since then, various studies have introduced the energy concept to design and seismic assessment [69, 73] Several researchers have agreed that the next generation building code would consider the energy principle . For instance, a proposal has been carried out to introduce the energy-based spectrum load into the Japanese building code [74]. Which was followed in other countries by various discussions on the same issue.

Donaire-Avila [75] has summarized the energy-based design process in four main issues:

(1) The input energy into the structure during earthquake ground motion;

(2) The distribution of the input energy throughout the structure;

(3) The energy absorption capacity of structural members;

(4) The relationship between the cumulative plastic strain energy and the maximum inelastic displacement, that is, the equivalent number cycle.

It has been clearly specified that each of the following issues required further investigation. As part of this dissertation, the first issue related to the evaluation of the input energy demand is addressed. The prediction of the seismic demand in terms of energy spectrum has received an increasing interest. In Seismic Hazard Analysis (SHA), probabilistic models are used to determine the intensity measure of the ground motions for a given hazard level. Compared to the amount of research performed on the parameters characterizing the strong ground motion, there are few works on energy-based parameters, in literature, a limited number of attenuation models have been proposed for elastic input energy by analyzing ground motion records collected from different regions [76-78]. Alici and Haluk (2016) [79] proposed two approaches for predicting input energy spectra, in the first approach; an attenuation model has been developed through nonlinear regression analysis while the second approach utilizes probabilistic seismic hazard maps. The seismic hysteretic energy spectra is proposed in the form of an attenuation relationship by Gong et al. (2012) [80], in which the hysteretic energy is expressed as a function of earthquake parameters such as earthquake magnitude, source-to-site distance, and site class. Alreja et al. (2015) [81] proposed a prediction model to estimate the hysteretic energy demand in steel moment-resisting frames, using Multivariate Adaptive Regression Spline (MARS) and Least Squares Support Vector Machines (LSSVMs). These models are used to establish a relation between the hysteretic energy demand and several effective parameters such as earthquake intensity, number of stories, soil type, period,

strength index. Zhai, Ji et al. (2018) [82] proposed a hysteretic energy prediction equation as a function of the vibration period, ductility value, and damping ratio.

Most of the prediction models of energy demand available in the literature are developed in form of attenuation relationship i.e. the energy input is expressed in terms of earthquake parameters such as magnitude and distance (see Figure II-14-a). Dindar [83] has attempted to incorporate the intensity measure parameter such as the PGA in addition to the structural proprieties, site condition, and target structural ductility as an input to predict energy demand spectra (see Figure II-14-b). In this dissertation, the hysteretic energy demand spectra are predicted by considering as inputs the Intensity measures (IMs) which characterize the main features of ground motion rather than expressing it in terms of earthquake parameters (see Figure II-14-c). The new approach is proposed in an attempt to reduce the uncertainties related to earthquake and seismological parameters.

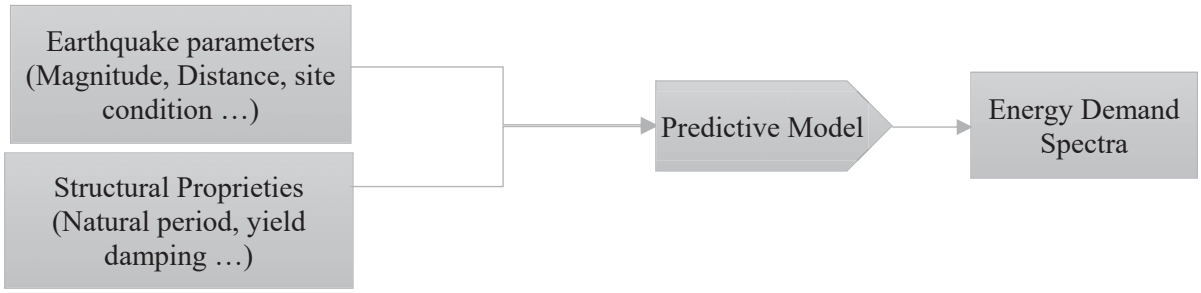

a. Approach commonly used in literature

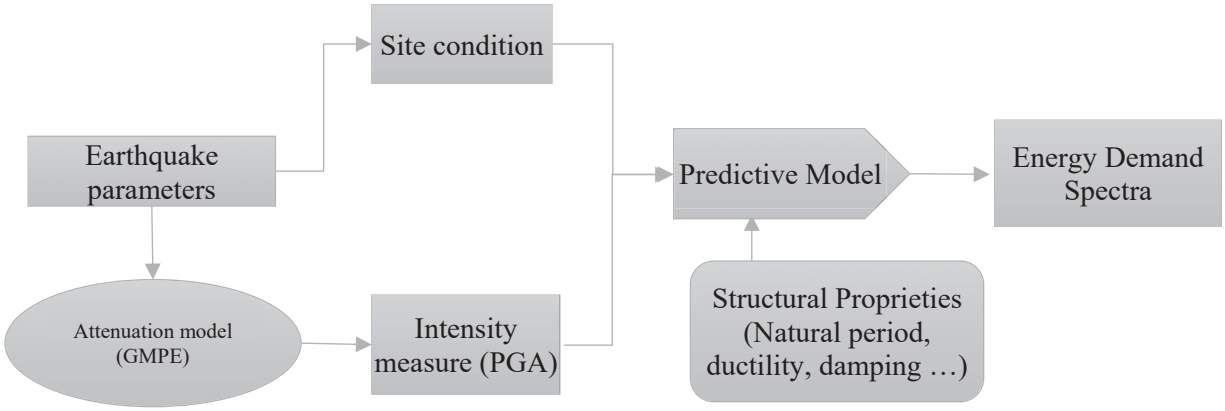

b. Dindar's model (2015) [16]: introducing PGA as an input

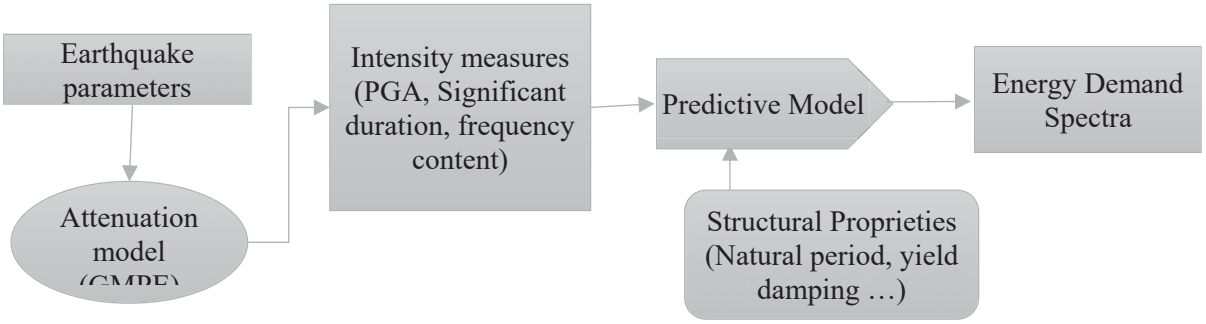

Figure II-14 Flowchart of procedures used in literature to predicting energy

II.9. Conclusion

A brief state of the art of the existing attenuation models for the intensity measures of ground motion has been presented. The intensity measure are parameters that describe quantitatively the main features of the earthquake ground motion namely, the amplitude, the cumulative effect and the frequency content. The earthquake parameters used to develop the ground motion prediction equation can be classified into three groups: 1) Source characteristics, 2) Path characteristics 3) Site characteristics.

In earthquake engineering, there is still a need to consider the directionality of ground motion effects. Various empirical relationships have been suggested in the literature in order to estimate the intensity measures of the ground motion; few researchers have addressed the directionality aspect of ground motion.

Researchers have chosen their techniques based on the available data from past earthquake, which varies greatly with geographical region. However, there is still a need to include more independent parameters into the attenuation models.

Chapter III. METHODOLOGY

III.1. Introduction

The characteristics of ground motion and Engineering demand measures of SDOF are investigated in this dissertation. The methodology can be summarized in three steps: (a) Data collection (b) Data modeling using artificial neural network (c) interpretation of results. The information collected from strong motion records is the basic input for Seismic Hazard Analysis (SHA) and earthquake-resistant structure design and rehabilitation. There is a large number of seismogram networks installed around the world, which provide valuable information and ground motion database. Various sources of the strong motion database are freely available to the research community, such as Pacific Earthquake Engineering Research (PEER), Consortium of Organizations for Strong-Motion Observation Systems (COSMOS), and National Research Institute for Earth (NIED).

For a given earthquake event, the strong motion database comprises:

(1) The strong motion file accelerogram records for each station.

(2) The metadata parameters such as magnitude, station location, epicenter location, and site condition parameters.

The ground motion database used in this dissertation is collected from the KiK-Net network. One of the major advantages of the KiK-Net database is that the borehole data set is available for each station, which is useful information to evaluate the site effects.

The Artificial neural network is used to analyze the data, which is highly recommended in such complex phenomena due to its ability to take into consideration the nonlinear relationships between the independent and the dependent parameters. An overview on the Artificial Neural Networks presented in this chapter

III.2. Ground Motion Data Set

III.2.1. Data acquisition

K-NET (Kyoshin Network) is a nation-wide strong-motion seismograph network, which consists of more than 1,000 observation stations distributed every 20 km uniformly covering Japan (see Figure III-1). KiK-Net has been operated by the National Research Institute for Earth Science

and Disaster Resilience (NIED) since June, 1996. At each K-NET station, a seismograph is installed on the ground surface with standardized observation facilities.

KiK-Net (Kiban Kyoshin Network) is a strong-motion seismograph network, which consists of pairs of seismographs installed in a borehole together with high sensitivity seismographs (Hi-net) as well as on the ground surface, deployed at approximately 700 locations nationwide. NIED constructed KiK-Net under the plan 'Fundamental Survey and Observation for Earthquake Research' directed by 'the Headquarters for Earthquake Research Promotion'.

The strong-motion data recorded by K-Net and KiK-Net are immediately transmitted to the data management center of NIED in Tsukuba. The observed strong-motion data are widely available to the public through the internet from the official web site. The soil condition data explored at K-NET stations and the geological and geophysical data derived from drilling boreholes at KiK-net stations are also available. [84]

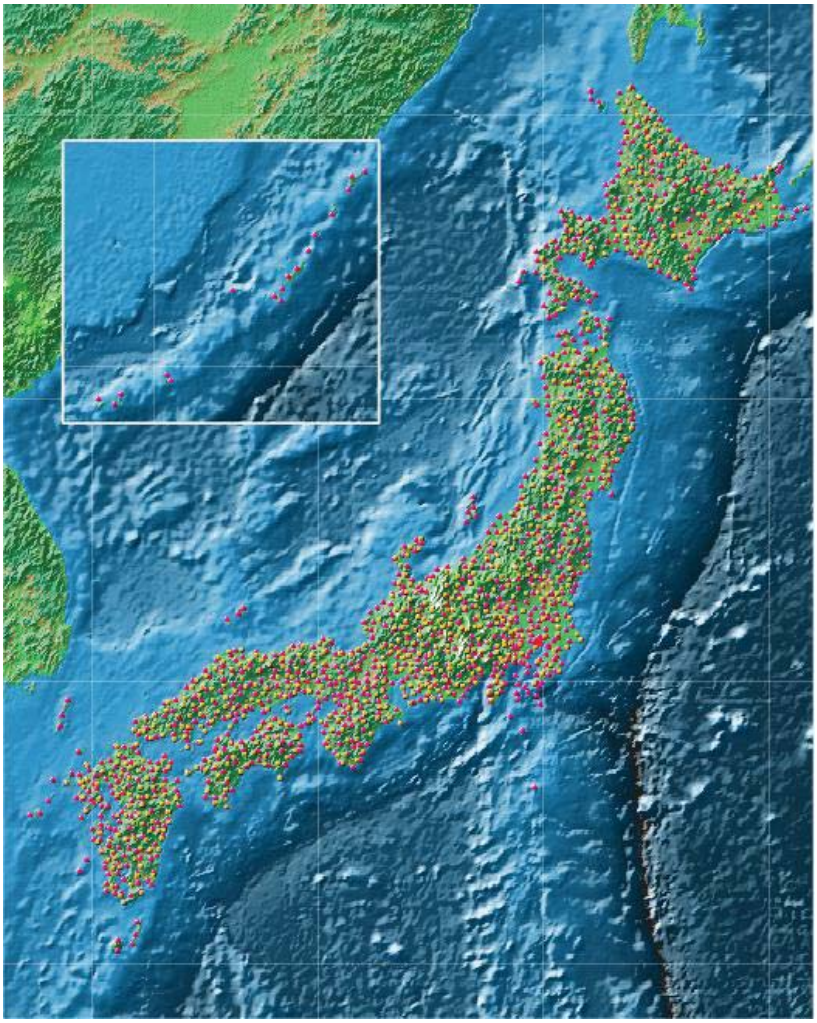

Figure III-1 K-NET & KIK-Net observation stations covering JAPAN

III.2.2. Statistics of strong Ground Motion Data Set

The strong motion database, collected for this study, includes 1 104 accelerograms from 10 earthquake events which magnitudes vary between M= 4.8 to 7.3, taken place in Japan during the period 2000-2016 (see

Table III-1). The earthquake ground motions were thoroughly selected from the KiK-Net database. The records distribution versus magnitude and Peak Ground Acceleration (PGA) are presented in chapter IV. The adequate selection of samples or data may significantly improve the performance of the predictive models. A complete list of the strong motion records selected for use in this study is included in Appendix.

A total set of 1,104 values is divided into three sets, [85, 86]

- The training dataset, used to train the model, represents 70% of the complete data.
- The validation dataset, used to avoid overtraining and monitor the training process, represents 15% of the complete data.
- And the testing dataset, used to judge the performance of the trained model, represents the remaining 15% of the complete data

Table III-1 Summury of the events collected for the ANN development (training and validation) freely available at: http://www.kyoshin.bosai.go.jp/

Origin Time	Latitude	Longitude	Depth	Magnitude	Earthquake name or epicenter region	Rupture process
2011/03/11-14:46	38.10N	142.86E	024km	M9.0	The 2011 off the Pacific coast of Tohoku Earthquake	Link
2008/06/14-08:43	39.03N	140.88E	008km	M7.2	The Iwate-Miyagi Nairiku Earthquake in 2008	Link
2007/07/16-10:13	37.56N	138.61E	017km	M6.8	The Niigataken Chuetsu-oki Earthquake in 2007	Link
2007/03/25-09:42	37.22N	136.69E	011km	M6.9	The Noto Hanto Earthquake in 2007	Link
2005/03/20-10:53	33.74N	130.18E	009km	M7.0	West off Fukuoka	Link
2004/10/23-17:56	37.29N	138.87E	013km	M6.8	The Mid Niigata prefecture Earthquake in 2004	Link
2000/10/06-13:30	35.28N	133.35E	011km	M7.3	The Western Tottori prefecture earthquake in 2000	
2016/04/16-07:23	32.79N	130.77E	012 km	M4.8		
2016/04/16-07:11	33.27N	131.40E	006 km	M5.4		
1998/04/22-20:32	35.17N	136.56E	010 km	M5.4		

2016/04/18-20:42	33.00N	131.20E	009 km	M5.8		
2011/03/23-07:12	37.08N	140.79E	008 km	M6.0		
2003/07/26-07:13	38.40N	141.17E	012 km	M6.2	Northern Miyagi prefecture	
2016/10/21-14:07	35.38N	133.85E	011 km	M6.6		

III.3. Data-modeling analysis: Artificial Neural Network (ANN)

III.3.1. Background and Basic concept

Artificial intelligence (AI) is the study and science of making intelligent systems, that are capable of receiving inputs from the environment, perceiving, thinking, learning, and adapting their behavior, to achieve a particular goal or objective over a period of time. Artificial intelligence techniques have proved their efficiency in almost all fields of science and engineering.

Various similar AI techniques were proposed and used, such as Neural networks, Fuzzy Systems, Genetic Algorithm, and Genetic Programming. These techniques are successfully used as an alternative to traditional mathematical models because of their faster computational efficiency. Artificial Neural Network (ANN) is the most popular AI technique that has been applied and proved its relevance.

The artificial neural network (ANN) is a computational model inspired by the way the human brain works, consisting of interconnected networks of simple processing units that attempt to recognize underlying relationships based on a set of data through a process of learning from experience by adjusting the connections.

The ANN is a very rough imitation of the brain's structure. The human nervous system is a complex neural network consisting of connected neurons (see Figure III-2). The nucleus is the center of the neuron and it is connected to other nuclei through the dendrites and the axon. This connection is called a synaptic connection. A typical neuron collects signals from others through a host of fine structures called dendrites. The neuron sends out spikes of electrical activity through the axon, which can split into thousands of branches. When a neuron receives enough electric pulses through its dendrites, it activates and fires pulse through its axon, which is then received by other neurons. In this way, information can propagate through the neural networks. The synaptic connections change throughout the lifetime of a neuron and the number of incoming pulses needed to activate a neuron (the threshold) also change. Learning occurs by changing the effectiveness of the synapses so that the influence of one neuron on other changes. [48, 87, 88]

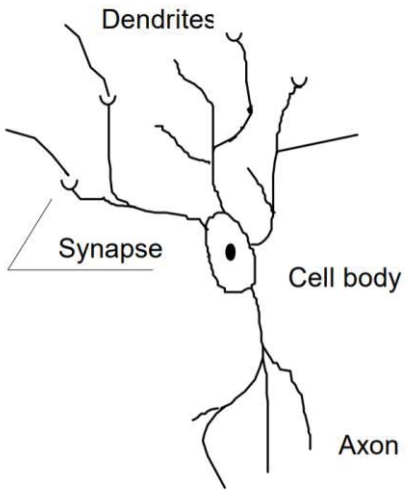

Figure III-2 A biological neuron

ANNs have been developed as generalizations of mathematical models of human cognition or neural biology, based on the assumptions that:

- Information processing occurs in many simple elements called *neurons*.
- Signals are passed between neurons over *connection* links.
- Each connection link has an associated *weight*, which, in a typical neural net, multiplies the signal transmitted.
- Each neuron applies an activation function (usually nonlinear) to its net input (sum of weighted input signals) to determine its output signal.

As illustrated in Figure III-3, a neuron consists of three main parts:

- A set of synapses, which connect the input signal xj to the neuron via a set of weights, wkj ;
- An adder uk which sums up the input signals, weighted by the respective synapses of the neuron;
- Activation function Ø (.) for limiting the amplitude of the output of the neuron. At times, a bias b_k *is* added to the neuron to increase or decrease the net output of the neuron.

Mathematically, a neuron *k* is described as (Haykin, 1994) [89]

$$u_k = \sum_{j=1}^{n} w_{kj} x_j$$

$$y_k = \emptyset(u_k + b_k)$$

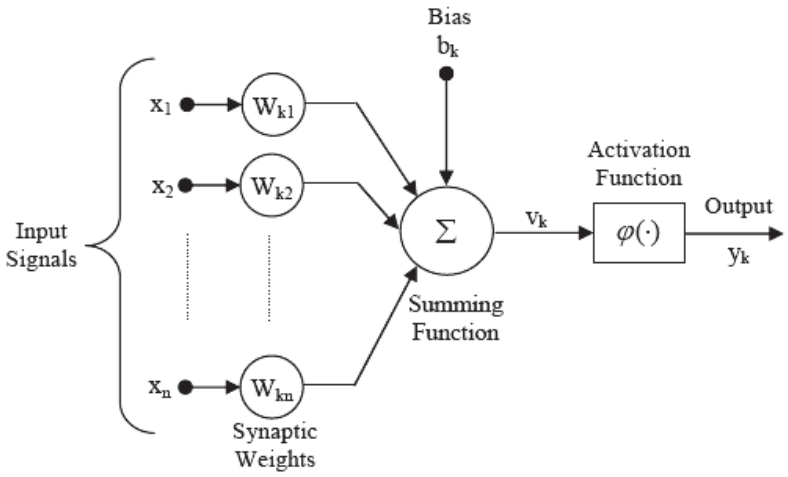

Figure III-3 The block diagram of a neuron (Haykin, 1994)

Where $x_1, x_2, x_3, \ldots, x_n$ are the input signals; $w_{k1}, w_{k2}, \ldots, w_{kn}$ are the weights for the neuron k; b_k is the bias; u_k is the adder or the linear combiner; $\phi(.)$ is the activation function; and y_k is the output signal of the neuron.

The selection of activation function is the most critical step in the development of Artificial-Neural-Network-based models, which allow capturing nonlinear behavior and dealing with complex phenomena. By definition, the activation function is a mathematical equation that delivers an output based on inputs. As shown in Figure III-4, several activation functions such as hyperbolic tangent, sigmoid and linear functions are commonly used in the mapping process. There is no systematic theory to determine the accurate architecture and define the number of hidden layer nodes. Thus, trial and error is a fundamental method used to select the optimal configuration of the neural network models.

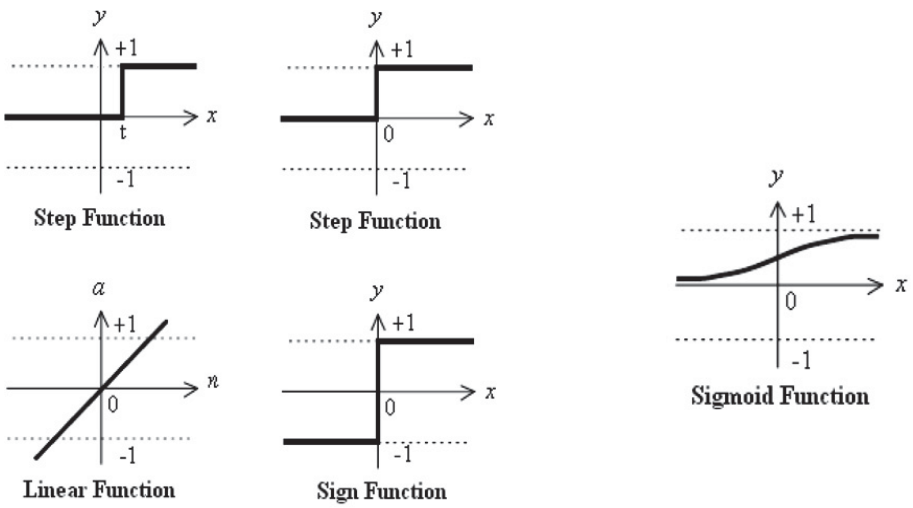

Figure III-4 some common activation functions

III.3.2. Areas of application

The development and application of neural networks is an extremely interdisciplinary field. The Artificial Neural Network has been used in every area of engineering to study and simulate various phenomena. Over the years, various researches have been conducted to incorporate the machine-learning concept in all fields of civil engineering such as structural engineering, geotechnical engineering, earthquake engineering, structural identification and control, transport infrastructure issues, management and technology in construction and installation issues. Abedi (1989) initially presented the first paper on the introduction of Neural Network in civil engineering. His groundbreaking study entitled " "Perceptron learning in engineering design", appeared in the journal "Microcomputers in Civil Engineering", which proposed an approach to introduce the machine learning model in engineering design of meal frame based on a concept of internal control parameters and perceptron [90].

In structural engineering, the neural network was largely used to develop a mechanism model that included factors that their effects on structural systems are poorly understood. The counter-propagation neural networks with competition and interpolation layers was presented and applied to several structural engineering issues such as [91]:

(1) Development of a mapping neural network that defines the relationship between the ultimate bending moment and the depth of a reinforced concrete beam with a rectangular cross-section.

(2) The prediction of the locations and magnitudes of maximum moments in a simply supported rectangular plate subjected to a unit concentrated load somewhere on the plate.

(3) The prediction of elastic critical lateral torsional buckling moments of wide-flange steel beams (W shapes) subjected to a uniform bending moment.

Other studies have used the NN for reinforced concrete structures, steel structures. Xu (2001) proposes an adaptive multiplayer perceptron (MLP) technique for the detection of cracks in anisotropic laminated plates [92]. Su and Ye (2005) developed A guided Lamb wave-based damage identification scheme monitoring of composite structures "in service", according to damage assessment[93]. Ganesh (2006) investigated the feasibility of using multilayer feed-forward neural networks to learn the complicated nonlinear mapping between the input parameters associated with profiled deck and the output parameters m and k associated with horizontal shear resistance of the composite deck [94]. Kumar (2008) developed a neural network approach for the identification and control of a smart composite laminated spherical shell [95]. Tsompanakis (2008) presented applications of soft computing techniques, involving ANNs, in computationally demanding tasks in

mechanics. The possibility to use ANNs for the approximation of the inverse structural mapping was investigated [96]. The identification of the damaged structures can be achieved with neural networks.

In 1992 Wu, Ghaboussi and Garrett presented a structural damage detection system using a backpropagation algorithm, the results of case studies indicated that neural networks are capable of learning about the behavior of undamaged and damaged structures and can identify the damaged member and the extent of the damage from patterns in the frequency response of the structure [97]. A method of identifying damage to steel moment-frame structures connected by welding subjected to seismic actions using frequencies and vibration modes is proposed [98]. Adeli (2009) presents a probabilistic neural network for predicting the magnitude of the largest earthquake in a pre-defined future time period in a seismic region using eight mathematically computed parameters known as seismicity indicators [99]. Calabrese (2013) used artificial neural network to implement, in order to determine the unknown nonlinear seismic and geotechnical input data versus the expected performance of the structural system [100].

The ANN has been successfully used for deriving fragility curves of the considered structures: A Soft Computing (SC) based framework for the fragility assessment of 3D buildings is proposed by Chara et al. (2011) [101]. Wang et al. (2018) proposed a methodology of ANN meta-models for the computation of fragility curves for nuclear power plant equipment. The ANN meta-model is utilized to build the statistical relation between the seismic intensity measures and the structural response [102]. Studies in the Structural identification and control problems area have attracted strong interest; The ANN is considered a powerful tool for identifying structural nonlinear dynamical systems. A review of journal articles published on system identification of structures was presented by Sirca and Adeli (2012) [103]. Facchini et al. (2014) proposed the application of neural networks for output-only modal identification of structural systems. Four frequency-dependent indicators, based on specific properties of the spectral tensor of vibration measurements, are defined and employed to build a likelihood function for the presence of structural resonances [104].

The computation of geotechnical engineering analysis is characterized by uncertainties on design values of geotechnical indices with significant impact. knowledge and experience are also the foundation for effective resolution of geotechnical problems. The Artificial Neural Networks are strongly recommended for modeling complex phenomena in geotechnical engineering (soil types and their associations in complex stratigraphic profiles), which by their nature, show a wide variety. The neural networks modeling does not need any assumptions about the fundamental rules governing the problem. Its capacity to learn from experiences gives neural network modeling superiority as an alternative to traditional methods.[105]

The difficulty encountered in geotechnical engineering problems due to the inhomogeneous soil, Neural Networks can be an optimal solution for modeling many problems in geotechnical engineering. Consequently, a large number of studies have been conducted to track the soil's behaviour and find its characteristics.

The application of ANNs in geotechnical engineering was initially discussed in the early 1990s by Goh (1994) and Ghaboussi and Sidarta (1998) [106, 107]. Basma (2004) investigated the feasibility of using neural networks to model the complex relationship between soil parameters, loading conditions, and the collapse potential using a backpropagation neural network process [108]. Several studies used various types of neural networks, such as backpropagation, probabilistic neural networks, and generalized regression, to estimate geotechnical slope stability and geometric parameters. [109-111]

The ANN has received, in recent years, a growing interest by the scientific community in the field of earthquake engineering and seismic risk assessment: Prediction of intensity measures of ground motion [46, 112]; generating artificial earthquakes and response spectra [113]; estimation of artificial time history and related spectral response [113, 114].

III.3.3. Type of ANN

ANNs are commonly classified by their network topology, node characteristics, learning, or training algorithms (Fausett, 1994). Based on the connection pattern (architecture), ANNs can be grouped into two categories (see Figure III-5) [115]

• Feed-forward networks, in which graphs have no loops, and

• Recurrent (or feedback) networks, in which loops occur because of feedback connections. [116, 117].

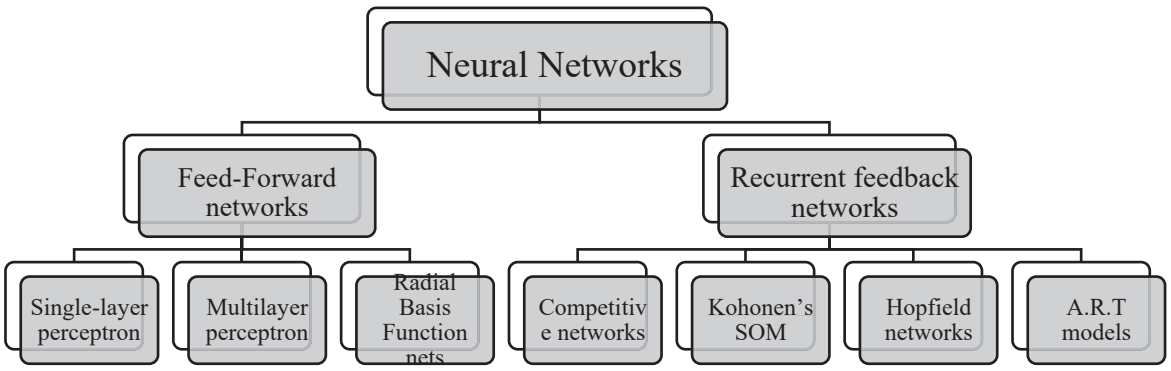

Figure III-5 A taxonomy of feed-forward and recurrent/feedback network architectures.

In a *feed-forward neural network* structure, Feedforward neural networks were the first type of artificial neural network invented and are simpler than their counterpart, recurrent neural networks. They are called feedforward because information only travels forward in the network (no loops), first through the input nodes, then through the hidden nodes (if present), and finally through the output nodes.

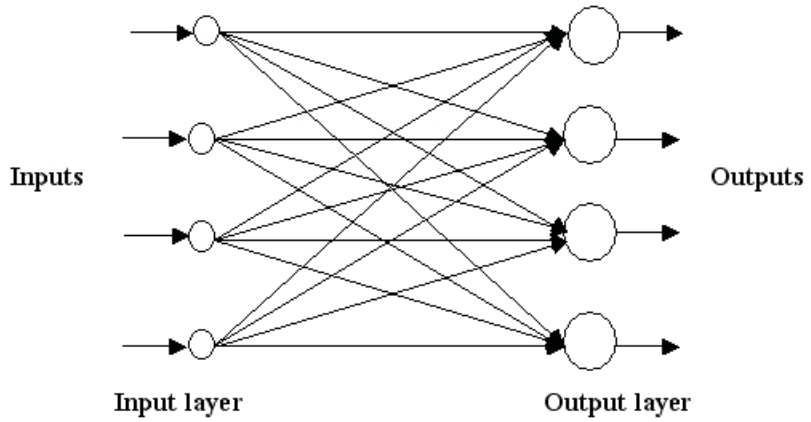

Figure III-6 A single layer feed-forward neural network

In Figure III-6, a single layer feed-forward neural network (fully connected) is shown. Including the input layer, there are two layers in this structure. In Figure III-7, a multi-layer feed-forward neural network with one "***hidden layer***" is depicted. As opposed to a single-layer network, there is (at least) one layer of "***hidden neurons***" between the input and output layers.

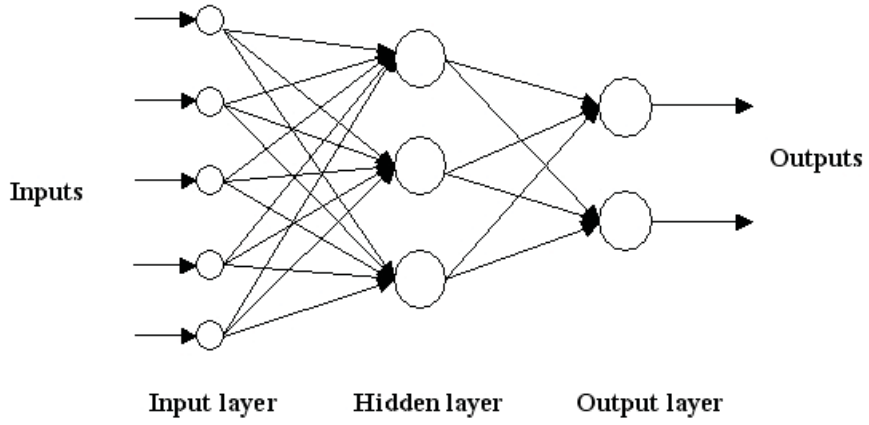

Figure III-7 A multi-layer feed-forward neural network

For *recurrent (or feedback) networks*, it include any network design in which the activity must go through the network more than once before the weights (output coefficients) are adjusted and the output is produced, the inputs of each layer can be affected by the outputs from previous layers (see Figure III-8).

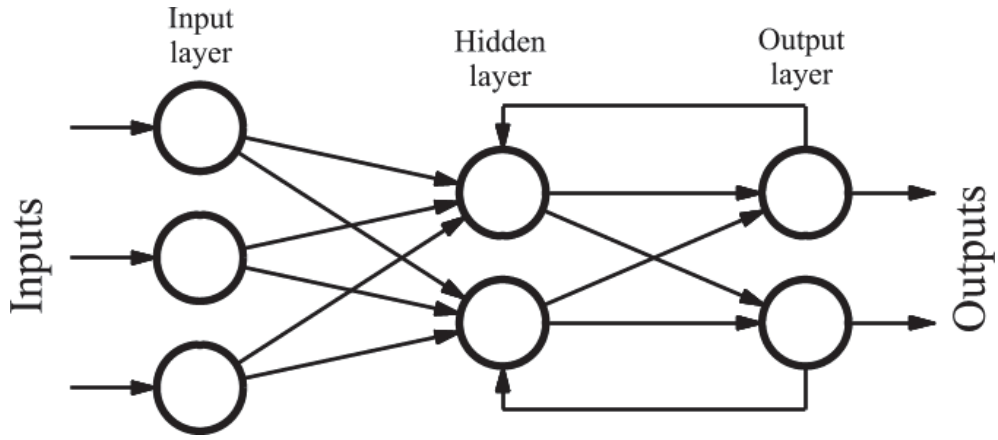

Figure III-8 recurrent (or feedback) networks

Another way of classifying ANNs is mode of training applied. Two modes of training are present in neural training, *supervised and unsupervised learning* networks (Konar, 1999) [118].

Supervised training: requires an external teacher to control the learning and incorporates global information. The teacher may be a training set of data or an observer who grades the performance. Examples of supervised learning algorithms are the least mean square (LMS) algorithm and its generalization, known as the back propagation algorithm, and radial basis function network. In supervised learning, the purpose of a neural network is to change its weights according to the input/output samples [119].

Unsupervised learning: When there is no external teacher, the system must organize itself by internal criteria and local information designed into the network. It is required in many recognition problems, where the target pattern is unknown. sometimes referred to as self-organizing learning, *i.e.* learning to classify without being taught. In this category, only the input samples are available and the network classifies the input patterns into different groups.

III.3.4. Backpropagation algorithm

The Feedforward backpropagation (FFBP) is considered as the most utilized forward neural network which is based on a mechanism updating the weights using gradient descent, It was first described by Rummelhart and McClelland (1986) [120], FFBP has a structure in which neurons are organized in successive layers. The first layer is referred to as the input layer, the last layer as the output layer, and all intermediate layers as the hidden layer. The backpropagation technique is a process of iteration in order to modify the weights from the output layer to input layer until no further correction is required (see Figure III-9). A simple hidden backpropagation neural network layer can generally approximate any nonlinear function with arbitrary precision [121, 122]. This

feature makes FFBP popular for predicting complex nonlinear systems [123, 124]. This type of ANN has evolved for a diverse range of engineering applications. It has been used and recommended to solve some of the difficult problems in various fields, including structural engineering. Various functions that can be used as activation or transfer functions such as hyperbolic tangent, sigmoid and linear functions. The type of activation function contributes significantly, and has a key role to introducing the nonlinearity so that it can deal even with complex phenomena. A systematic theory to determine the number of input nodes and hidden layer nodes is unavailable [122]. The most common means to determine the appropriate number of inputs and hidden layer is via experiments or by trial and error based on the performance assessment criteria.

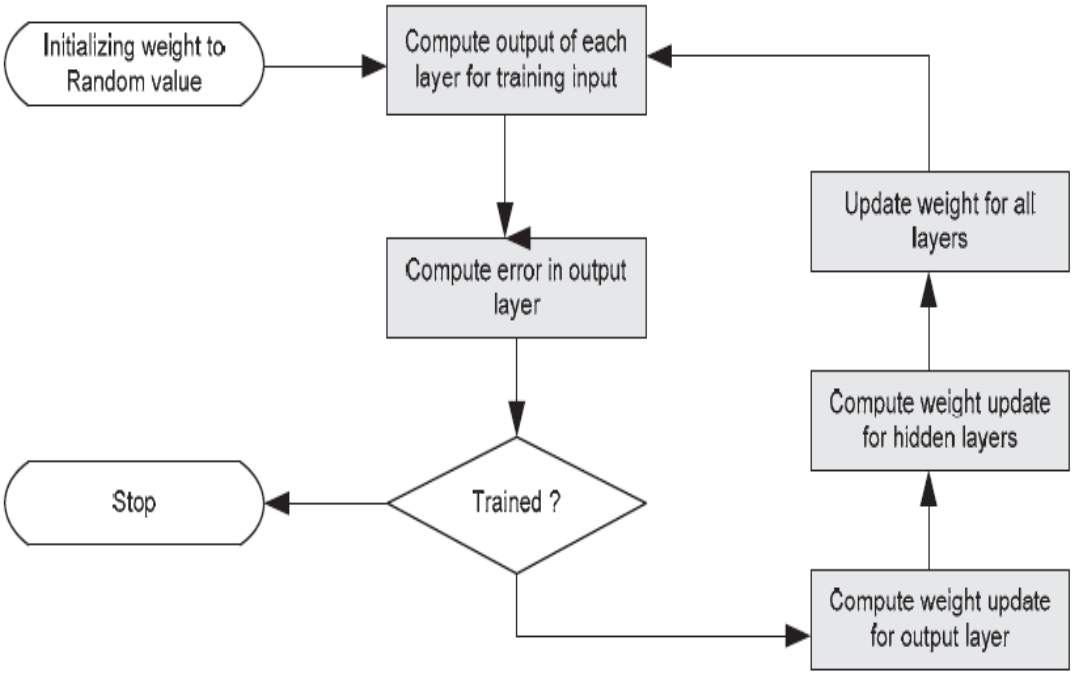

Figure III-9 Back-propagation training algorithm

III.3.5. Data Normalization

An optimal efficiency of the ANN requests a prior data conditioning, i.e. all the data are normalized [85, 86, 125]. The data set used in the present dissertation , including inputs and target outputs are scaled as follows::

$$\mathbf{P_n} = 2\frac{(\mathbf{P} - \mathbf{I}.\mathbf{P_{min}})}{(\mathbf{P_{max}} - \mathbf{P_{min}})} - 1$$
$$\mathbf{T_n} = 2\frac{(\mathbf{T} - \mathbf{I}.\mathbf{T_{min}})}{(\mathbf{T_{max}} - \mathbf{T_{min}})} - 1 \quad (6)$$

Where: P, P_n are respectively matrix and scaled matrix of input vectors; T, T_n are respectively matrix and scaled matrix of output vectors; P_{min}, P_{max} are respectively minimal and maximal component value of each input vectors; T_{min}, T_{max} are respectively minimal and maximal values of each output vectors; ***I*** is the vector unity.

The developed neural network models are trained using the data derived from the scaling process, whereas the target output becomes:

$$\mathbf{T} = 0.5\,.\,(\mathbf{T_n} + 1).\,(\mathbf{T_{max}} + \mathbf{T_{min}}) + \mathbf{T_{min}} \quad (7)$$

III.4. Conclusion:

The strong motion database, collected for this study, includes 1,104 records from 10 events ranging in magnitude from M= 4.8 to 7.3, occurred in Japan during the period 2000-2016. A complete list of the strong motion records selected for use in this study is included in Appendix. The adequate selection of samples or data may considerably increase the efficiency of prediction model.

The artificial neural network (ANN) technique is used as an alternative to regression methods. The ANN with Back-Propagation (BP) learning algorithm is strongly recommended for highly nonlinear modeling problems. A theoretical framework for the artificial neural network is presented in this chapter.

Chapter IV. PREDICTION OF INTENSITY MEASURES

IV.1. Introduction

The characterization of ground motion is a fundamental step in seismic analyses of structures subjected to earthquake ground motion. The effects of seismological parameters on seismic action are not explicitly incorporated in current design practice. The prediction of the intensity measures of the ground motion for a given earthquake parameter is an essential step in hazard and risk seismic analysis. Three parameters are considered PGA, SD, and Tm. Each of these measures characterize a feature of ground motion, namely, amplitude, cumulative effect, and frequency content. The independent seismological parameters used in this study are the magnitude (M_{jma}), the epicentral distance (R_{epi}), the shear-wave velocity (V_{s30}), the resonant frequency (f_{800}), the focal depth (d), and the angle epicenter-station (θ). The ANN with Back-Propagation (BP) learning algorithm is used as an alternative to regression methods, which is strongly recommended for highly nonlinear modeling problems.

IV.2. Directionality effect:

In earthquake engineering, there is still a need to consider the directionality of ground motion effects. Various empirical relationships have been suggested in the literature to estimate the intensity measures of the ground motion; few researchers have addressed the directionality aspect of ground motion.

The component of ground motion corresponding to an azimuth given by an increment of rotation angle is determined as a function of two ground motion components (EW and NS) as follow: [46, 126, 127]:

$$a_{rot}(t,\theta) = a_1(t)\cos(\theta) - a_2(t)\sin(\theta) \quad (8)$$

θ: rotational angle

a_1, a_2: horizontal component acceleration *E-W* et *N-S*

a_{rot}: horizontal component corresponding to a rotational angle θ

t: time.

According to Eqn.(8), The two ground motion components (EW and NS) are combined into a single component corresponding to an increment of rotation angle. For each set of two as-recorded

orthogonal-component time series, the ratio between the maximum value and the recorded value of the PGA in the EW and NS is determined. The procedure steps are described as follows [128]:

- In the orientation set to 0 degree, calculate the target characteristics of ground motion such as PGA value
- Rotate the horizontal component by an increment of 1 degree and calculate the characteristics
- Repeat the steps a and b for θ range between 0 to 180 degree
- Calculate the target intensity measure (PGA value) for all the rotation angles.
- Sort the maximum for each of the target intensity measures (PGA value).

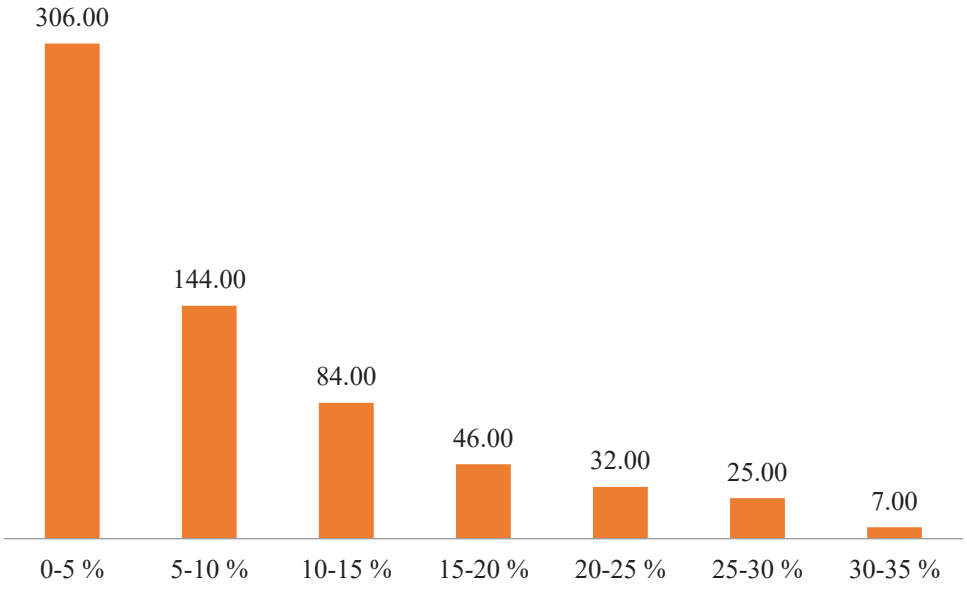

Figure IV-1 PGA variation according to critic direction

As presented in Figure IV-1, the results show the effect of directionality on the PGA values. The ratio of the maximum to the minimum may reach up to 1.35 (increase of 35%). In an attempt to consider this effect, new input parameters "angle epicenter-station" that characterize the direction source-to-site is introduced an earthquake parameter.

The angle epicenter-station parameters is defined as the angle between the orientation of the epicenter-station path and the direction of the component (see II.4.2 section). This parameter is used among other inputs in the ANN model to predict the peak acceleration of the strong ground motion.

IV.3. Peak ground acceleration

Peak ground acceleration (PGA) is one of the key measures employed to assess the importance of seismic action and is still often used as a parameter to describe strong ground motion and to scale earthquake design spectra. The question that then arises is how to estimate the PGA at a site where no recording station is installed. The prediction of the PGA in terms of seismological parameters is developed in this section. As presented in chapter 3 the ground motion database was obtained from the KiK-Net nationwide strong motion networks, the records used to develop the prediction model have been carefully selected from the database depending on the type of the parameter (i.e. IM or EDP). The distributions of ground motion records versus earthquake magnitude and PGA in Figure IV-2.

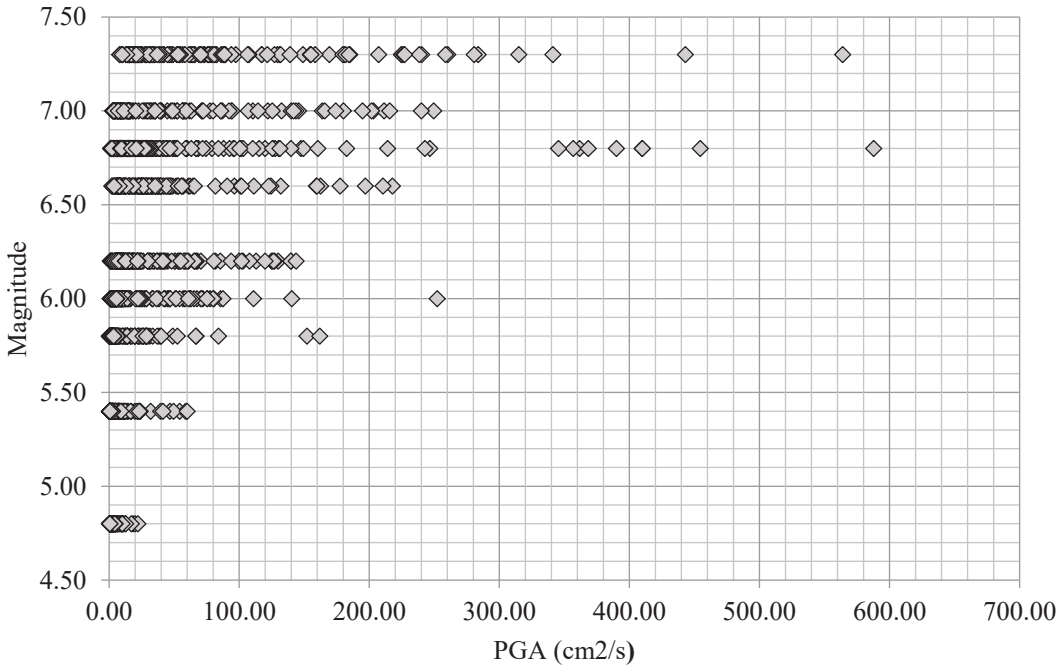

Figure IV-2 Magnitude versus PGA distribution

IV.3.1. Artificial Neural Network Model

The selection of the optimal architecture of an ANN is not an easy task as it is necessary to test a large number of architectures to achieve the best one. The results show that the configuration with a **hyperbolic tangent function for the hidden layer and for the output layer** gives the best results. (see Table IV-1, Table IV-2)

According to the above provisions, inputs to the network are defined here by the values of magnitude (M_{jma}), epicentral distance (Repi), shear-wave velocity (V_{s30}), resonant frequency (f_{800}), the focal depth (d) and the angle epicenter-station (θ). The output node is represented by peak ground

acceleration PGA (Figure IV-3). A standardization of all data was performed to improve the performance of the model.

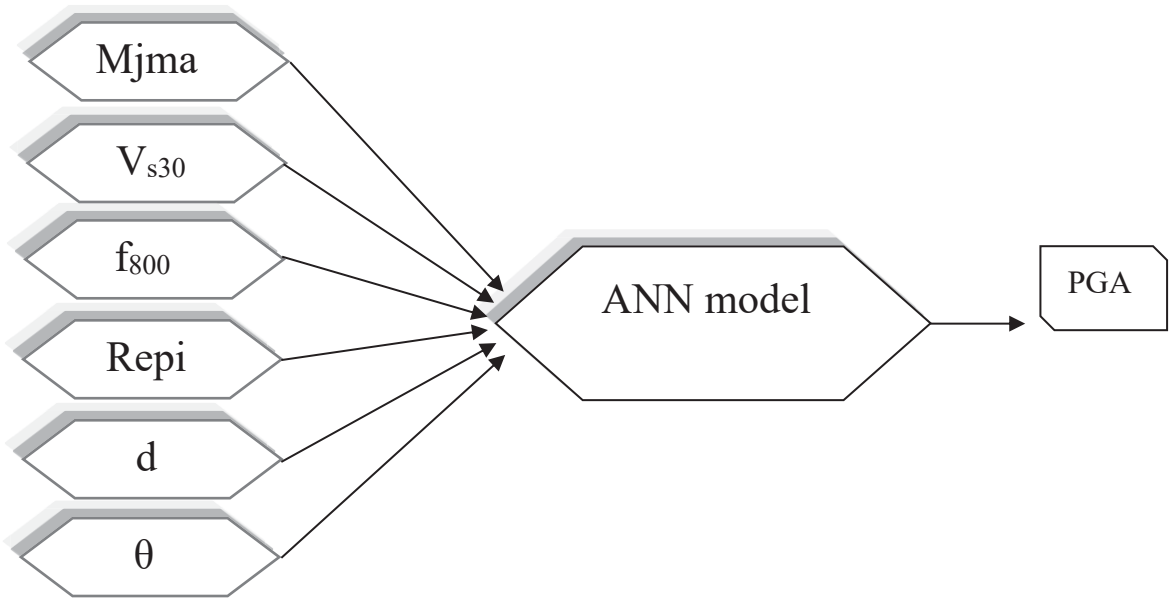

Figure IV-3 Input /Output of PGA models developed

A total of 1104 values have been divided into three sets:

The training set, which is about 70% of the complete database, has been used to train the network; the validation set, which is about 15%, has been used for the purpose of monitoring the training process, and to guard against overtraining; and the testing set, which is about 15%, has been used to judge the performance of the trained network. The training was stopped when the cross-validation error began to increase, i.e., when the cross-validation error reached a minimum, the training should be stopped.

In this dissertation, a large number of architectures were tested using various parameters in order to obtain the best ANN model.

The performance of the developed neural network models is carried out by comparing the target PGA and those predicted by the ANN model. Figure IV-4 shows the regression curves for all data (1104 samples) which reveal a coefficient of correlation R equal to 0.86.

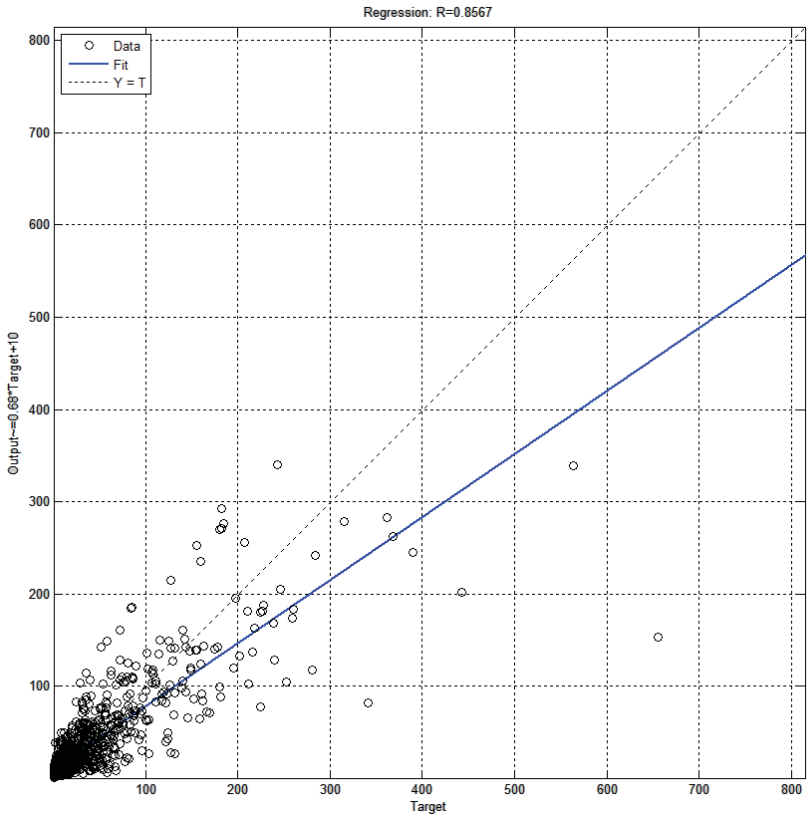

Figure IV-4 Linear regression between the target and predicted PGA

Because the predictive model depends on multiple variables (inputs), the plots of residuals against the main variables are used here to evaluate the accuracy of the model and the correlation of the variables with the predicted values. In Figure IV-5 the residuals, expressed by:

$$e_i = \log_{10}\left(\frac{obsPGA_i}{prePGA_i}\right) \quad (4)$$

Where:

obsPGA$_i$ and prePGA$_i$ are the recoded and predicted PGA

The residuals plots are plotted against the epicentral distance, the magnitude and the focal depth (see Figure IV-5) the plots are pretty symmetrically distributed, tending to cluster towards the middle of the plots showing no bias or trend in the residuals in any of these plots.

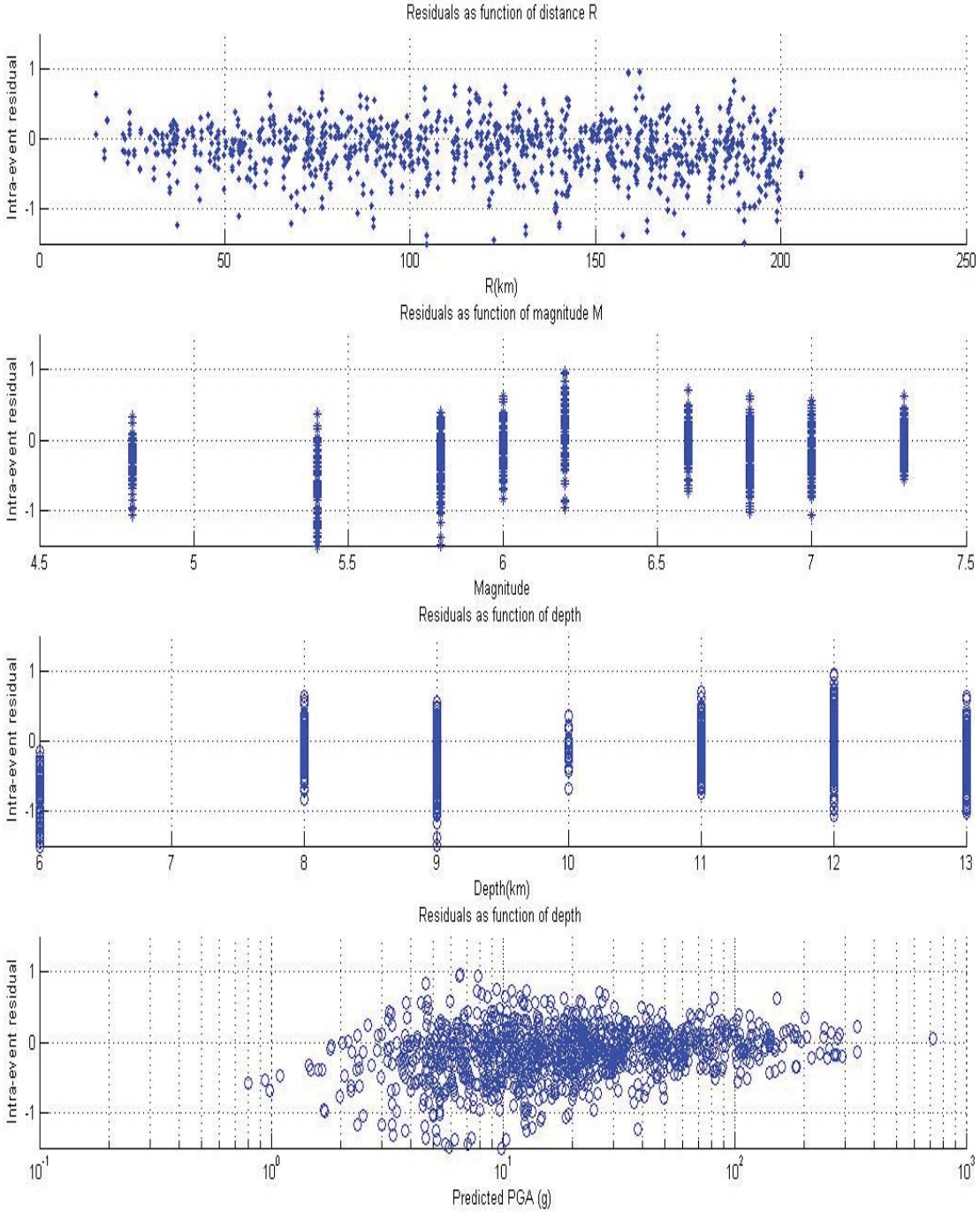

Figure IV-5 Intra-Event Residuals of PGA as function of distance Repi and magnitude and Depth

IV.3.2. Results and discussions

IV.3.2.1. Neural network topology optimization

As it was described before, to determine the optimal architecture of an ANN it was necessary to test a large number of neural topologies. Table IV-1 shows the activation function used for layers and lists for each configuration the correlation coefficient for each subset: training, validation and test (R_{train}, R_{valid} and R_{test}).The obtained results in this study are presented in Table IV-2.

The accuracy of the prediction is evaluated by comparing the performance criteria; Table IV-1 shows the performance of the four ANN architectures, along with their respective prediction accuracy. On one hand it is observed that the best value of correlation coefficient (R) with small value of Mean Square Error (MSE) is associated with the combinations (tanh-sigmoid – tanh-sigmoid) as a function activation, on the other hand it has been found that the neuron number considered of the hidden layer have approximately same prediction accuracy which mean that the number of neurons used in the hidden layer has no influence on the performance of this particular models. This table lists the MSE and R for different tests using different combinations. Following various tests on the different combinations and architectures used, it can be concluded that the PGA predicted by the ANN with six inputs using the combination of activation function (tanh-sigmoid – tanh-sigmoid) with ten neurons has been found to be more accurate.

Table IV-1 Test of different combination of activation function

		PGA			
Layer 01	Layer 02	R_{train}	R_{valid}	R_{test}	MSE
log-sigmoid	log-sigmoid	<0.1	<0.1	<0.1	>0.5
log-sigmoid	linear	0.89	0.88	0.88	0.01
Tanh-sigmoid	linear	0.9	0.88	0.85	0.01
Tanh-sigmoid	Tanh-sigmoid	0.88	0.84	0.84	0.004

Table IV-2 Influence of number of neuron activation function (tanh-sigmoid – tanh-sigmoid)

		PGA			
Neuron	Rtrain	Rvalid	Rtest	RAll	MSE
5	0.92	0.82	0.83	0.89	0.005
10	0.88	0.84	0.84	0.86	0.004
15	0.9	0.87	0.89	0.89	0.01
20	0.92	0.86	0.9	0.9	0.008

IV.3.2.2. Effect of magnitude, epicentral distance and soil velocity on the peak ground acceleration

The PGA is plotted against epicentral distance on Figure IV-6. It can be noticed that the trend of the variation of the PGA is more sensitive to the magnitude and is almost decreasing with distance.

As illustrated in Figure IV-6, comparisons are made between the predicted PGA in three types of site: A site characterized by a shear-wave velocity V_{S30}= 200m/s (f_{800}=1.67Hz soft soil) and the other one characterized by a shear-wave velocity V_{S30}= 800m/s (f_{800}= 6.68 Hz Rock site). This figure shows clearly for both cases that the PGA decreases with the distance. It can be noted that the soft soil (V_{s30}=200m/s; f_{800}=1.67 Hz) produces more than 50 % greater PGA value than those on the rock site.

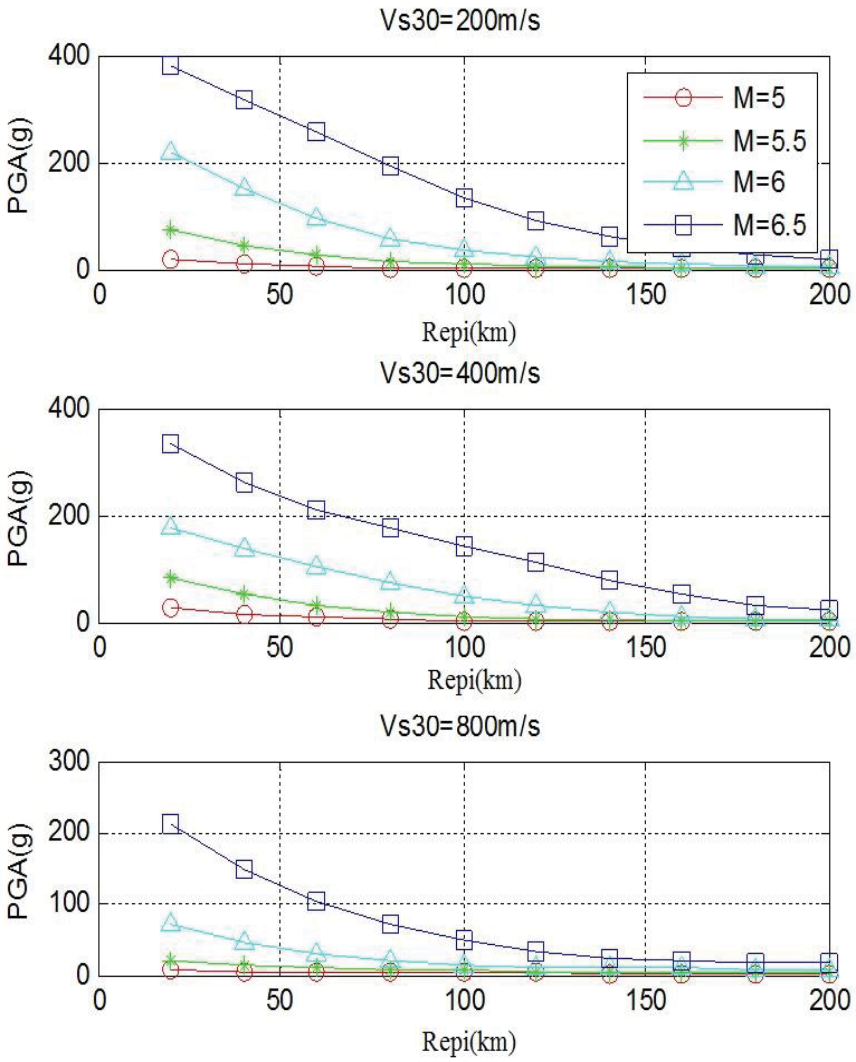

Figure IV-6 Predicted PGA for Vs30 of 200m/s and 400m/s, 800m/s and Mw 5-5.5-6-6.5

IV.3.3. Comparison with existing models

The model proposed in this study is compared with four existing PGA attenuation relationships: Zhao and al. (2006), Cotton and al. (2008), Kanno and al (2006) and Derras and al (2010) [18, 124, 129, 130]. The common characteristic of these four existing models is the source of the database used (K-Net and KiK-Net).

Figure IV-7 compares the predicted value of PGA, for magnitude earthquakes M=6 for site class (V_{s30} = 600 m/s and f_{800}=5hz), and those provided by four empirical relationships.

For the sites characterized by epicentral distance (R) lesser than 15 km, the proposed model predicts PGA value which is 20% smaller than those from the empirical models.

Conversely, for distance range between 15 and 200 km, the proposed ANN provides values falling between the empirical attenuation relationships predictions. This distance range represents the validity limits of the developed model.

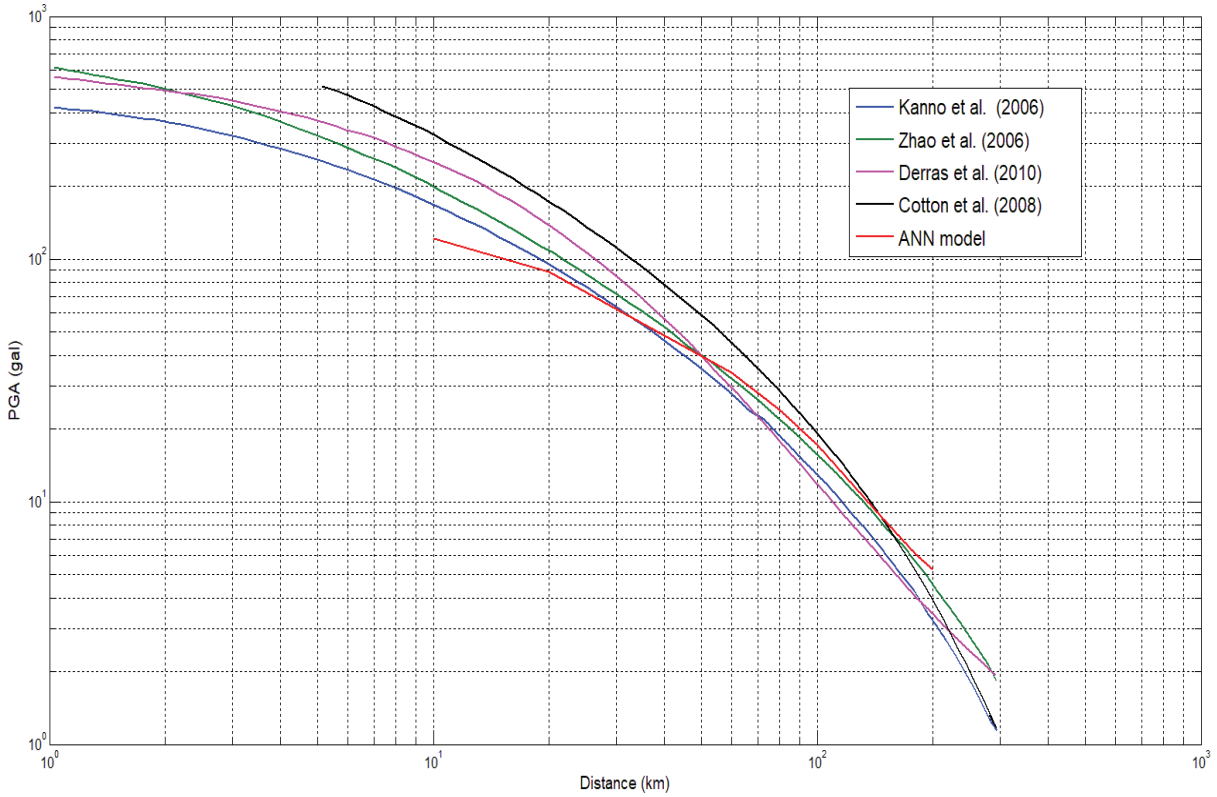

Figure IV-7 Comparison of proposed PGA model with existing relationships Mja= 6; Vs30=600 m/s; principal direction.

IV.3.4. Sensitivity Analysis

A sensitivity analysis for the input variables was performed in order to quantify the influence of each of the earthquake parameters on the IMs and EDPs considered. In this dissertation, percentages of synaptic weight, P_i, that correspond to each of the six parameters were computed using the following equation [131]:

$$P_i = \frac{\sum_{j=1}^{Nh} |w_{ij}^h|}{\sum_{i=1}^{N} \sum_{j=1}^{Nh} |w_{ij}^h|} \quad (9)$$

Where: w_{ij}: synaptic weights of the ANN;

For PGA neural model $1 \leq i \leq 6$ *and* $1 \leq j \leq 10$

Nh: number of hidden neurons Nh=10; N: number of input variables N=6

This analysis was conducted for the models developed and the overall results are summarized in Figure IV-8. As can be seen on this figure, the inputs parameters have almost the same effects on the PGA except that the soil frequency parameter f_{800} which has less influence.

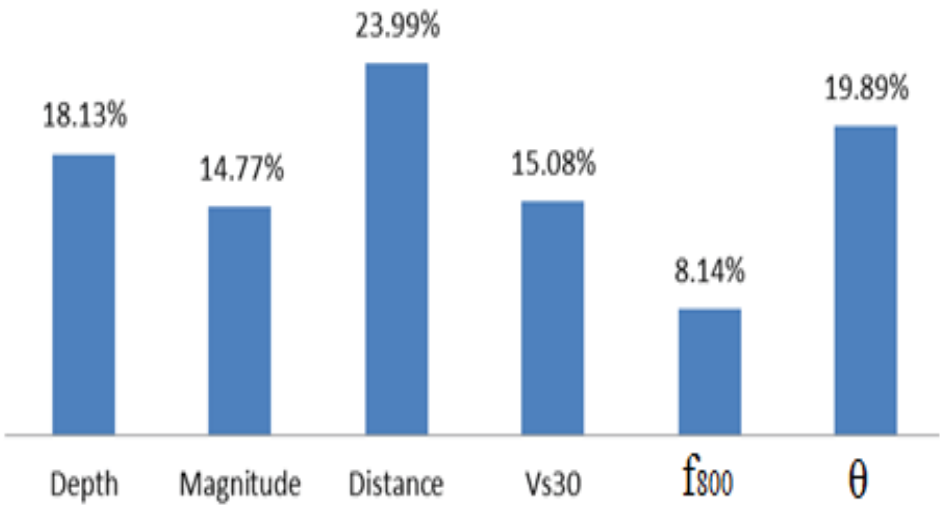

Figure IV-8 . Input sensitivity analysis for PGA

IV.4. Significant duration.

The second IM parameter considered in this dissertation is the duration of the strong ground motion. In the present study, the adopted definition of the significant duration is the one given by Trifunac and Brady (1975) which is detailed in the chapter II.

In recent years, there has been growing interest in the influence of the duration of ground motion on the behaviour of structures [132, 133]. Therefore, significant correlations were revealed between significant duration and potential damage of the earthquake [134-136].

In the present section, the artificial neural network (ANN) is considered as an alternative option to multiple regression analysis, The objective is to predict the significant duration (fractiles 5%, 75% and 95%: SD595 and SD575) of the ground motions records. It investigates also the influence of seismological parameters.

The earthquake ground motions were thoroughly selected from the KiK-Net database prepared as a part of this dissertation. The records distribution versus magnitude and Significant Duration (SD595) are presented in Figure IV-9. The adequate selection of samples or data may significantly improve the performance of the trained neural network training.

IV.4.1. Artificial neural network model

As mentioned before, the most common means to determine the appropriate number of inputs and hidden layers is via experiments or by trial and error based on the performance assessment criteria. For achieving the best ANN model, several architectures are tested. The results summarized in Table IV-3 and Table IV-4, As illustrated in the tables that the configuration that presents optimal result is based on hyperbolic tangent sigmoid as an activation function for the hidden layer. Therefore, as shown in Figure IV-10, the inputs to the network are presented by the magnitude (M_{ja}), epicentral distance (R), shear wave velocity (V_{s30}), resonant frequency (f_{800}), the focal depth (D) and the angle epicenter-station (θ). Two neural-network models are proposed to predict the significant duration: SD575 and SD595. Both models are developed with **six inputs and one output** (SD575 or SD595). To strengthen the model performance, a prior standardization of all data (Input/Output) is performed.

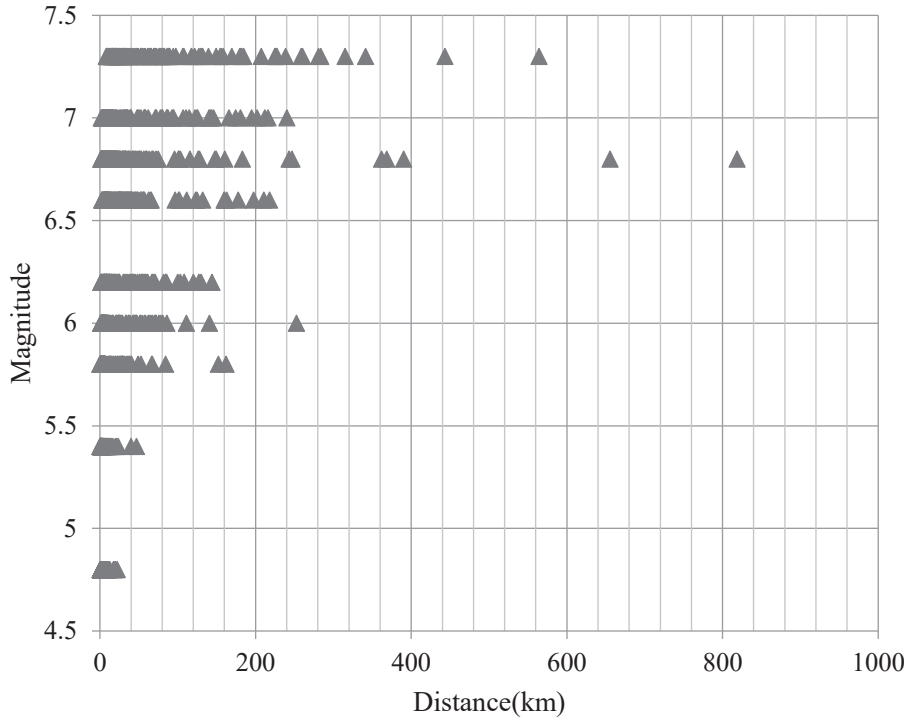

Figure IV-9 Magnitude versus Distance.

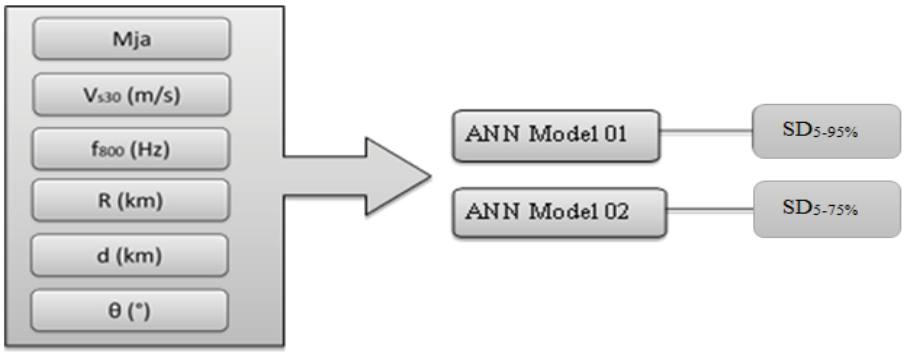

Figure IV-10 Input /Output of models developed

The training process is stopped once the cross-validation reaches its minimum. The performance of the developed ANN is carried out by comparing the target significant durations and those predicted by the models. Figure IV-11 and Figure IV-12 shows the regression curves for all data (1,104 samples) which reveal a correlation coefficient R equal to 0.95 for SD595 and 0.98 for SD575.

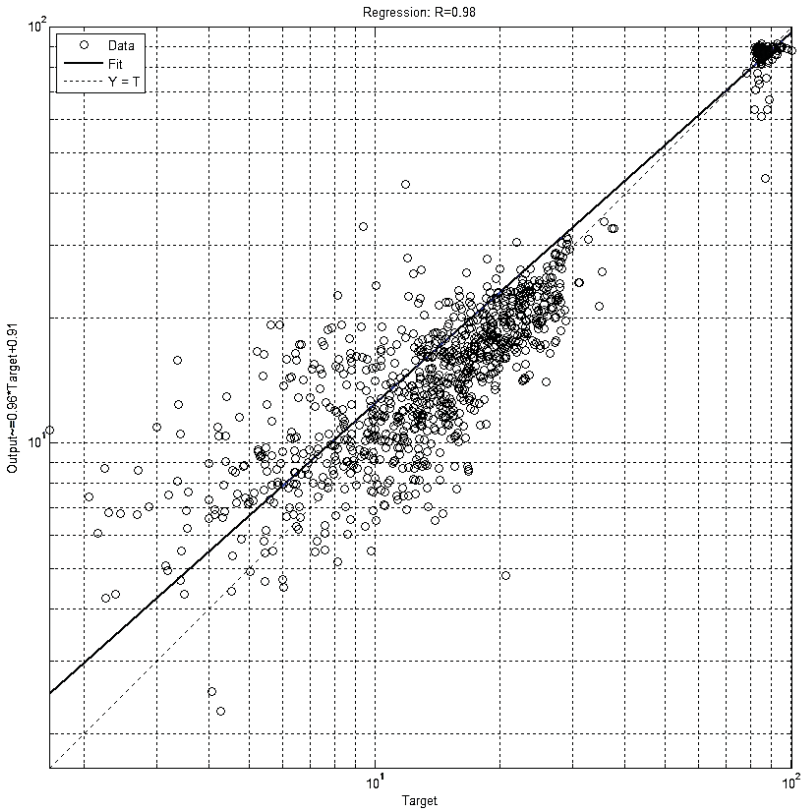

Figure IV-11 Linear regression between the target and predicted SD. SD575 Model

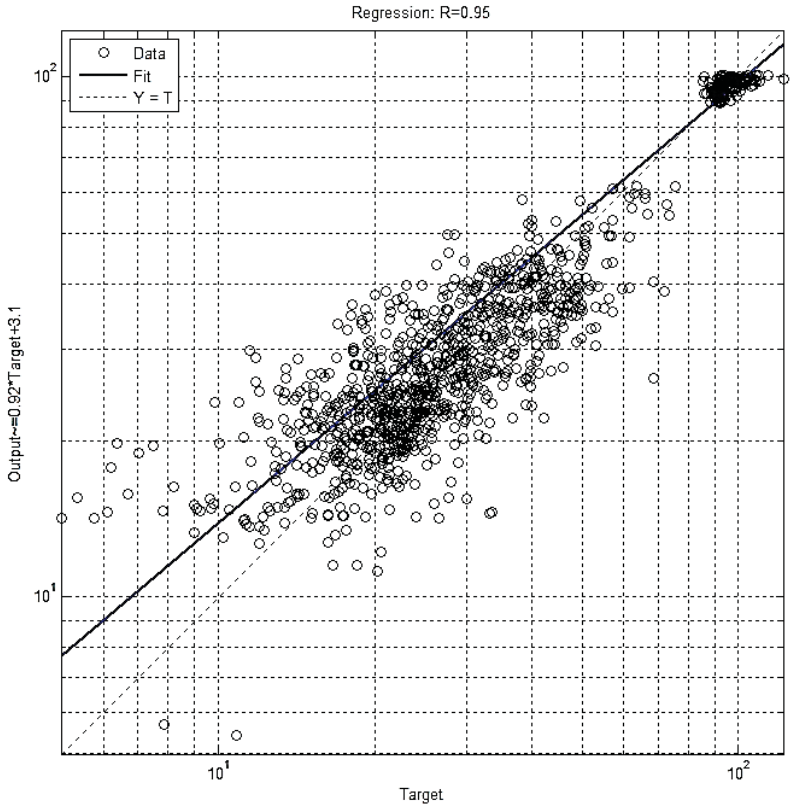

Figure IV-12 Linear regression between the target and predicted SD. SD595 Model

Since the predictive model depends on multiple variables (inputs), the plots of residuals against the main variables are drawn in Figure IV-13 and Figure IV-14 to evaluate the accuracy of the model and the correlation of the variables with the predicted values., the residuals are expressed by:

$$e_i = \log_{10}\left(\frac{obsSD_i}{preSD_i}\right) \quad (10)$$

Where: obsSDi and preSDi are the observed (recorded) and predicted significant durations. The residuals are plotted against the epicentral distance, the magnitude and the focal depth. For both predictions SD575 and SD595, the plots are pretty symmetrically distributed, tending to cluster towards the middle of the plots showing no bias or trend in the residuals in any of these plots.

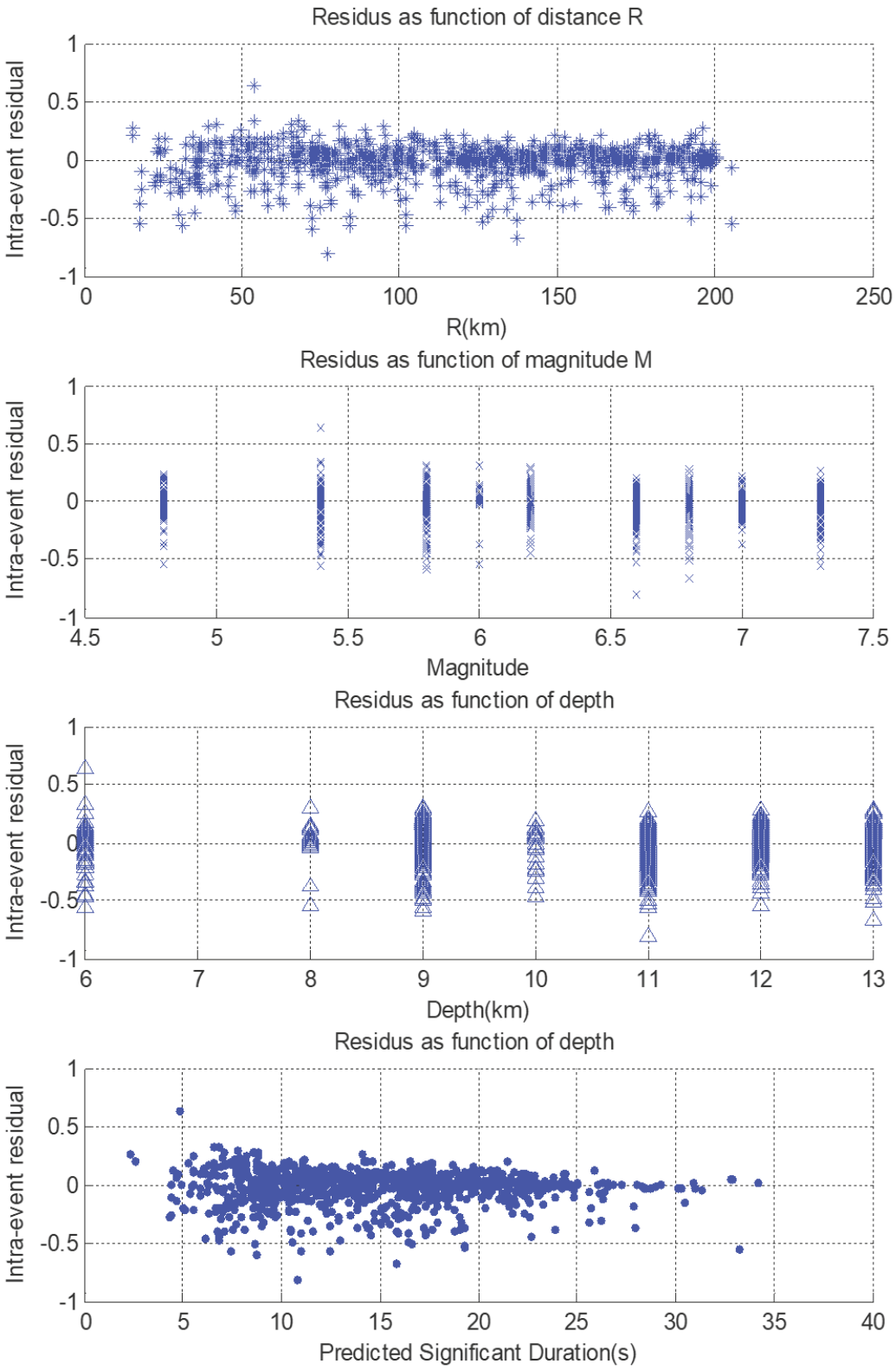

Figure IV-13 Intra-event residuals as function of distance R, magnitude and Depth. SD575 Model

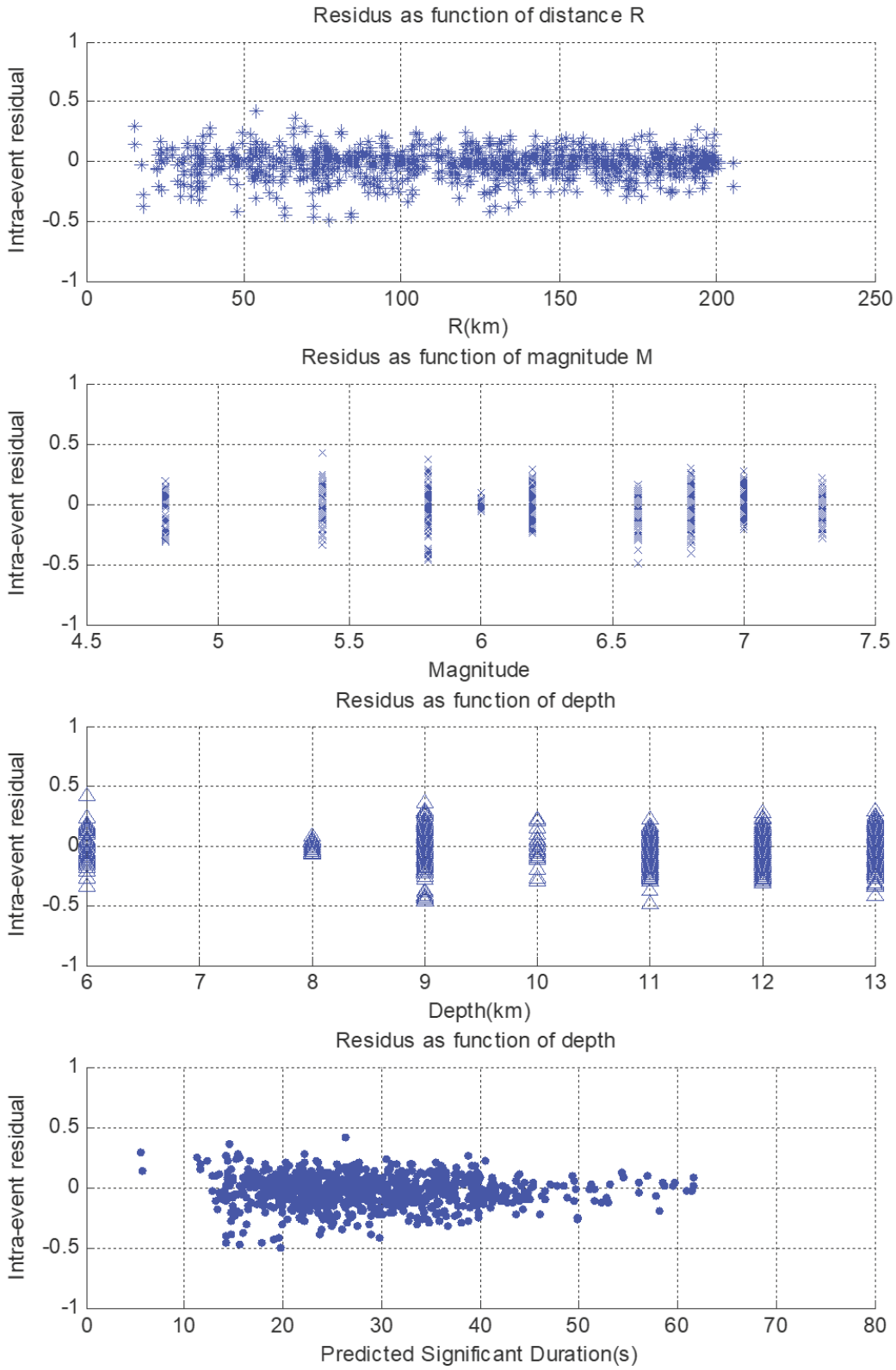

Figure IV-14 Intra-event residuals as function of distance R, magnitude and Depth. SD595 Model

IV.4.2. Results and discussions

IV.4.2.1. Neural network topology optimization

In order to define the optimal architecture of a neural model, it is necessary to test various neural typologies. The results are presented in Table IV-3 and Table IV-4, which list the Mean Square Error (MSE) and correlation coefficient (R) for different tests using different combinations. Following various tests on the different combination and architecture. The findings indicate that the significant duration measures (SD595 and SD575) predicted by the proposed models with six inputs using the combination of tangent hyperbolic function (tanh-sigmoid) as an activation function for both the hidden layer and output layer, with ten neurons, appears to be the most accurate.

Table IV-3 Test of different combination of activation function

		SD595				SD575			
Layer 01	Layer 02	R_{train}	R_{valid}	R_{test}	MSE	R_{train}	R_{valid}	R_{test}	MSE
log-sigmoid	log-sigmoid	<0.1	<0.1	<0.1	>0.5	<0.1	<0.1	<0.1	>0.5
log-sigmoid	linear	0.95	0.95	0.95	0.017	0.98	0.98	0.97	0.01
Tanh-sigmoid	linear	0.96	0.93	0.91	0.019	0.98	0.98	0.97	0.007
Tanh-sigmoid	Tanh-sigmoid	0.96	0.95	0.94	0.018	0.98	0.98	0.98	0.007

Table IV-4 Influence of number of neuron activation function (tanh-sigmoid – tanh-sigmoid)

	SD595					SD575				
Neuron	R_{train}	R_{valid}	R_{test}	R_{All}	MSE	R_{train}	R_{valid}	R_{test}	R_{All}	MSE
5	0.93	0.93	0.94	0.94	0.024	0.98	0.97	0.98	0.97	0.007
10	0.96	0.95	0.94	0.95	0.018	0.98	0.98	0.98	0.98	0.007
15	0.96	0.94	0.92	0.95	0.02	0.99	0.95	0.97	0.97	0.011
20	0.97	0.94	0.85	0.96	0.017	0.99	0.93	0.97	0.97	0.016

IV.4.2.2. Effect of magnitude, epicentral distance and soil velocity on the significant duration

The significant durations SD595 and SD575 are plotted against epicentral distance, see Figure IV-15 and Figure IV-16. It can be noticed that the variation trend of the SD575 is less sensitive to the magnitude and is almost linearly increasing with distance. However, the SD595 is more sensitive to magnitude in far field, which means that the weakest part of the motion tends to last longer with higher magnitudes and longer distances. It is also noticed that soft soil tends to expand more the SD595, according with distance for low amplitudes.

Figure IV-17 and Figure IV-18 shows the variation of the significant duration with respect to distance from the source, for soft and rock soil types, at three levels of magnitude M=5, 5.5 and 6.

The soft soil is characterized by a shear wave velocity V_{S30} = 200m/s (f_{800}=1.67 Hz), the rock soil (reference site) has a shear wave velocity V_{S30} = 800m/s (f_{800}= 6.68 Hz). It is clearly shown that, in both cases, the significant duration increases with the distance and the site effect is more important on SD595 duration compared to SD575. The soft soil produces more than 60% elongation of the significant duration, in the case of rock site at low magnitudes. Figure IV-17 compares the trend in the variation of the two significant duration measures SD575 and SD595 with respect to the distance from the source. It shows that the significant duration D575 has better stability than the D595, especially for greater amplitudes.

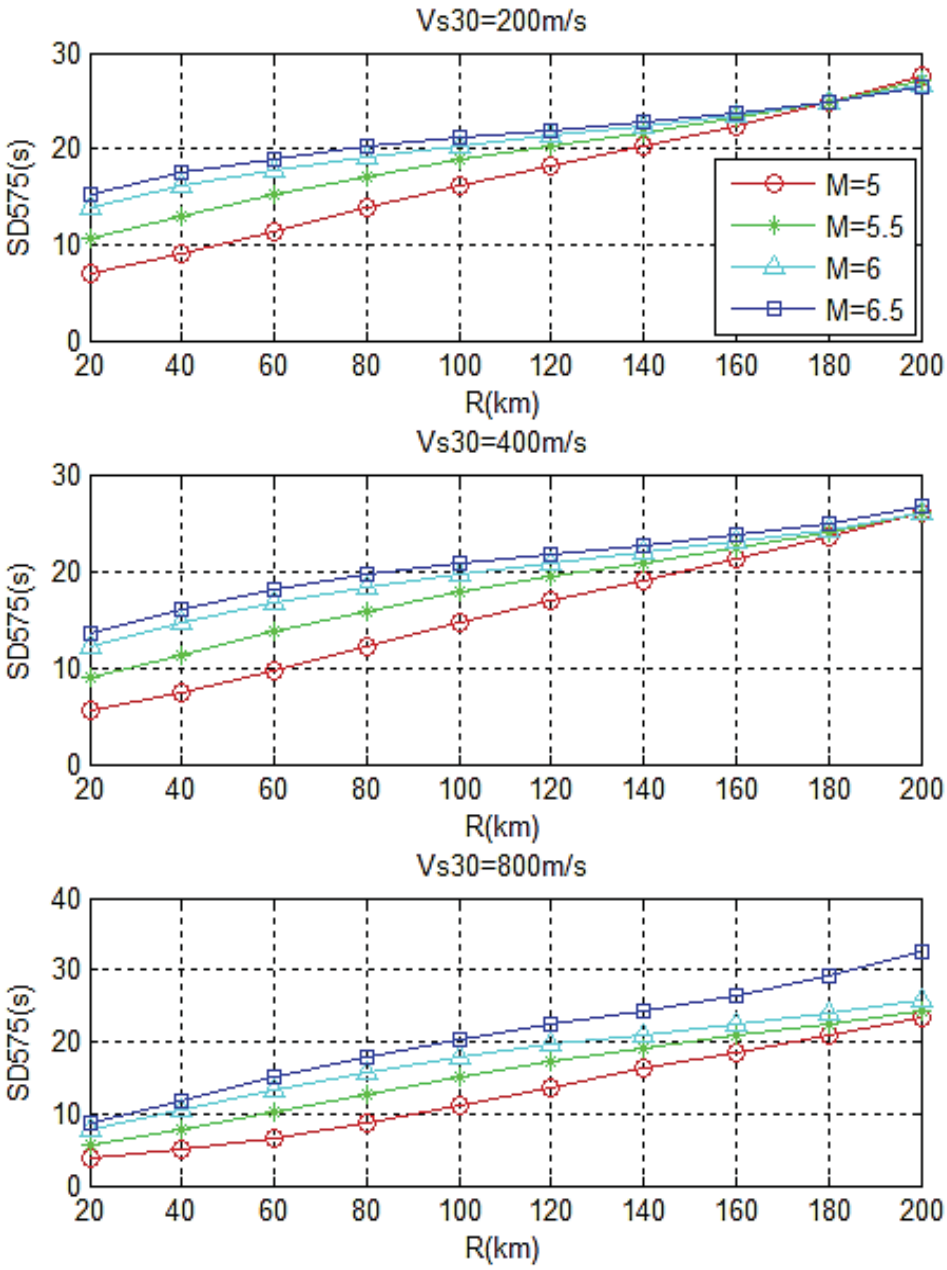

Figure IV-15 Predicted significant duration for Vs30 in {200m/s, and 400m/s, 800m/s}wc and Mw in {5, 5.5, 6, 6.5}. SD575 Model

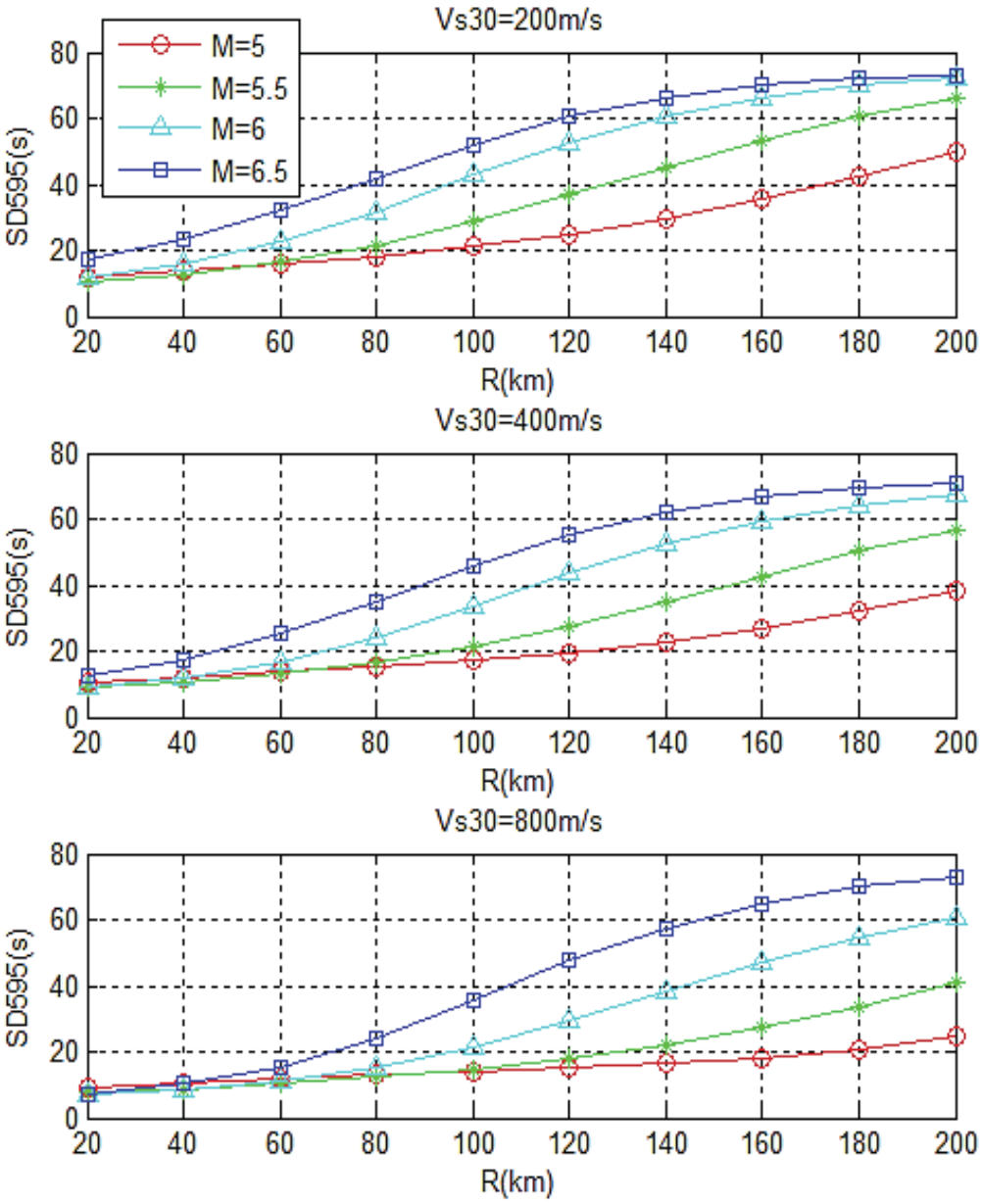

Figure IV-16 Predicted significant duration for Vs30 in {200m/s, and 400m/s, 800m/s} and Mw in {5, 5.5, 6, 6.5}. SD595 Model

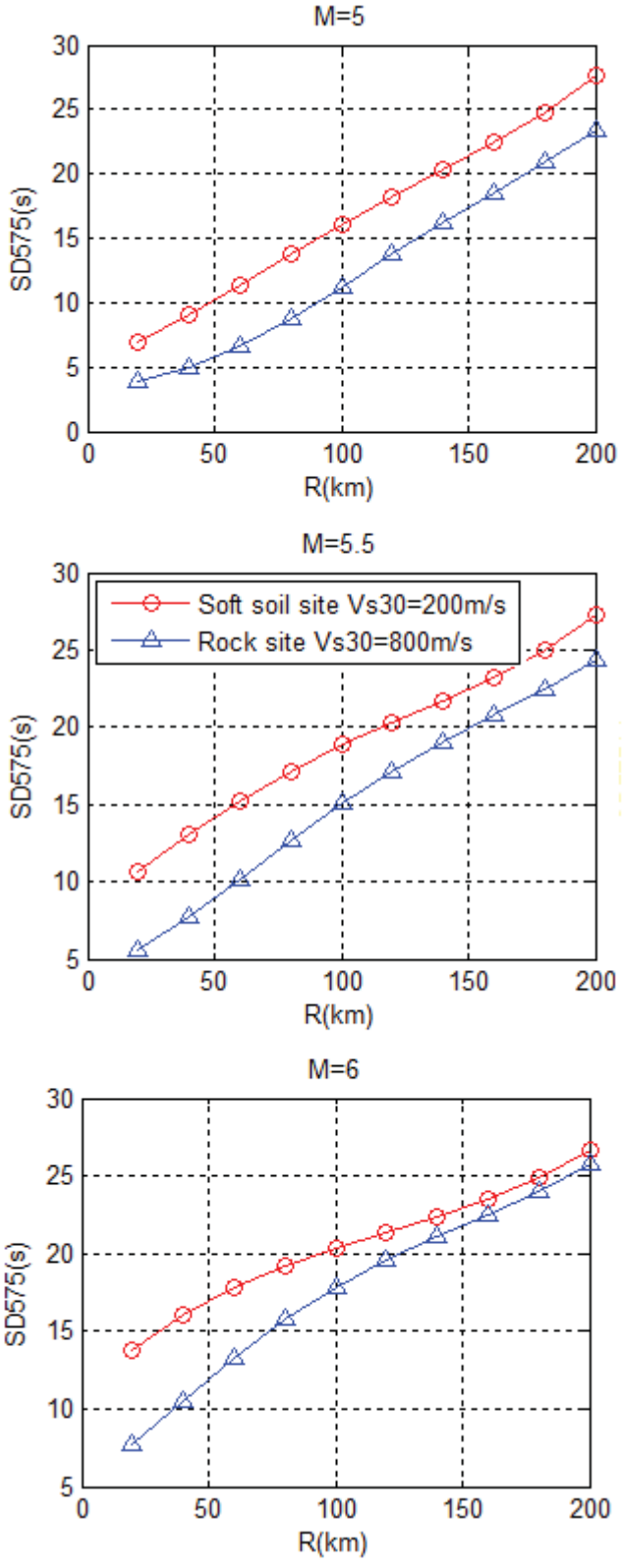

Figure IV-17 Effects of distance and site class on predicted models for M in {5, 5.5, 6}.SD575 Model

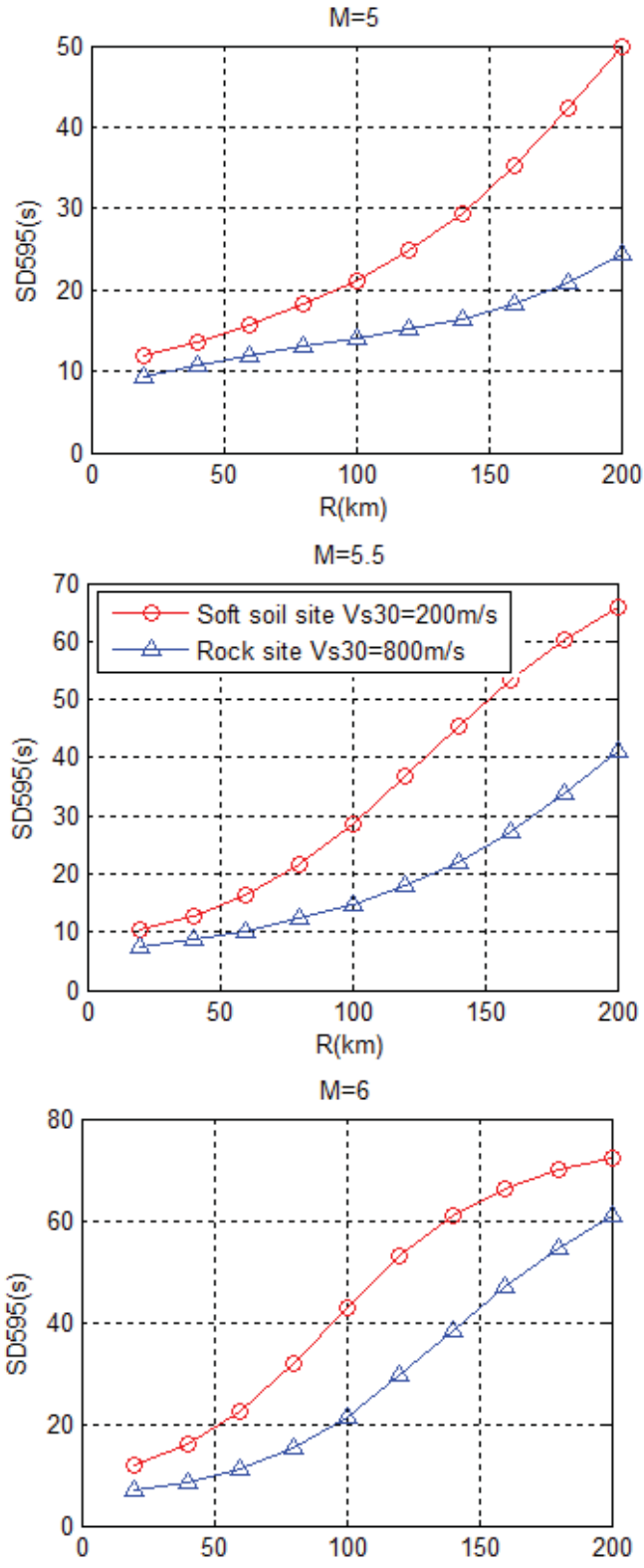

Figure IV-18 Effects of distance and site class on predicted models for M in {5, 5.5, 6}.SD595 Model

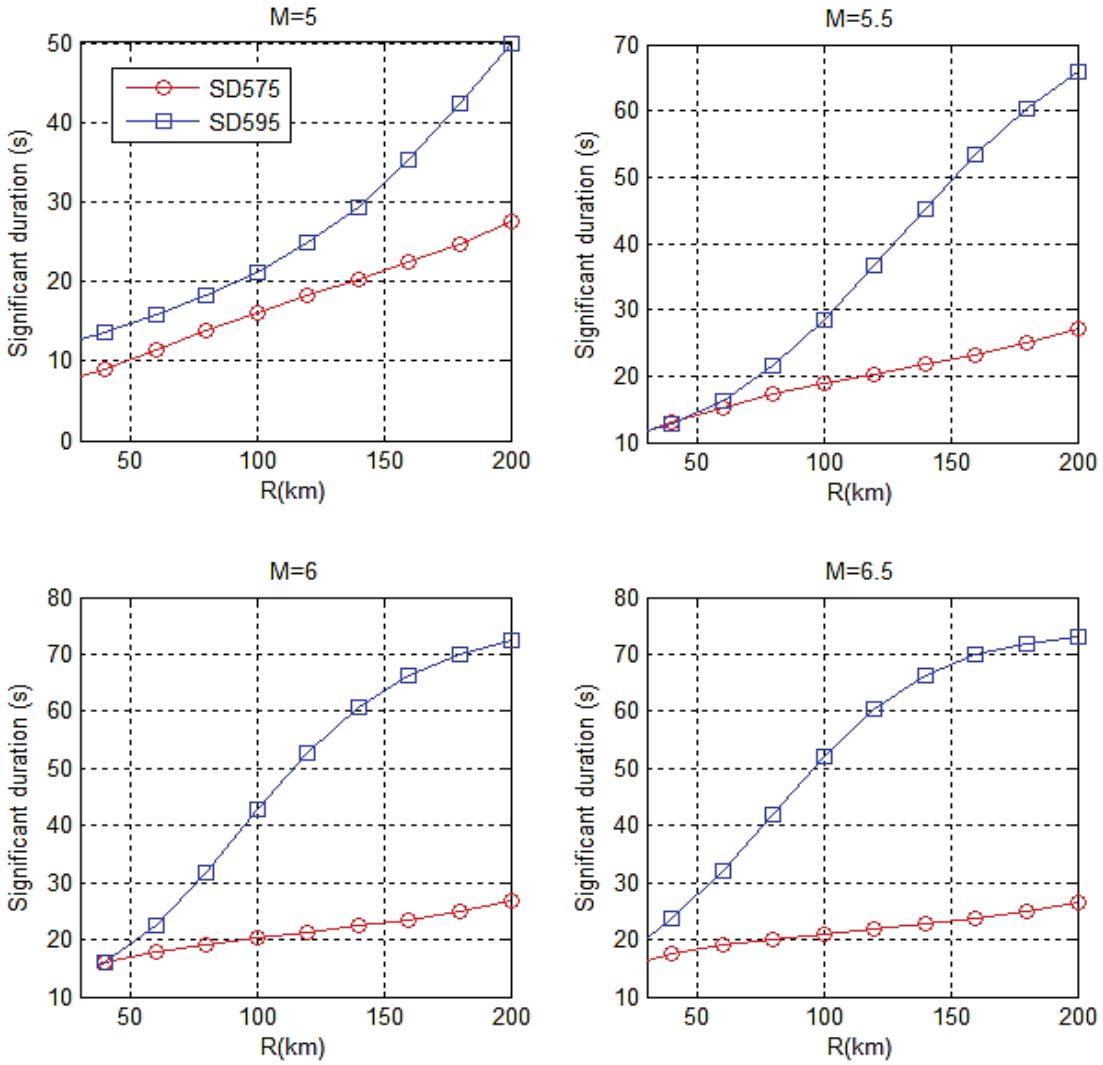

Figure IV-19 Comparison of proposed Model Prediction SD575 and SD595 for Vs = 200m/s.

IV.4.1. Comparison with existing models

The model proposed in this study is compared with two existing significant duration relationships: Abrahamson and Silva (1996) and Afshari and Stewart (2016). Figure IV-20 compares the predicted value of both significant duration definitions (SD595 and SD575), for magnitude earthquakes equal to 5.5 for site class D (V_{s30} = 200 m/s), and those provided by three empirical relationships: the one proposed in this study and those proposed by Abrahamson and Silva (1996) and Afshari and Stewart (2016). These two laters (empirical attenuation relationships) use an additive site effect term (rock or soil parameter for Abrahamson and V_{s30} for Afshari and Stewart 2016). [3, 49]

For the sites characterized by epicentral distance (R) greater than 100 km, the proposed model predicts significant duration value which is 30% greater than those from the two empirical relationships. Conversely, for distance range between 0.0 and 100 km, the proposed ANN provides values falling between the two empirical attenuation relationships predictions.

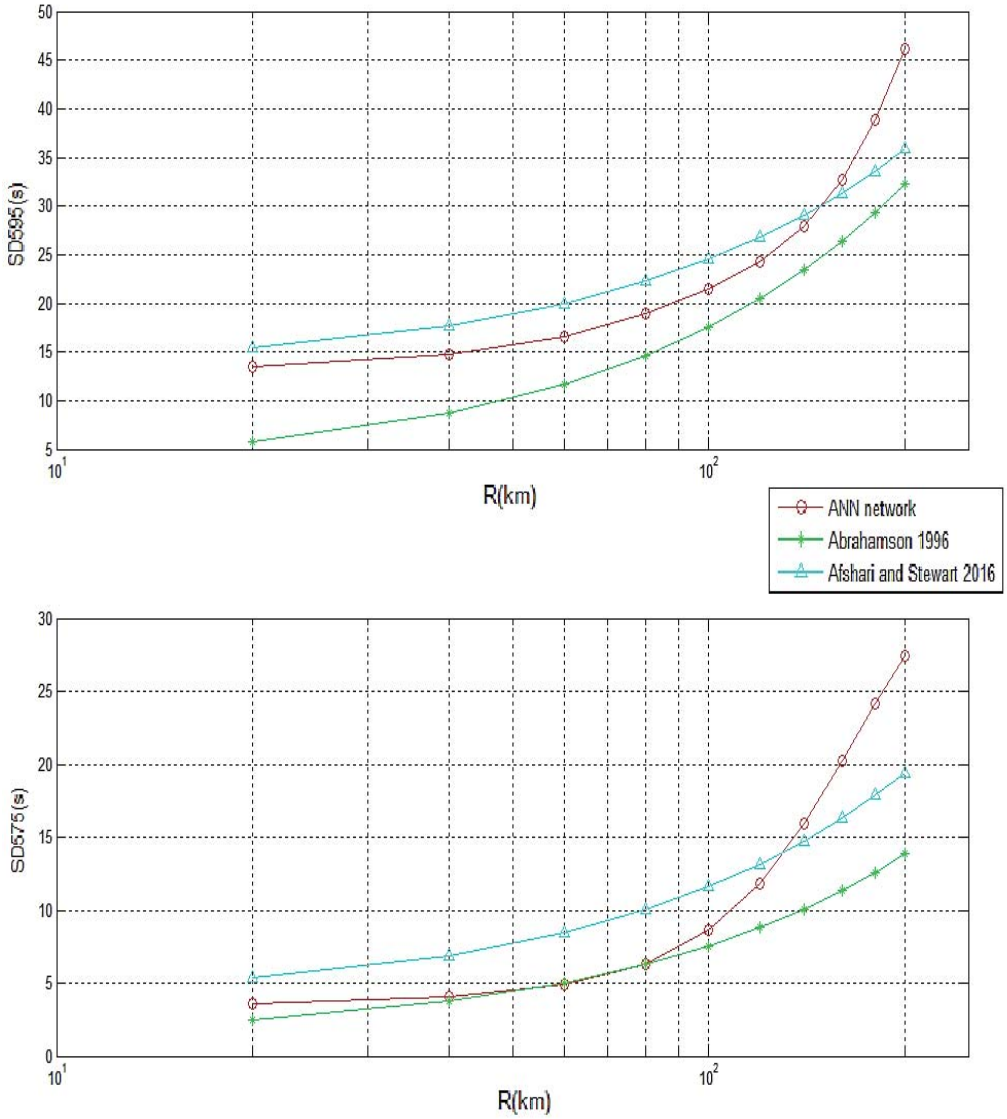

Figure IV-20 Comparison of proposed significant duration model with two existing relationships Mja= 5.5; Vs30=200 m/s; principal direction.

IV.4.2. Sensitivity analysis

A sensitivity analysis investigates how the different inputs affect the significant duration models. the overall results are summarized in Figure IV-21 and Figure IV-22, which shows that the inputs parameters have almost the same effects on the significant duration, whereas the depth parameter is dominant and the radial angle has less influence.

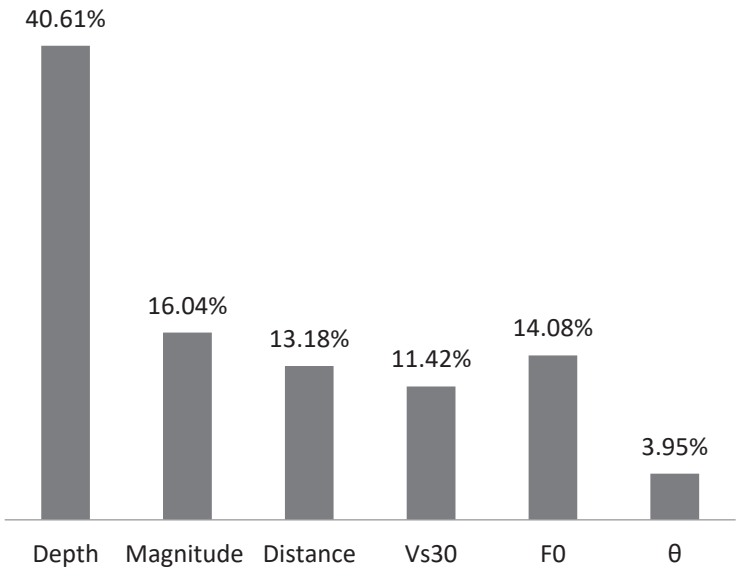

Figure IV-21 Input sensitivity analysis. SD575 Model

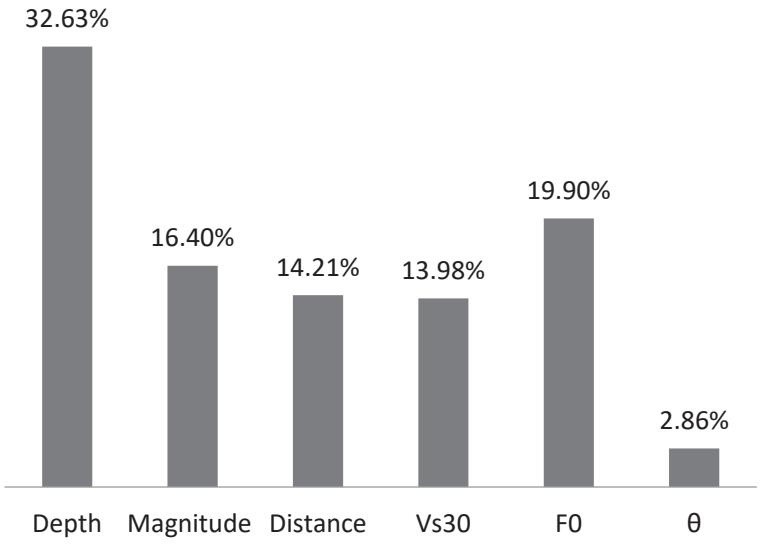

Figure IV-22 Input sensitivity analysis. SD595 Model

IV.5. Frequency content

The mean period parameter (Tm) of a ground shaking is considered as a simplified parameter to describe the frequency content. This parameter is preferred due to its ability to distinguish between various spectral shapes of ground motion, and its relationship with seismological parameters.

The objective of this section is to predict the mean period (Tm) of the strong ground motions and analyze the effects of seismological parameters using feed forward artificial neural network (ANN) with a gradient back-propagation rule for the training. The inputs are the magnitude, the focal depth, the epicentral distance, the shear wave velocity and the radial angle epicenter-station while the target outputs are represented by the mean period (Tm). Then, a sensitivity analysis is carried out in an attempt to capture the influence of the seismological parameters on the mean period of the ground motion.

IV.5.1. Artificial Neural Network Model

The results show that the configuration with a hyperbolic tangent function for the hidden layer and linear function for the output layer gives the best results.

According to the above provisions, inputs to the network are defined here by the values of magnitude (Mjma), epicentral distance (Repi), shear-wave velocity (V_{s30}), resonant frequency (f_{800}), the focal depth (d) and the angle epicenter-station (θ). The output node is represented by mean period (Tm) (Figure V-26). A standardization of all data was performed to improve the performance of the model.

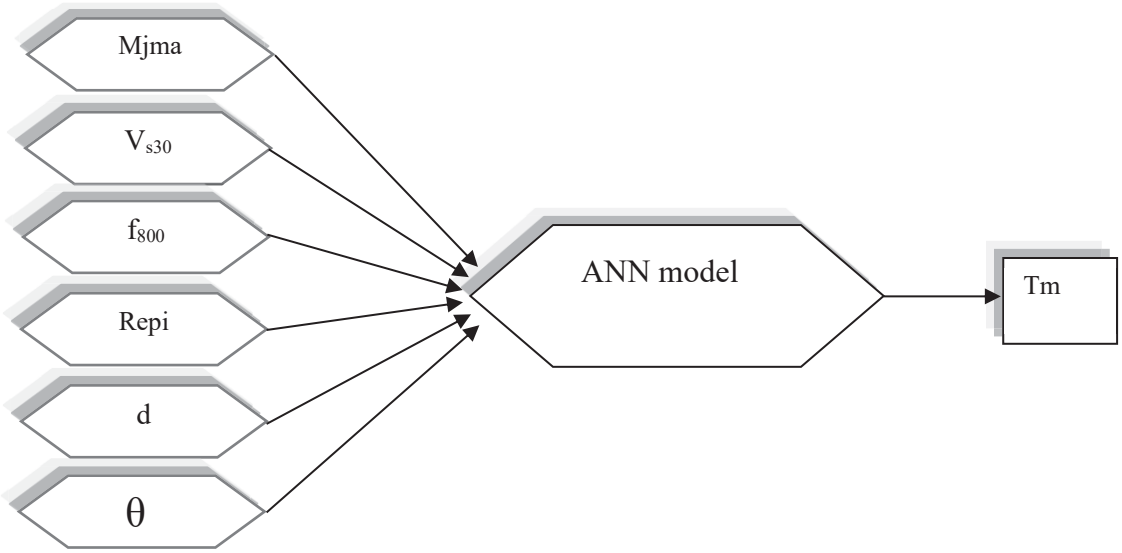

Figure IV-23 Input /Output of models developed

In this section, a large number of architectures were tested using various parameters in order to obtain the best ANN model.

The performance of the developed neural network models is carried out by comparing the target Tm and those predicted by the models. Figure IV-24 shows the regression curves for all data (1104 samples) which reveal a coefficient of correlation R equal to 0.8.

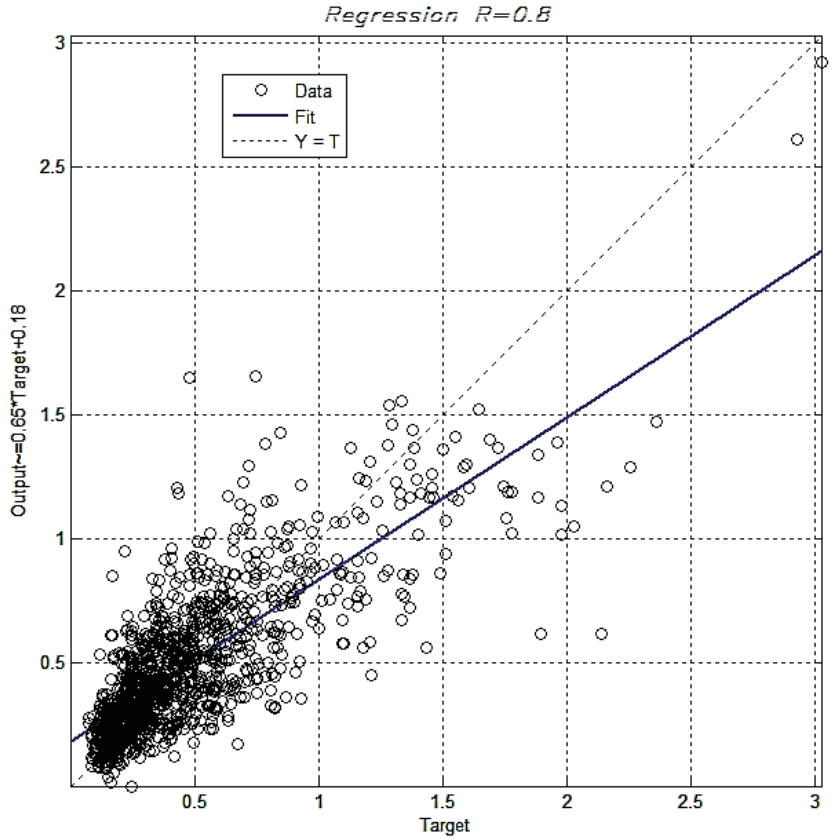

Figure IV-24 Linear regression between the target and predicted Tm

IV.5.2. Results And Discussions

As it was described before, to determine the optimal architecture of an ANN it was necessary to test a large number of architectures. To train and test the ANN models, a computer program was developed that includes routines for MATLAB Neural Network Tool Box. All architecture used and the results obtained in this study are presented in Table IV-5 and Table IV-6.

The accuracy of the prediction is evaluated by comparing the performance criteria; Table IV-5 shows the performance of all the three ANN architectures, along with their respective prediction accuracy. On one hand it is observed that the best value of R with small value MSE associated with the combinations (tanh-sigmoid –linear) as function activation, on the other hand it has been found that the neuron number considered of the hidden layer have approximately same prediction accuracy

which mean that the number of neurons used in the hidden layer has no influence on the performance of this particular models. This table lists the MSE and R for different tests using different combinations, Summing up the results it can be concluded that the Tm (Mean period) predicted by the ANN with ten neurons for the activation function using the combination of activation function (tanh-sigmoid –linear) has been found to be more accurate.

Table IV-5 Test of different combination of activation function

Layer 01	Layer 02	R_{train}	R_{valid}	R_{test}	R_{all}	MSE
log-sigmoid	log-sigmoid	<0.1	<0.1	<0.1	<0.1	>0.5
log-sigmoid	linear	0.78	0.71	0.76	0.76	0.032
Tanh-sigmoid	linear	0.81	0.8	0.77	0.8	0.027
Tanh-sigmoid	Tanh-sigmoid	0.84	0.73	0.76	0.81	0.038

Table IV-6 Influence of number of neuron activation function (tanh-sigmoid –linear)

Neurone nbr	*Rtrain*	*Rvalid*	*Rtest*	*RAll*	*MSE*
5	0.75	0.77	0.7	0.75	0.025
10	0.806	0.8	0.77	0.8	0.019
15	0.8	0.67	0.8	0.78	0.024
20	0.82	0.72	0.81	0.8	0.027

IV.5.3. Sensitivity Analysis:

This analysis was conducted for the models developed and the overall results are summarized in Figure IV-25. As can be seen on this figure, the shear-wave velocity down to a depth of 30m (V_{S30}) and the resonant frequency f_{800} are the most influent parameters, followed by the magnitude and focal depth. Nevertheless, the distance and the orientation of path turned out to be less influential.

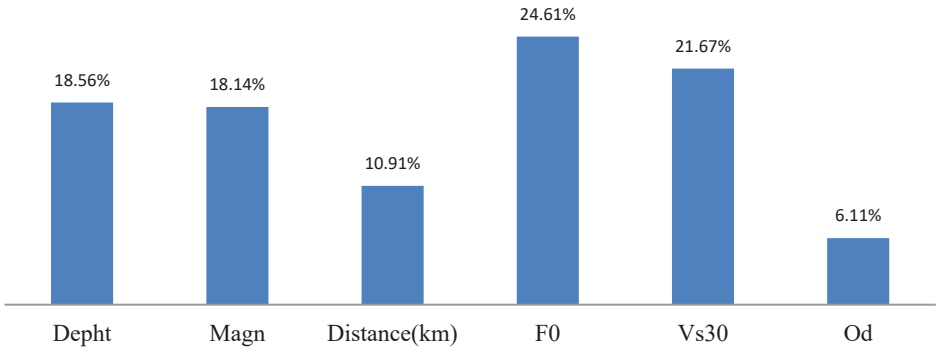

Figure IV-25 Input sensitivity analysis for Tm

IV.6. The functional form

The functional form for each of the developed model is expressed in Equation (11), for any given set of input data, the first step is the normalization preprocessing according to Equation (6), to get Pn.. The output of the model is then obtained through the ANN according to Equation:

$$T_n = \mathrm{Tanh}\left(\{b_2\} + [w_2] \times Tanh(\{b_1\} + [w_1] \times \{P_n\})\right) \quad (11)$$

where :

w1: is the (Nh, N) matrix of synaptic weights between the input parameters and the hidden layer;

w2: is a vector of size Nh that contains the synaptic weights between the hidden layer and the single-output parameter;

{b1} and {b2}: are the bias vectors of the hidden layer and output layer, respectively. The values of the synaptic weight matrices and bias vectors for each of the ANN models developed are included in the appendix. The scaled output Tn is then unscaled, using Equation (7).

The Tanh dependency is related to the selection of the Tanh-sigmoid activation function.

For each of the earthquake parameters considered as an input the validation limits are summurized in Table IV-7.

Table IV-7 Validation limits

	f_{800}	V_{s30}	M_w	R	Depth
min	0.12	144	4.8	15	16
max	20	1500	7.3	205	13

IV.7. Conclusion

The prediction of the intensity measures of ground motion for a given site is of paramount importance in many practical applications of earthquake engineering. In this chapter of the dissertation, a neural network based method has been used to predict the intensity measures for a given set of seismological parameters.

The elaborated models have six input factors: the magnitude (M_{jma}), the epicentral distance (R_{epi}), the shear-wave velocity (V_{s30}), the resonant frequency (f_{800}), the focal depth (d) and the angle of the epicenter-station (θ).

A large number of ground motions extracted from the KiK-Net strong motion database were used to train the ANN. Performance criteria such as mean square error (MSR) and correlation

coefficient are used to evaluate accuracy. It is found that the predicted values of the intensity measures by the neural network correlate well with the observed ones.

Moreover, in previous models, the intensity measure variation due to different orientations was not explicitly incorporated and it was based on the geometric mean or the maximum of the two orthogonal components. The ANN models proposed take into account both components of the ground motions, and consider the directionality effect through the radial angle as an input parameter.

For the PGA model, the results show that the configuration with a hyperbolic tangent function for both the hidden layer and output layer gives the best PGA, which converges to the recorded value with the highest level of correlation coefficient, equal to 0.86.

The PGA increases with magnitude and decreases with increasing distance and V_{s30} (stiffer sites). These observations are consistent with those shown in previous studies. On the basis of a sensitivity analysis, it can be concluded that all input parameters are comparably influencing the PGA, including the newly introduced parameter θ.

For the Significant Duration (SD) model, the results confirm previous studies outcomes, i.e. Abrahamson and Silva (1996), Afshari and Stewart (2016). They are all in good accordance as long as distance is less than 100km. However, the ANN model provides a slightly higher duration at distance greater than 100km. The discrepancies, at distances greater than 100km, are attributed to the significantly enriched far field content (site at distance greater than 100km) of the collected database.

A sensitivity analysis concludes that the magnitude and the focal depth are first order parameters influencing the significant duration, in comparison to the epicenter distance and shear wave velocity down to 30 m, which have a small impact. The additional parameter "θ" defined as the angle formed between the orientation of the path epicenter-station and the direction of a component (EW or NS) improves further the performance of the models despite its small effect on the models compared to others inputs.

For the mean period, the sensitivity analysis shows that the shear wave velocity and the resonant frequency are, first order parameters influencing the mean period compared to the magnitude and the depth, which have a small impact.

Chapter V. PREDICTION OF ENGINEERING DEMAND PARAMETERS (EDPS)

V.1. Introduction

Engineering Demand Parameters (EDPs) are structural response measures that can be used to evaluate the damage to different components structural and non-structural. Various EDPs parameters are proposed in literature to quantify the response of structures such as inter-story drift or floor acceleration. As a part of probabilistic based seismic design, Estimate the EDPs for a given hazard level is an essential step, which are often used to assess the amount of damage (structural, non-structural and content), The EDPs used in this study are based on equivalent SDOF. As illustrated in Figure V-1 the selected EDPs are the inelastic response and the hysteretic energy, which correlate well with the potential damage of the earthquake. The objective of this chapter is to propose predictive models for EDPs and analyze the effect of seismological parameters and intensity measures.

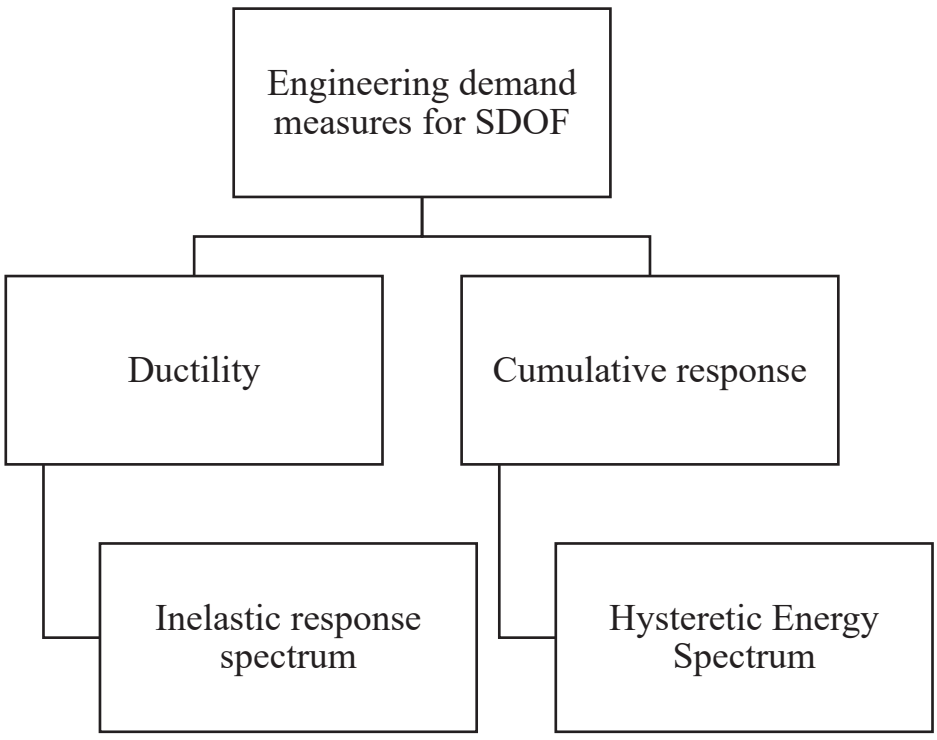

Figure V-1 EDPs considered in this dissertation

V.2. Inelastic Response Spectra

V.2.1. Computation of inelastic response spectrum

Equivalent single-degree-of-freedom (ESDOF) systems are commonly used in the field of earthquake and structural engineering [54, 55] to approximate the response of multi-degree-of-freedom (MDOF) structures, including regular RC buildings, when the response is dominated by a single mode with a high modal participation factor. Different methods also make use of equivalent SDOF systems to predict damage in structures. [56, 137]

Most of the Ground Motion Prediction Equations for elastic and inelastic response spectra proposed in literature are based on the response of constant-ductility systems and are developed for design purpose [9]. Furthermore, the seismic assessment and design verification are based on the evaluation of the ductility demand of structures with given strength, stiffness and restoring force characteristics. This investigation is predicated on the constant-strength approach. Consequently, five-yield strength reduction factors (q) equal to 1,2,3,4 and 5 are considered.

A set of 21 SDOF systems are considered to cover periods of vibration ranging from 0.1 sec to 4 sec (step 0.2 sec). Yielding strength values (fy) are computed dividing the elastic strength (Fe), corresponding to the period of interest, by a yield strength reduction factor (q). A total number of 21 000 nonlinear time history analyses were carried out. As illustrated in Figure V-2, an Elastic-Perfectly-Plastic (EPP) model is used.

For an inelastic damped SDOF system subjected to ground acceleration, the differential equation of motion can be expressed as follows:

$$m\ddot{x}(t) + c\,\dot{x}(t) + f(x,x) = -m\,\ddot{x}_g(t) \tag{12}$$

Where: m, c and f represent the mass, damping and resisting force of the inelastic system, respectively; $\ddot{\boldsymbol{x}}_{\boldsymbol{g}}(\boldsymbol{t})$ denotes the ground acceleration; $\ddot{\boldsymbol{x}}, \dot{\boldsymbol{x}}, \boldsymbol{x}$ represent respectively the acceleration, velocity and deformation of a SDOF.

In this investigation, Bouc-Wen model is selected for its simplicity, stability and it can simulate any extended plastic deformation [138]. Runge-Kutta method is adopted to solve the model differential equation numerically [139]. According to Bouc-Wen, the resisting force $\boldsymbol{f}(\boldsymbol{t})$ is defined as the sum of the linear part and the hysteretic part, and depends on history of deformation.

$$f(t) = k_p\,x(t) + Q\,z(t) \tag{13}$$

Where: $\boldsymbol{k_p}$ is the post-yield stiffness; Q is the yield strength (ordinate at origin of creeping part) whereas $\boldsymbol{f_y}$ represents the yielding force; and the adimensional variable z(t) which characterizes the Bouc-Wen hysteresis model :

$$\dot{z}(t) = \frac{\dot{x}(t)}{x_y}\left[A - |z|^{\lambda}\,(B.sign(\dot{x}z) + \beta)\right] \tag{14}$$

Where: z(t) depends on the yield displacement fy, as well as A, B, λ and β that are the parameters that control the shape of the hysteresis loop. The adopted values are:

A=1, B=0.1, λ=0.9, β=6 and $\boldsymbol{k_p = 0}$ for bilinear elastic-perfectly plastic system

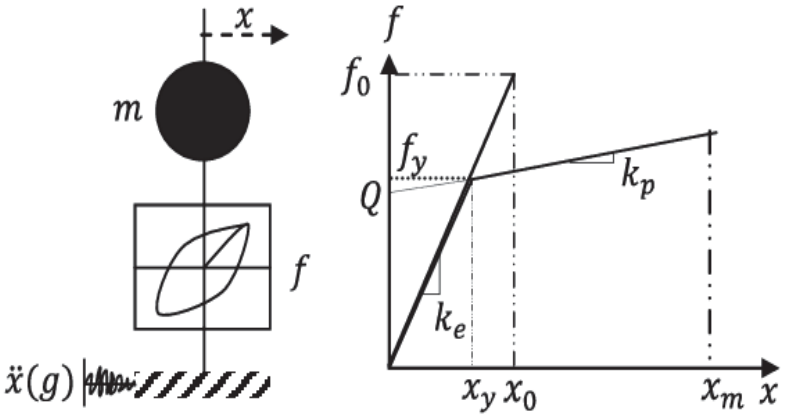

Figure V-2 Elastic-Perfectly-Plastic relationship of inelastic single-degree-of-freedom

V.2.2. Artificial neural network

There are several functions such as hyperbolic tangent, sigmoid and linear functions that can be used as activation or transfer function. The type of activation function plays an important role, and allows the introduction of nonlinearity so that it can deal even with complex phenomena. The concept of the ANN in estimating the inelastic response spectra is illustrated in Figure V-5 together with a schematic representation of the input and output parameters.

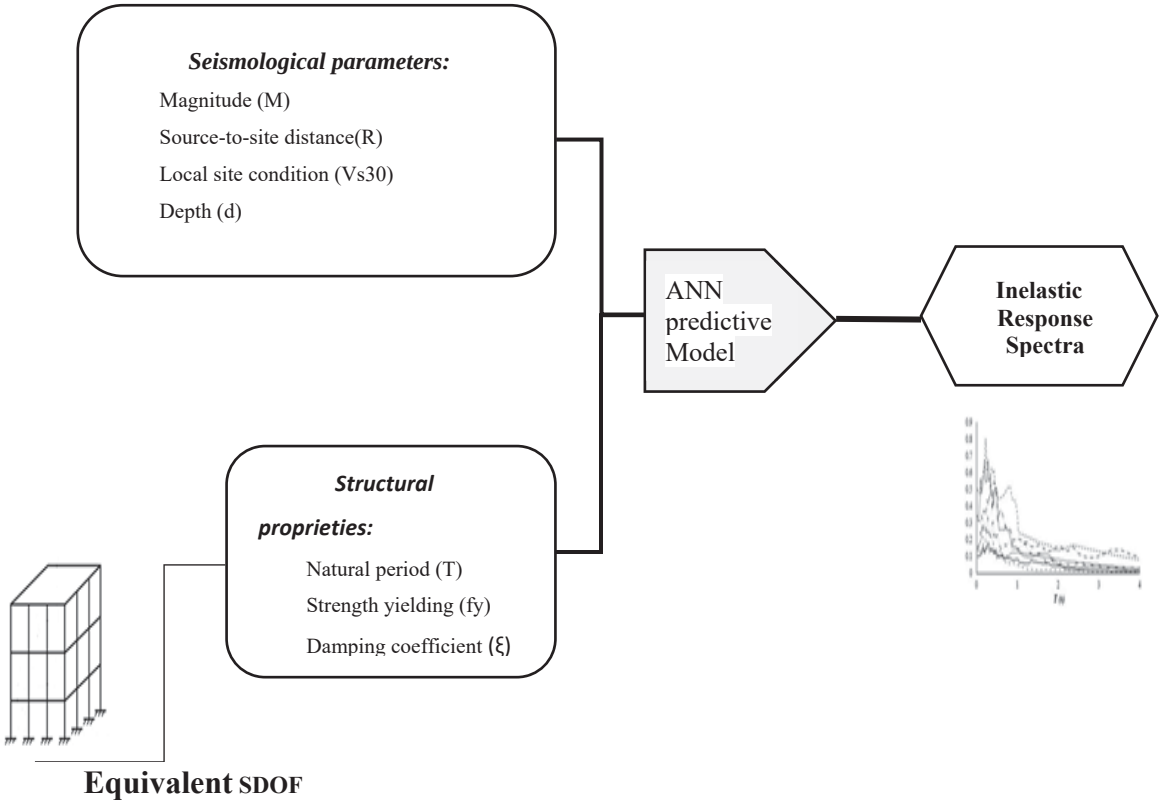

Figure V-3 Process of estimating the inelastic response spectra (Sd)

Figure V-3 and Figure V-4 shows the flowchart for the process of computation of the inelastic response spectra. The constant-strength inelastic response is calculated by reducing the elastic strength of SDOF system from the corresponding reduction factor. A global flowchart of the procedure used in this study is shown in Figure V-4. The selected ground motions from the KiK-Net database are first used to construct the ANN database using the constant-strength approach and then introduced to train, test and validate the ANN model.

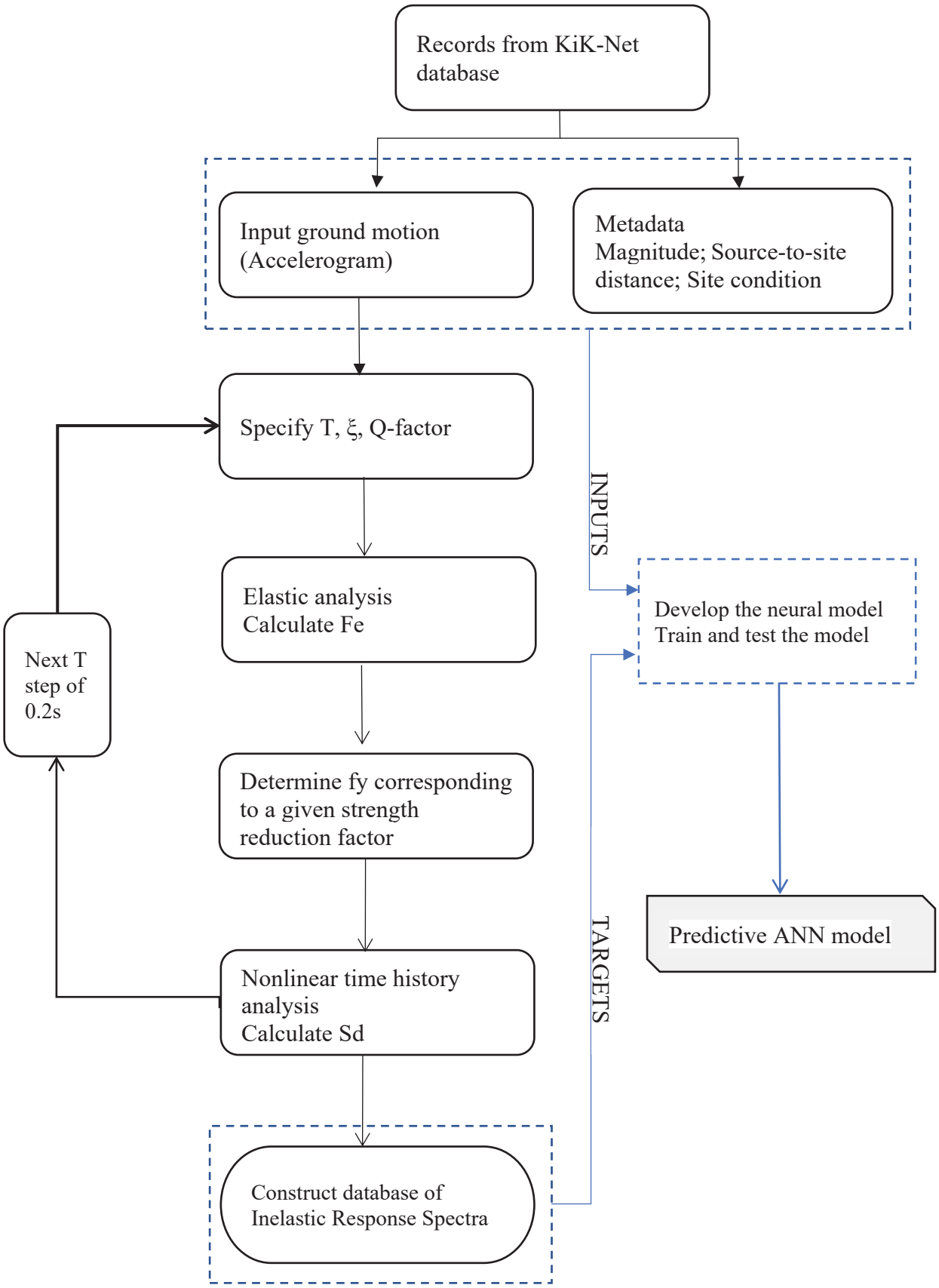

Figure V-4 Flowchart presented overall procedure for predicting inelastic response spectra

V.2.3. Results and discussion

V.2.3.1. Neural network topology optimization

Various neural typologies were tested to define the optimal architecture of a neural model. The results are presented in Table V-1, which list the Mean Square Error (MSE) and correlation coefficient (R) for different tests using different combinations. Following various tests on the different combination and architecture. It turned out that the inelastic response spectra predicted by the proposed models with five inputs using the combination of tangent hyperbolic function (tanh-sigmoid) as an activation function for the hidden layer and linear function (lin) for the output layer, with ten neurons, appears to be the most accurate (Figure V-5). [140]

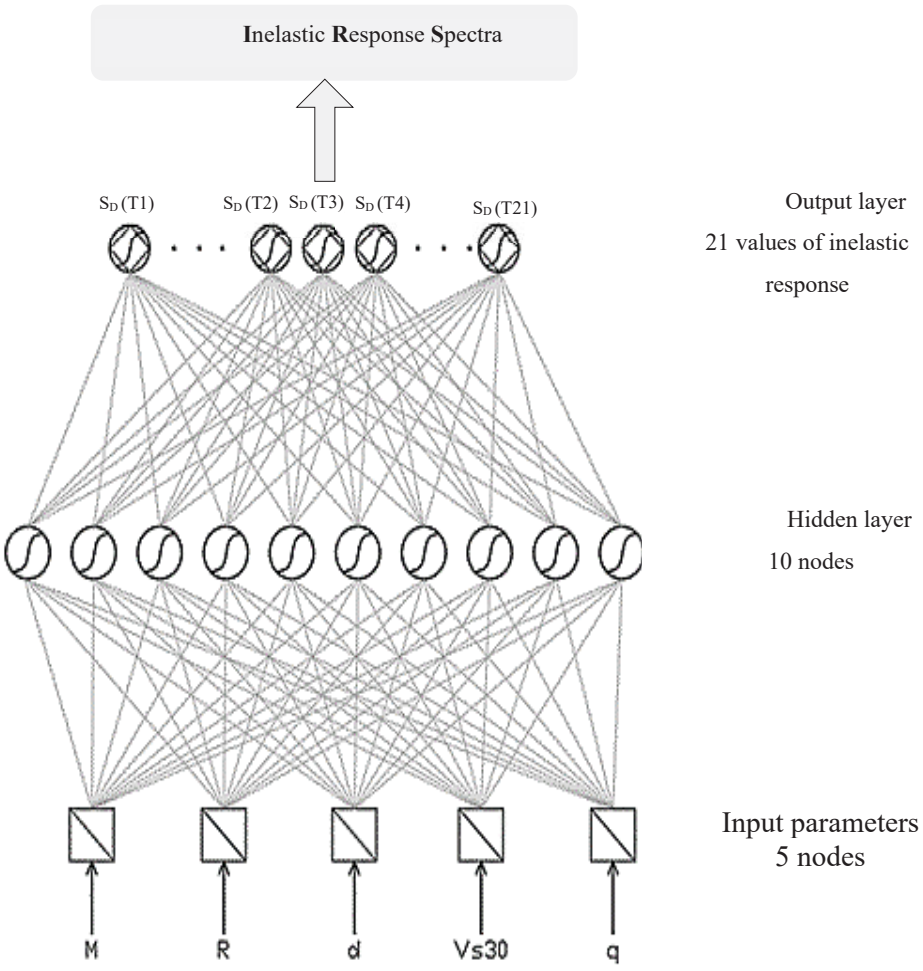

Figure V-5 Structure of ANN model

Figure V-6 shows the regression curve, which plots the values of the inelastic response estimated by the proposed model against the calculated values. The correlation coefficient (R) shows that the values predicted by the neural model are in good agreement with the target values (R=0.93).

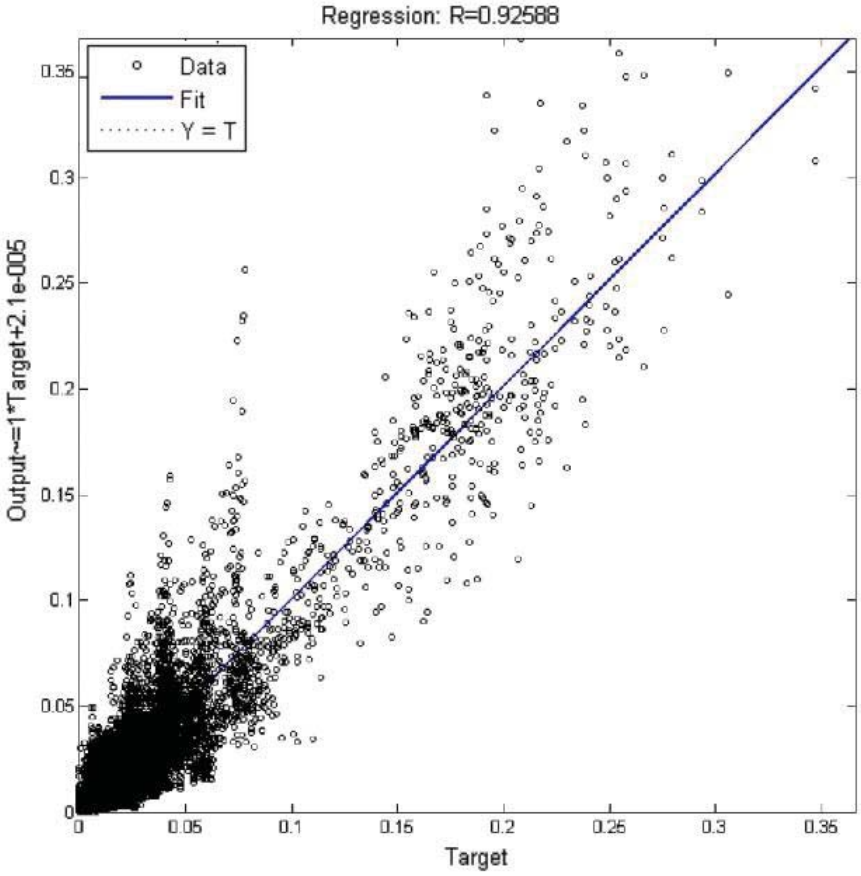

Figure V-6 Linear regression between the target and predicted Sd

To evaluate the statistical behavior of the developed model the residuals are plotted against the M, the R and the Vs30 for predicted inelastic response spectra. As illustrated in Figure 8, generally there is no bias of trend in the residuals. However, It should be noted that in small magnitude events (M=4.5) and in the large distance (R>150km; Far field) significant bias values were observed with respect to Magnitude and distance. The bias in the model is attributed to insignificant response amplitudes due to the attenuation of the ground motion with Magnitude and Distance.

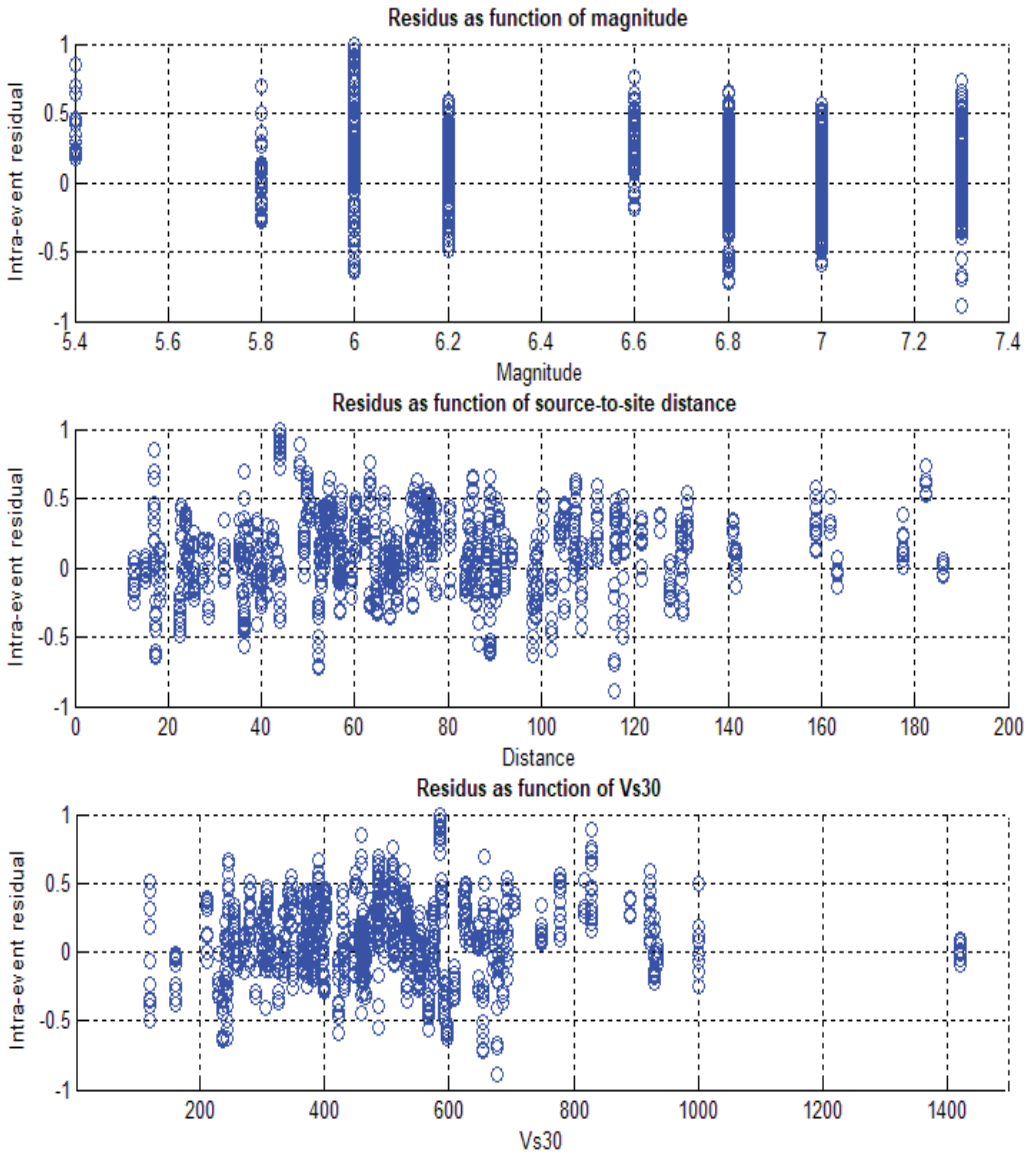

Figure V-7 Intra-event residuals as function of distance R, magnitude and Vs30.

Table V-1 Test of different combination of activation function

ACTIVATION FUNCTION		PERFORMANCE CRITERIA				
Layer 01	Layer 02	R_{train}	R_{valid}	R_{test}	R_{all}	MSE
log-sigmoid	log-sigmoid	<0.1	<0.1	<0.1	<0.1	>0.5
log-sigmoid	linear	0.95	0.92	0.91	0.93	***0.008***
Tanh-sigmoid	linear	0.94	0.92	0.92	0.93	0.007
Tanh-sigmoid	Tanh-sigmoid	0.86	0.83	0.87	086	0.018

V.2.3.2. Effect of intensity measures on Inelastic response spectra

This section presents the effect of the chosen vector-valued seismological parameters on the inelastic response spectra predicted by the ANN model. Figure V-8 shows the variation of the S_d amplitudes with natural periods for three values of magnitude (M 5.5,6 and 6.5) while keeping the same values of: source-to-site distance (R 50km), Depth (d 10km) and Shear wave velocity (Vs30 180m/s). The trend of variation for all magnitudes is similar and tends to increase the inelastic displacement demand further in the long-period region (2s<T<3.5s).

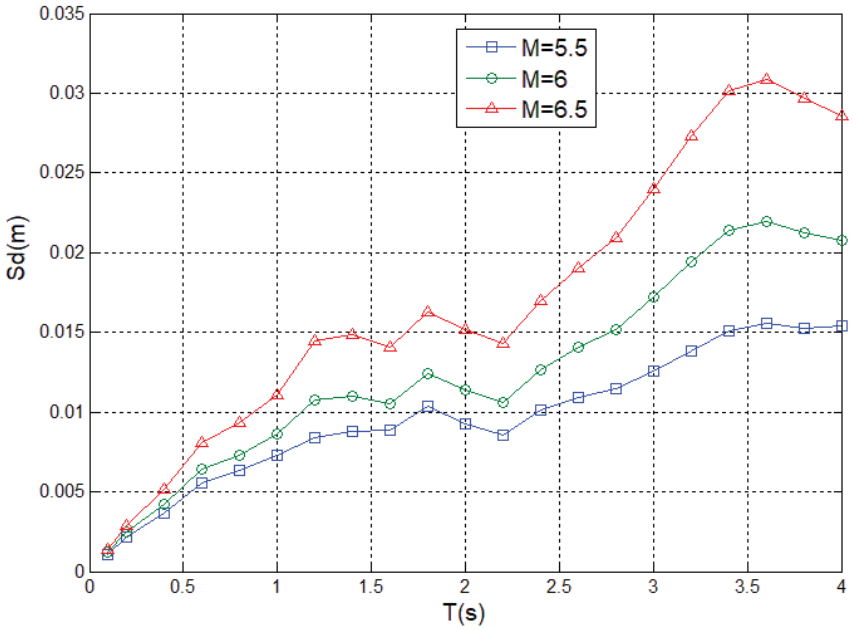

Figure V-8 Predicted inelastic response spectra for M in (5.5, 6, 6.5).

Source-to-site distance-dependent inelastic response spectra are shown in Figure V-9 for two scenario: Near field (R 20km) and Far Field (R 70km) with the same M, d and Vs30. The results indicate clearly that the inelastic deformation demand is still more pronounced in the long-period region with the same trend for both the near and far field scenario. Logical trend is observed, there is systematic increase in the S_d spectra with a decrease in the source-to-site distance.

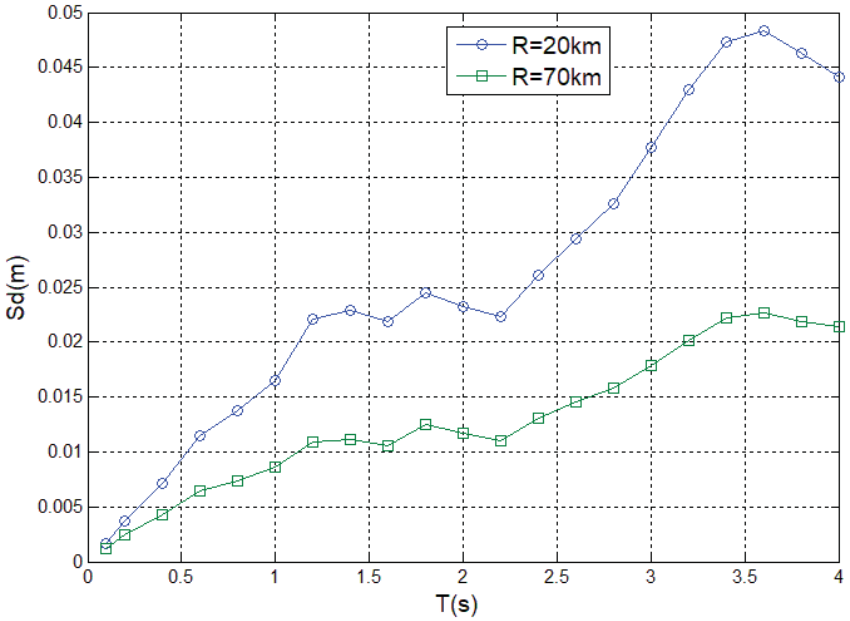

Figure V-9 Predicted inelastic response spectra for R in (20km, 70km).

To highlight the influence of the site condition on the inelastic response spectra, the curves corresponding to the spectra predicted by the ANN model are plotted in Figure V-10 for three values of Vs30 (180m/s, 270m/s and 360m/s). It shows that the effect of the Vs30 is similar to the previous parameters and small values of Vs30 (soft soil) produce larger response than site with high values of Vs30.

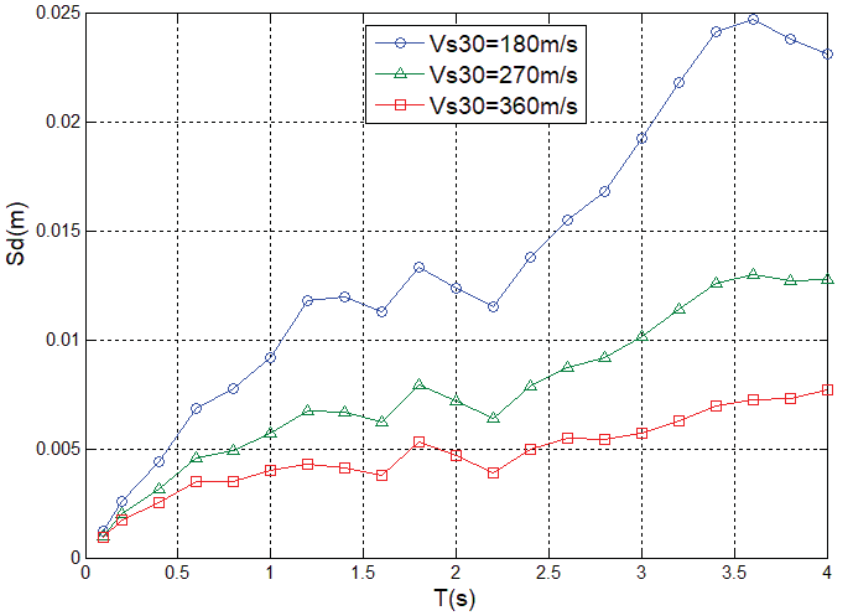

Figure V-10 Predicted inelastic response spectra for Vs30 in (180m/s, 270m/s, 360m/s).

The reduction factor is used to reduce the yielding strength obtained from a linear analysis in order to take into account the non-linear structural capacities. Figure V-11 elucidate further the

influence of reduction factor on the inelastic response spectra where each increment of q-factor leads to decreasing nonlinear response.

Based on the results illustrated in Figures 7, 8, 9 and 10, the relation between the inelastic response spectra and seismological parameters present a similar trend and all the parameters considered as inputs are more effective in the large-period region.

The

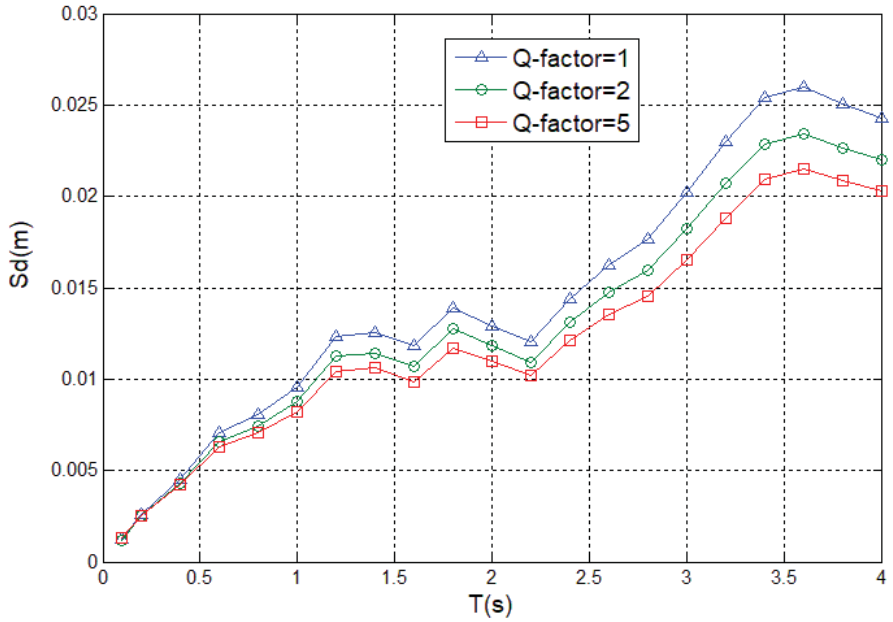

Figure V-11 Predicted inelastic response spectra for Q-factor in (1,2,5).

dependence of the inelastic response spectra on seismological parameters, such as magnitude, distance, and soil condition, was investigated. The obtained results are well substantiated by the physical meaning of the magnitude as an increase in the magnitude values leads to consistent increase of inelastic response demand. It is well known that strong ground motions attenuate with distance, this was clearly reflected in Figure V-9 where significant reduction in the inelastic response spectra is observed in the far fields. On the other hand, as expected, structures on soft soil foundations are exposed to higher ductility demands than those on stiff soil foundations.

V.2.4. Sensitivity analysis

A sensitivity analysis of the seismological input parameters is performed, in order to gauge the individual influence of each parameter on the Sd spectra. Percentages of synaptic weight Pi that corresponds to each of the four parameters are computed using the following equation :

$$P_i = \frac{\sum_{j=1}^{Nh} |w_{ij}^h|}{\sum_{i=1}^{N} \sum_{j=1}^{Nh} |w_{ij}^h|} \qquad (15)$$

w_{ij}: synaptic weights of the ANN where $i \in [1..N]$ and $j \in [1..N_h]$, with N=10 and N_h=4.

The overall results are summarized in Figure V-12, which shows that the seismological parameters have almost the same effects on the Sd spectra, whereas the depth has less influence.

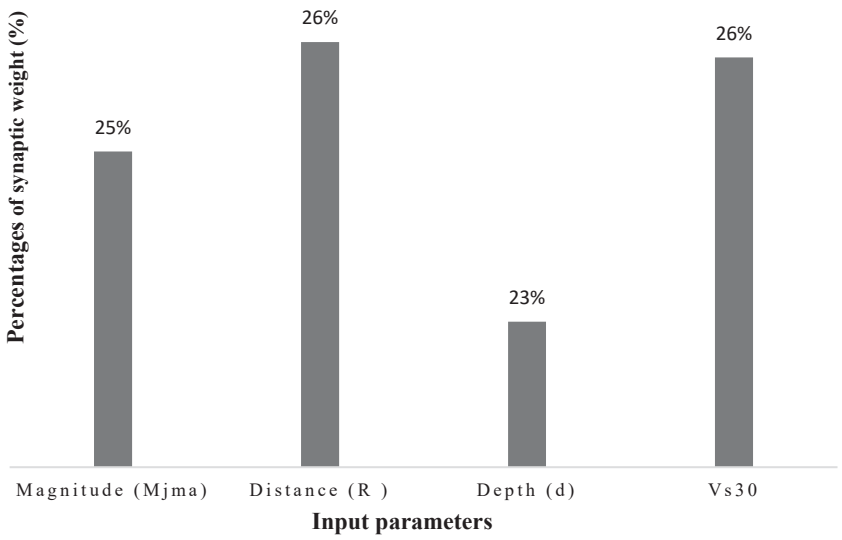

Figure V-12 Input sensitivity analysis

V.3. Hysteretic energy demand spectra

The different types of seismic energy component imparted to structures are presented in chapter II. In this section, we investigated the hysteretic energy component. This objective is to predict the hysteretic energy demand spectra by considering as inputs the Intensity measures (IMs) which characterize the main features of ground motion rather than expressing it in terms of earthquake parameters (see Figure V-13). The proposed approach is intended to reduce the uncertainties related to earthquake and seismological parameters using feed forward Artificial Neural Network (ANN) with gradient back-propagation rule for the training. For this purpose, a database of hysteretic energy response spectra is constituted using 5% damped Single-Degree-Of-Freedom (SDOF) systems subjected to 570 strong ground motion components judiciously extracted from the KiK-Net strong-motion network.

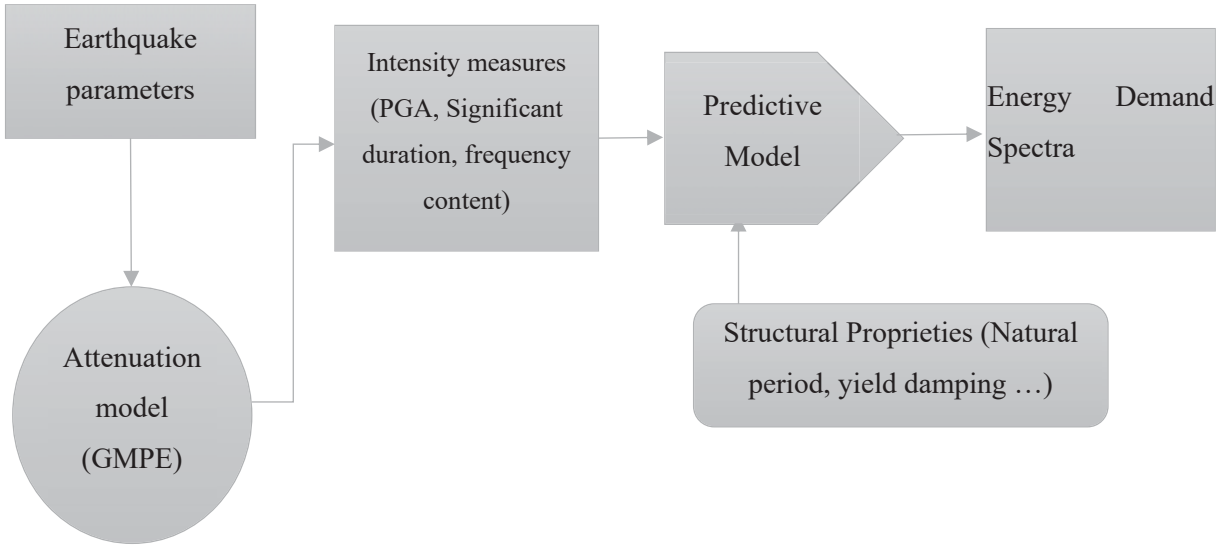

Figure V-13 the approach used to predict the hysteretic energy demand

The earthquake ground motions were attentively selected from the KiK-Net database prepared initially, the distributions of the records in terms of intensity measures are presented in Fig. V-14, V-15 and V-16. The intensity measures (IMs) considered in this study are strategically selected to take into consideration the three essential features of the ground motion; the Peak Ground Acceleration (PGA) for the amplification, the Significant Duration (SD) for the duration, and the mean period (Tm) for the frequency content.

As illustrated in Fig. V-14, More than 70% (414 records) of the ground motion records used in this study to train the neural network, have a PGA range between 50 to 250 gal.

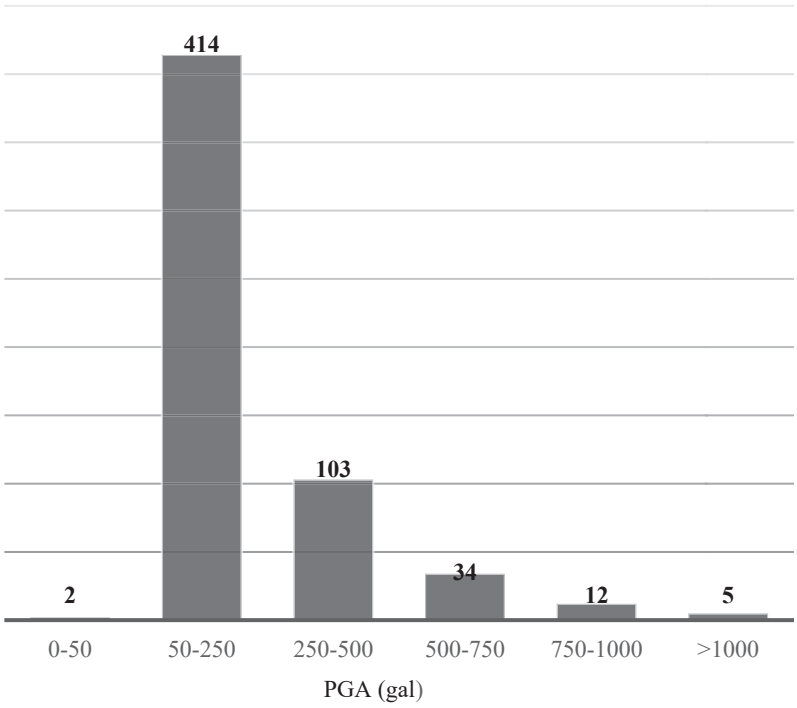

Figure V-14 PGA distribution

More than 50% (280 records) of the ground motion records used in this study to train the neural network, have a significant duration range between 5 to 25 s (Fig. V-15).

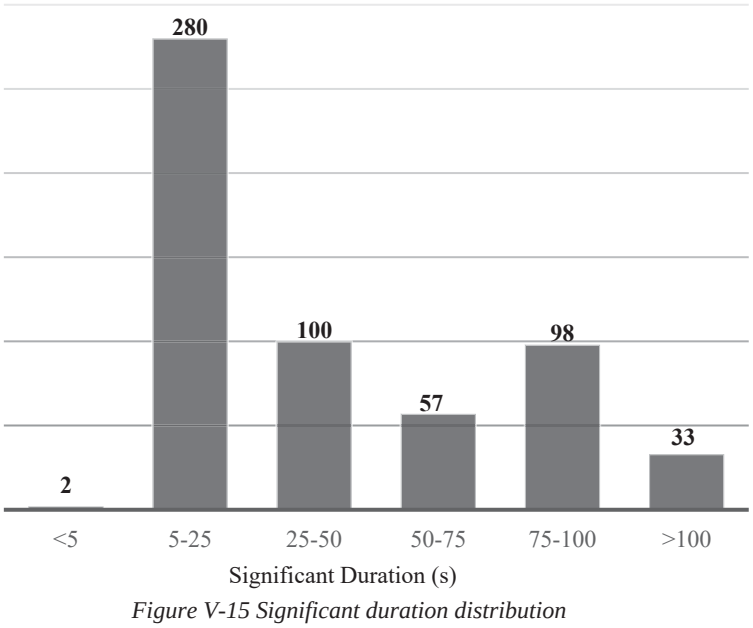

Figure V-15 Significant duration distribution

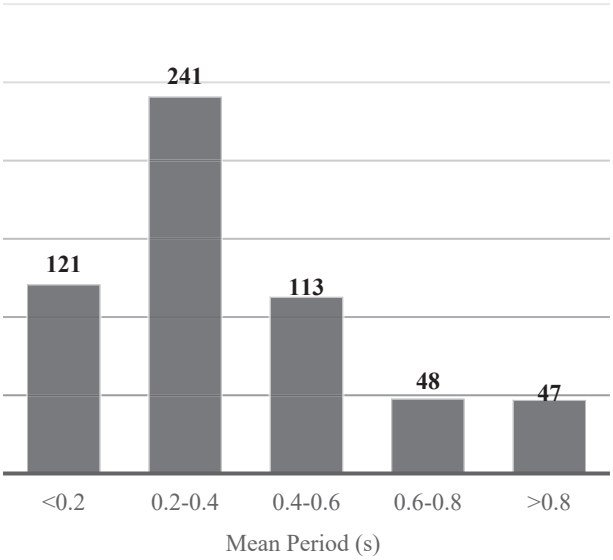

Figure V-16 Mean period distribution

A computer algorithm was developed to compute the energy response time-histories of SDOF systems under the selected earthquake ground motions. Consequently, a dataset of hysteretic energy demand spectra was constructed and used in the learning process. To this end, a range of SDOF systems is considered. Each SDOF system is characterized by a natural period (T), a critical damping ratio (ζ) and a mass-normalized yield strength (Cy), which is defined as:

$$C_y = \frac{F_y}{m} \qquad (16)$$

Where, *Fy* is the yield force of the system. The force-deformation relation of the system is elastic-perfectly-plastic and damping ratio is taken 5% of critical damping. The interval of variation of the natural period is composed of 14 values ranging from 0.1 sec to 2.5 sec.

Most of the Ground Motion Prediction Equations for energy demand spectra proposed in literature are based on the response of constant-ductility systems and are developed for design purpose [83]. Furthermore, the seismic assessment and design verification are based on the evaluation of the ductility demand of structures with given strength, stiffness and restoring force characteristics. As illustrated in Figure V-17, this investigation is predicated on five levels of mass-normalized yield strength (C_y) equal to 10,5,2,1 and 0.5 m/s^2. A total number of 39 900 nonlinear time history analyses were computed. For an inelastic damped Single-Degree-of-Freedom (SDOF) system subjected to ground acceleration.

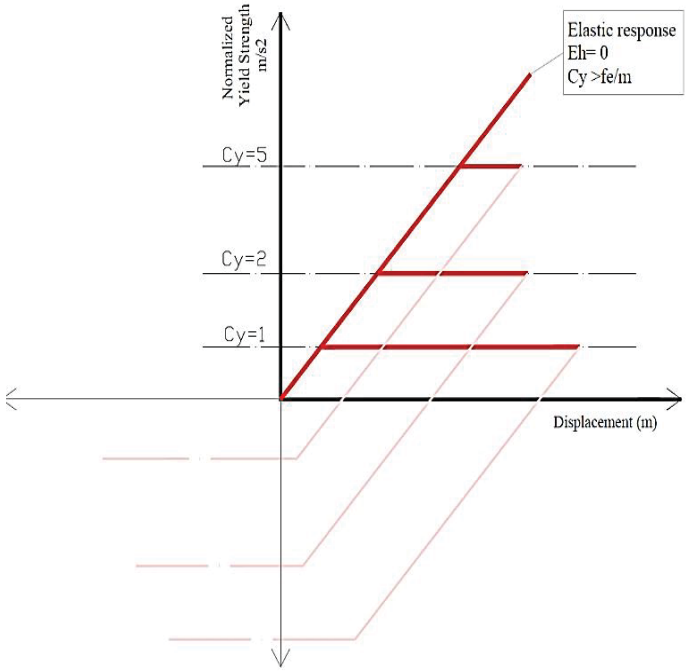

Figure V-17 levels of normalized yield strengths

V.3.1. Artificial neural network

There are several functions such as hyperbolic tangent, sigmoid and linear functions that can be used as activation or transfer function. The type of activation function plays an important role, and allows to deal even with complex phenomena. A systematic theory to determine the number of input nodes and hidden layer nodes is unavailable.

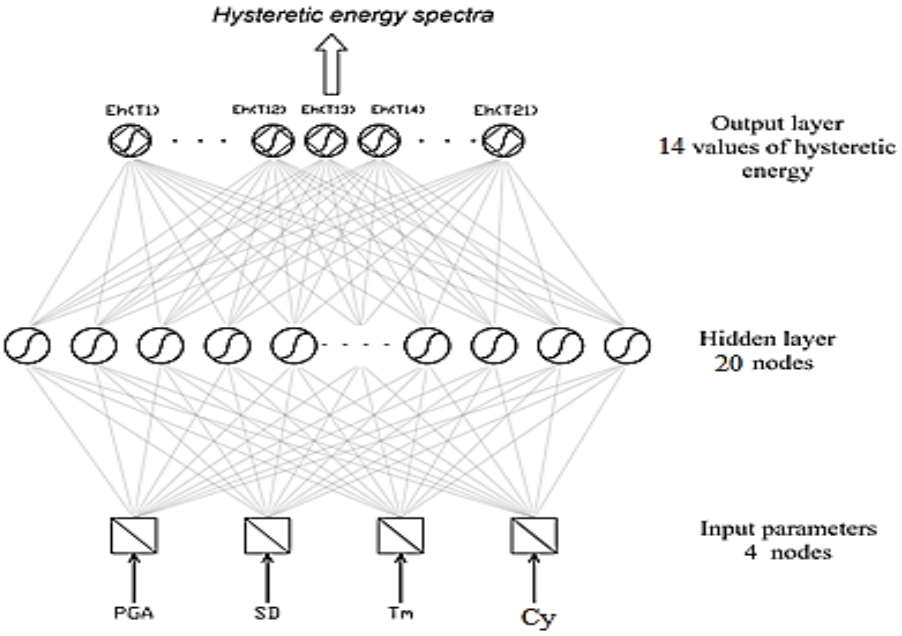

Figure V-18 Structure of ANN model

Therefore, the selection of an architecture of the neural network is determined by trial and error [141]. In this paper, a large number of architectures are tested by using various parameters in order to obtain the best ANN model. The model is developed with four inputs and 14 output neurons and a 20 nodes hidden layer as illustrated in Figure V-18.

Various neural typologies were tested to define the optimal architecture of a neural model. The results are presented in Table V-2, which list the Mean Square Error (MSE) and correlation coefficient (R) for different tests using different combinations. After several trials on the different combination and architecture, it turned out that the hysteretic energy spectra predicted by the proposed models with four inputs using the combination of tangent hyperbolic function (tanh-sigmoid) as an activation function for the hidden layer and the linear function for the output layer, with twenty neurons, is the most accurate.

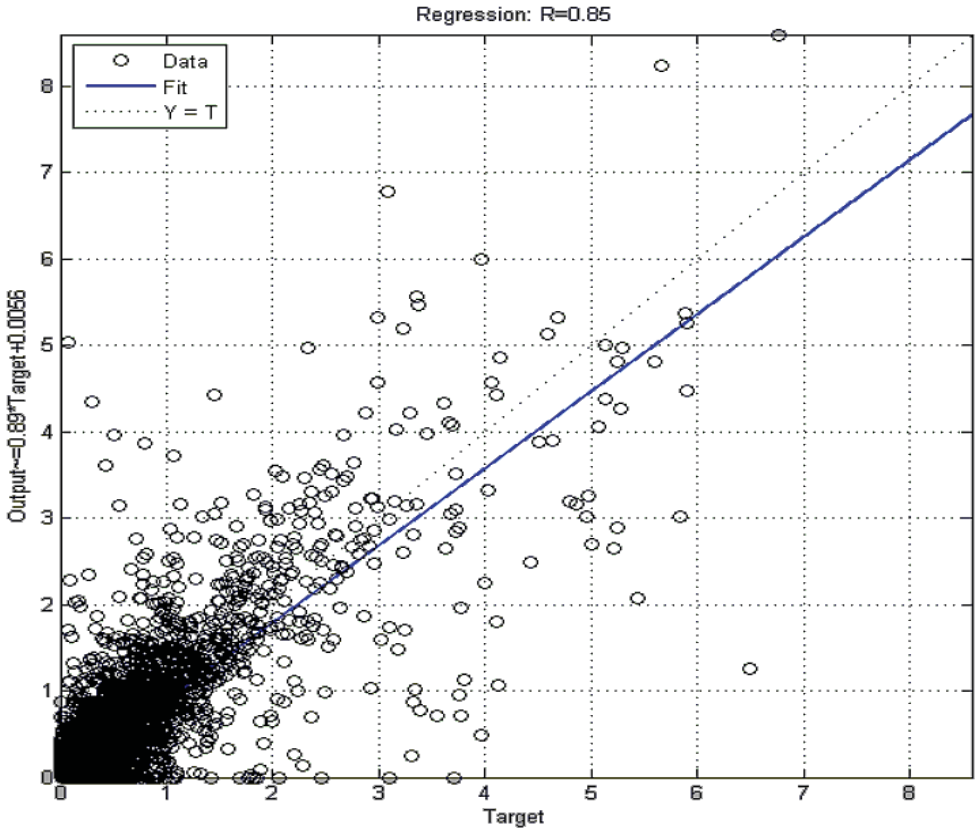

Figure V-19 Linear regression between the target and predicted Sd

Table V-2 Test of different combination of activation function

Activation Function		Performance Criteria				
Layer 01	Layer 02	Rtrain	Rvalid	Rtest	Rall	MSE
log-sigmoid	log-sigmoid	<0.1	<0.1	<0.1	<0.1	>0.5
log-sigmoid	linear	0.88	0.73	0.89	0.85	***0.005***
Tanh-sigmoid	linear	0.86	0.83	0.86	0.85	0.004
Tanh-sigmoid	Tanh-sigmoid	0.85	0.73	0.70	0.80	0.006

V.3.2. Results and discussion

V.3.2.1. Neural network topology optimization

Figure V-19 shows the regression results which compare the value of the hysteretic energy estimated by the proposed model and the calculated values. The correlation coefficient (R=0.85) indicates that the values estimated by neural model are in agreement with the calculated target values.

To evaluate the statistical behavior of the developed model, the residuals are plotted against the PGA, the SD and the Tm for predicted hysteretic energy spectra. As illustrated in Figure V-20, the plots are fairly symmetric and tend to cluster towards the middle showing no bias or trend in the residuals.

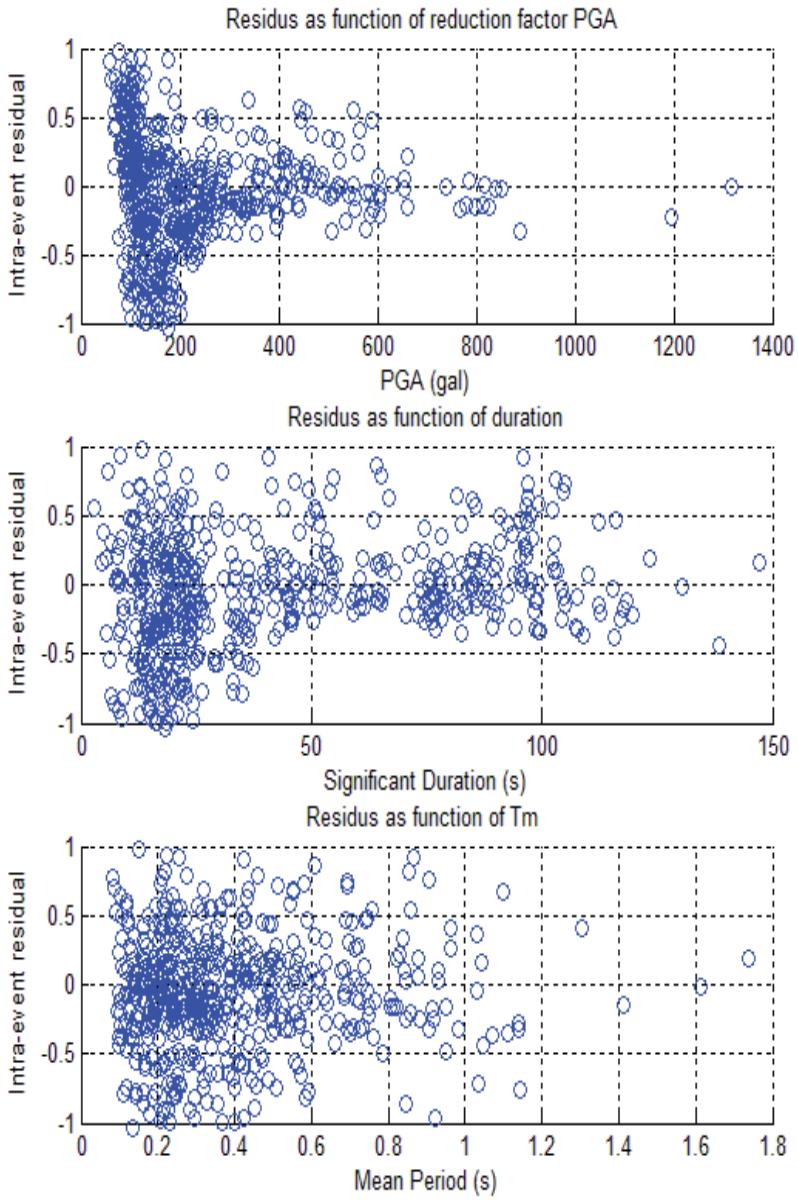

Figure V-20 Intra-event residuals as function of PGA, SD and Tm

V.3.2.2. Effect of intensity measures on the hysteretic spectra

The effect of the intensity measures on the predicted hysteretic energy spectra is presented in this section. Figure V-21 shows Five curves of the predicted hysteretic energy demand spectra corresponding to increasing values of PGA (PGA 0.2g, 0.4g, 0.6g, 0.8g and 1.0g) while keeping the same values of the significant duration (SD 15s), the mean period (Tm 0.4s) and the normalized yield strength (Cy=1 m^2/s^2).

The effect of PGA is mostly felt in the short-period region (T<0.7s). The hysteretic energy demand depends strongly on the PGA, an increase in the PGA leads to consistent increase of hysteretic energy demand.

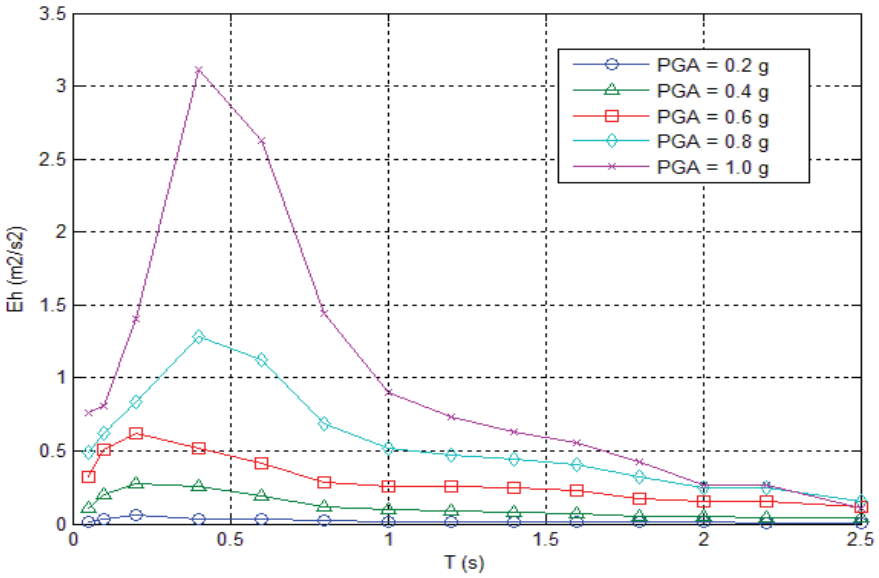

Figure V-21 Predicted Eh spectra for PGA in {0.2g, 0.4g, 0.6g, 0.8g and 1.0g}

Duration-dependent hysteretic energy spectra obtained for three scenarios (SD 5 s), (SD 20 s) and (SD 40 s) with the same PGA and Tm (PGA 0.5g and Tm 0.4s) are depicted in Figure V-22. It is clearly shown that, for T<0.8s the long duration (SD 40s) procures more than 75% growth of the hysteretic energy compared to the short duration (SD 5s). The results indicate clearly that the effect of significant duration attenuate as we increase the naturel period value. Therefore, the duration effect is more pronounced in the short-period region (T<0.7s) while the large-period region is less sensitive to the duration of the strong motion. In the other hand, there is significant increase in the hysteretic energy demand with an increase in the duration. This lends support to previous finding in literature. [142]

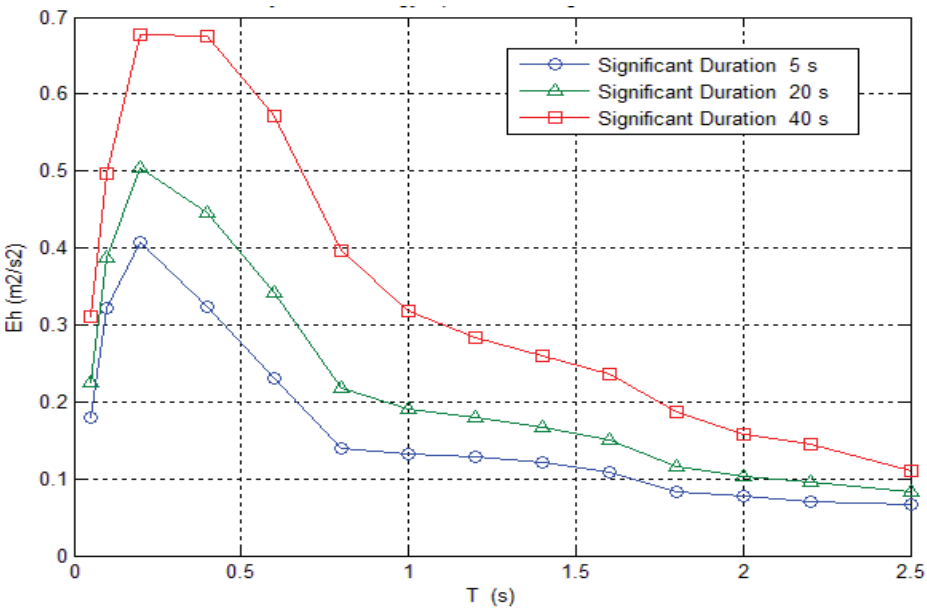

Figure V-22Predicted Eh spectra for SD in {5s, 20s and 40s}

To highlight the influence of the frequency content on the hysteretic energy. The latter is predicted for short period ground motion (Tm 0.2 s) and long period ground motion (Tm 0.8 s). and plotted in Figure V-23.

The spectral shape of hysteretic energy spectra depends on the mean period (Tm). The short period ground motion affects more the system in short period region (0.2s<T<0.5s) while the systems in period greater than 0.5s, the hysteretic energy demand are consistently smaller. Compared to the short period ground motion (Tm 0.2s), the long period ground motion (Tm 0.8) produces more than 200% increase of the hysteretic energy demand in period greater than 0.5s.

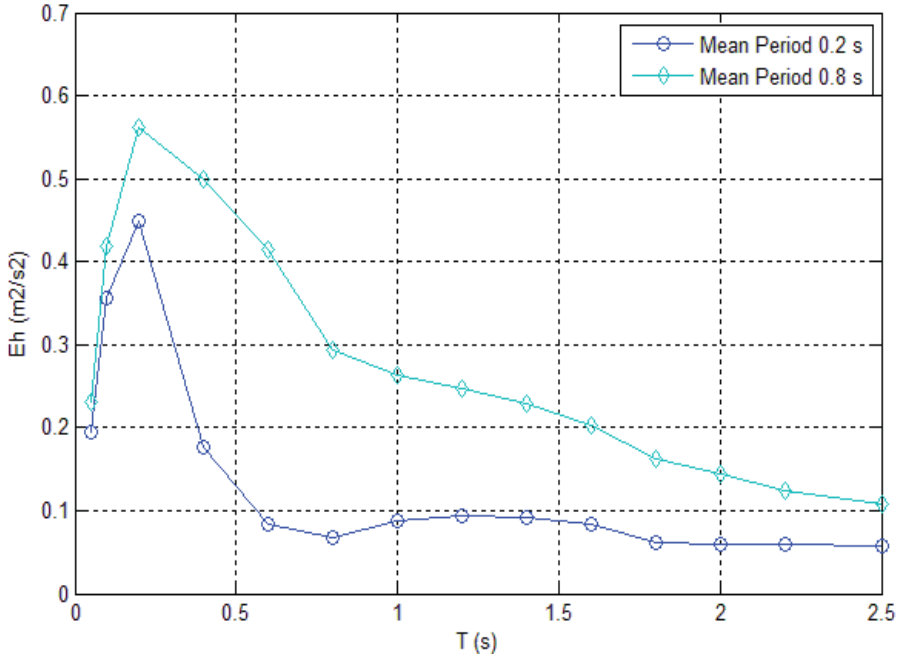

Figure V-23 Predicted Eh spectra for Tm in {0.2s and 0.8s}

The proposed model is based on the response of constant-strength oscillators which is useful for seismic evaluation of existing structures. Figure V-24 clarify further the influence of mass normalized yield strength (Cy) on the hysteretic energy demand spectra. As expected an increase of Cy leads to an extended elastic phase, which consequently is reflected by a consistent decrease in the amplification shape of the hysteretic energy demand spectra.

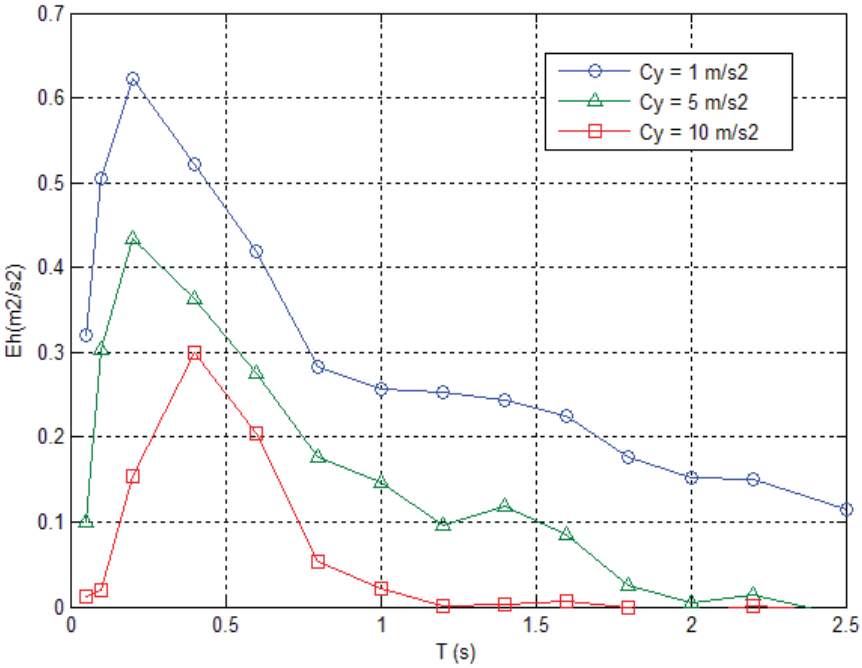

Figure V-24 Predicted Eh spectra for Cy in {1,5 and 10}

V.3.3. Numerical comparison with existing models

The model proposed in this study is compared with two existing empirical relationships: Decanini and Mollaioli (2001) and Dindar et al. (2015) [83, 143].

Figure V-25 compares the hysteretic energy spectrum computed on the basis of the intensity measures values corresponding to Kobe record and the parameters given in Table V-3.

Table V-3 Input parameters used to construct hysteretic energy spectra

PGA (g)	SD (s)	Tm (s)	μ	Site class	ξ (%)
0.8	40	0.5	4	Stiff soil	5

Note that the existing models are based on the response of a constant-ductility ratio, while the proposed model is developed for a constant-strength ductility. To conduct the comparison the mass normalized yield strength is calculated for each period.

Figure V-25 shows that the overall trends of the spectra of the proposed model and those of Decanini and Mollaioli (2001) and Dindar et al. (2015) are similar.

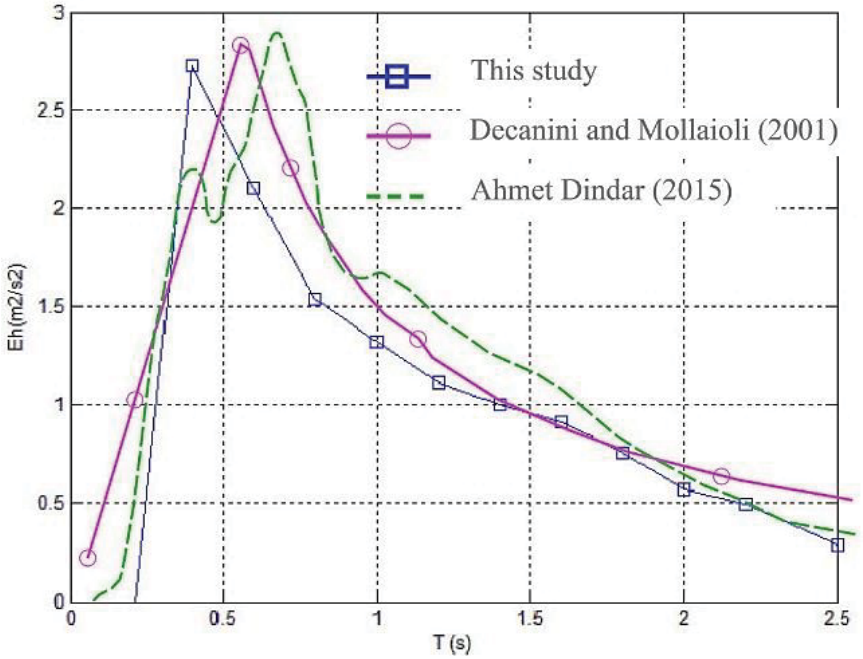

Figure V-25 Comparison with existing models

V.3.4. Sensitivity analysis

A sensitivity analysis for the input variables is performed in order to quantify the individual influence of each parameter on the hysteretic energy demand spectra.

The results of the sensitivity analysis are plotted in Figure V-26, which shows that the IMs parameters have almost the same effects on the hysteretic energy demand spectra, whereas the Cy has less influence.

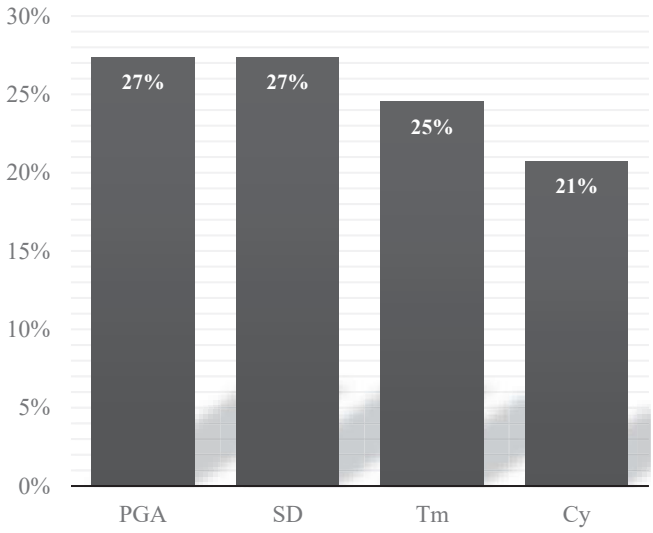

Figure V-26 Input sensitivity analysis

V.4. Conclusion

In this chapter, a neural network based method is developed, in order to predict the inelastic displacement and the hysteretic energy spectra, for a given set of structural proprieties and intensity measures of ground motion.

The proposed hysteretic energy model adopts four input parameters: the peak ground acceleration (PGA), the significant duration (SD), the mean period (T_m) and the mass-normalized yield strength (C_y). The database is constructed using nonlinear time history analysis (NLTHA) of SDOF systems subjected to ground motion records that has been selected from the KiK-Net network. The test phase shows that the predicted values of the hysteretic energy demand spectra by the neural network are reasonably close to the target values and show also a similar trend with existing empirical formulations. A parametric study shows the hysteretic energy demand spectra increase with peak ground acceleration and significant duration in short-period region. In large period range, the hysteretic energy spectrum is less sensitive to the characteristics of the ground motion. Similarly, the short-period ground motion influences more the SDOF systems in the short period region while the long-period ground motion influence covers a wide range of period. The resulting synaptic weights of the trained NN reveal that the intensity measures represented by: PGA, SD and Tm are first order parameters influencing the hysteretic energy demand spectra, in comparison to the Cy, which have a lesser impact.

As for the inelastic response spectra, Unlike most of previous studies based on the constant-ductility approach, this investigation adopt the constant-strength approach in the development of GMPE, which is useful for evaluating the seismic performance of the existing structures. Based on performance criteria such as mean square error (MSR) and correlation coefficient (R), the proposed ANN model predicts the inelastic response spectra with an acceptable precision compared to the real spectra. The result of residual analysis corroborate the model reliability with some bias and poor performance in the small magnitude and far field, this weakness can be justified by the insignificant response amplitudes due to the attenuation of the ground motion with Magnitude and Distance. The use of this GMPE is recommended for events with larger magnitude ($M>5.5$) in the near fields ($R<150$ km). A sensitivity analysis concludes that the seismological parameters have almost the same influence on the inelastic response spectra as predicted by the ANN model except the depth parameter which has a reduced impact.

Chapter VI. CONCLUSION

This dissertation investigated the effects of the seismological parameters on the structural response on two stages. Firstly, we interested on the ground motion characteristics and how it is affected by the seismological parameters. Afterward, the structural aspects is addressed, the influence of the earthquake parameters on the nonlinear behavior of structures is investigated.

The methodology can be summarized in three steps: (a) Data collection (b) Data analysis using artificial neural network (c) interpretation of results. The ground motion database developed in this dissertation is obtained from the nation-wide strong-motion seismograph network KiK-NET (Kyoshin Network), which consists of more than 1,000 observation stations distributed every 20 km uniformly covering Japan

The Artificial neural network is used to analyze the data, which the artificial neural network (ANN) is considered as an alternative option to multiple regression analysis, the ANN with back-propagation (BP) is an efficient way of solving nonlinear modelling problems.

In the **chapter 4**, the intensity measures (IMs) considered in this study are strategically selected to take into consideration the three essential features of the ground motion; the Peak Ground Acceleration (PGA) for the amplification, the Significant Duration (SD) for the duration, and the mean period (Tm) for the frequency content.

Neural models are developed to predict the intensity measures (IMs). The models are then used to investigate also the influence of seismological parameters.

The governing input parameters are the magnitude, the focal depth, the epicentral distance, the shear wave velocity, the resonant frequency and the radial angle epicenter-station. The target outputs correspond to intensity measures (IMs). Compared to the existing attenuation models, in addition to the earthquake independent parameters used for attenuation relationships, a new aspect is considered in this dissertation called directionality.

An analysis of the effect of directionality on the PGA was performed; the findings of this analysis highlight the effects of directionality on the amplitude of ground motion. the ratio (max/min) may reach up to 1.35 (increase of 35%). Therefore, a radial angle parameter has been included in the input of the predictive model.

The database used in most recent Ground Motion Prediction Equations (GMPEs) is based on one record at each station derived from the combination of two horizontal components EW and NS (usually the geometric mean). Compared to previous research works, one of the most important

advantage in introducing the angle epicenter-station (θ) as an input model parameter is that both components E-W and N-S are considered apart in the database.

Performance criteria such as mean square error (MSR) and correlation coefficient are used to evaluate the accuracy. It is shown that the predicted values of the intensity measures (IMs) by the neural network are in good accordance with the observed ones.

A sensitivity analysis investigates how the different inputs affect the significant duration models, it has been found that:

- For the significant duration, the inputs parameters have almost the same effects on the significant duration, whereas the depth parameter is dominant and the radial angle has less influence. The additional parameter "θ" defined as the angle formed between the orientation of the path epicenter-station and the direction of a component (EW or NS) improves further the performance of the models despite its small effect on the models compared to others inputs.
- For the PGA, The inputs parameters have almost the same effects on the PGA except that the soil frequency parameter f_{800}, which has less influence.
- For the mean period, the shear-wave velocity down to a depth of 30m (V_{S30}) and the resonant frequency f_{800} are the most influent parameters, followed by the magnitude and focal depth. Nevertheless, the distance and the orientation of path turned out to be less influential.

The structural behavior is addressed in **chapter 5**, the ductility and dissipated energy, which correlate well with the structural damage during an earthquake are investigated. Equivalent SDOF systems are considered with a set of 21 periods of vibration ranging from 0.1 sec to 4 sec (step 0.2 sec). Based on the response time history of SDOF systems subjected to ground motion records selected attentively from the database, two engineering demand measures are considered: (1) the inelastic displacement response spectra. (2) Hysteretic energy demand spectra.

A Ground Motion Prediction Equations (GMPEs) is developed to predict the inelastic response spectra without the need to resort first to elastic spectra. The inelastic response is expressed in terms of seismological parameters and structural proprieties using feed forward artificial neural network (ANN) with a gradient back-propagation rule.

The use of this GMPE is recommended for events with larger magnitude ($M > 5.5$) in the near fields ($R < 150$ km). A sensitivity analysis concludes that the seismological parameters have almost the same influence on the inelastic response spectra as predicted by the ANN model except the depth parameter that has a reduced impact.

The energy concept is addressed in the second section of **chapter 5** by considering the hysteretic energy demand spectra. A neural model is developed by considering as inputs the Intensity measures (IM_s) which characterize the main features of ground motion rather than expressing it in terms of earthquake parameters. The proposed approach is intended to reduce the uncertainties related to earthquake and seismological parameters using feed forward Artificial Neural Network (ANN) with gradient back-propagation rule for the training.

A parametric study shows the hysteretic energy demand spectra increase with peak ground acceleration and significant duration in short-period region. In large period range, the hysteretic energy spectrum is less sensitive to the characteristics of the ground motion. Similarly, the short-period ground motion influences more the SDOF systems in the short period region while the long-period ground motion influence covers a wide range of period.

The resulting synaptic weights of the trained NN reveal that the intensity measures represented by: PGA, SD and Tm are first order parameters influencing the hysteretic energy demand spectra, in comparison to the Cy, which has a lesser impact. For the engineering demand measure considered in this dissertation, the performance of the developed model reveals a good match between the computed and predicted values of hysteretic energy demand spectra.

The results of this study were compared to those of the previous study on significant duration and hysteretic energy spectra. The proposed models are in good accordance with the existing models.

From a practical perspective, the ANN model with only one hidden layer and a limited number of neurons has been implemented in a simple computer program (see appendix). Therefore, the developed models can be routinely integrated into engineering applications and for probabilistic seismic hazard analysis (PSHA) studies.

REFERENCE

[1] Kempton, J.J. and J.P. Stewart, Prediction Equations for Significant Duration of Earthquake Ground Motions Considering Site and Near-Source Effects. Earthquake Spectra, 2006. 22(4): p. 985-1013.

[2] Bommer, J., P.J. Stafford, and J. Alarcón, Empirical equations for the prediction of the significant, bracketed, and uniform duration of earthquake ground motion. Bulletin of the Seismological Society of America, 2009. 99(6): p. 3217-3233.

[3] Afshari, K. and J.P. Stewart, Physically Parameterized Prediction Equations for Significant Duration in Active Crustal Regions. Earthquake Spectra, 2016. 32(4): p. 2057-2081.

[4] Hammal, S., N. Bourahla, and N. Laouami, Significant duration prediction and evaluation of the effects of seismological parameters using neural networks, in The 2017 World Congress on Advances in Structural and Engineering Mechanics ASEM17 Seoul Korea. 2017.

[5] Rathje, E.M., N.A. Abrahamson, and J.D. Bray, Simplified frequency content estimates of earthquake ground motions. Journal of Geotechnical and Geoenvironmental Engineering, 1998. 124(2): p. 150-159.

[6] Rathje, E.M., et al., Empirical Relationships for Frequency Content Parameters of Earthquake Ground Motions. Earthquake Spectra, 2004. 20(1): p. 119-144.

[7] Lee, J., Engineering Characterization of Earthquake Ground Motions. 2009.

[8] Yaghmaei-Sabegh, S., New models for frequency content prediction of earthquake records based on Iranian ground-motion data. Journal of Seismology, 2015. 19(4): p. 831-848.

[9] Bozorgnia, Y., M.M. Hachem, and K.W. Campbell, Ground motion prediction equation ("attenuation relationship") for inelastic response spectra. Earthquake Spectra, 2010. 26(1): p. 1-23.

[10] Tothong, P. and C.A. Cornell, An empirical ground-motion attenuation relation for inelastic spectral displacement. Bulletin of the Seismological Society of America, 2006. 96(6): p. 2146-2164.

[11] Krawinkler, H., Van Nuys hotel building testbed report: exercising seismic performance assessment. Pacific Earthquake Engineering Research Center. University of California at Berkeley, Berkeley, California, 2005.

[12] Baker, J.W., An introduction to probabilistic seismic hazard analysis (PSHA). White paper, version, 2008. 1: p. 72.

[13] Kanamori, H., The energy release in great earthquakes. Journal of geophysical research, 1977. 82(20): p. 2981-2987.

[14] Hanks, T.C. and H. Kanamori, A moment magnitude scale. Journal of Geophysical Research: Solid Earth, 1979. 84(B5): p. 2348-2350.

[15] Katsumata, A., Comparison of magnitudes estimated by the Japan Meteorological Agency with moment magnitudes for intermediate and deep earthquakes. Bulletin of the Seismological Society of America, 1996. 86(3): p. 832-842.

[16] McGuire, Seismic hazard and risk analysis. Monograph MNO-10, Earthquake Engineering Research Institute, Oakland, USA, 2004.

[17] Douglas, J., Earthquake ground motion estimation using strong-motion records: a review of equations for the estimation of peak ground acceleration and response spectral ordinates. Earth-Science Reviews, 2003. 61(1-2): p. 43-104.

[18] Zhao, J.X., et al., Attenuation relations of strong ground motion in Japan using site classification based on predominant period. Bulletin of the Seismological Society of America, 2006. 96(3): p. 898-913.

[19] McVerry, G.H., et al., Crustal and subduction zone attenuation relations for New Zealand earthquakes. Bulletin of the New Zealand Society for Earthquake Engineering, 2006. 39(1).

[20] Boore, D.M., W.B. Joyner, and T.E. Fumal, Estimation of response spectra and peak accelerations from western North American earthquakes: an interim report. 1994, US Department of the Interior, US Geological Survey.

[21] Ambraseys, N.N., The prediction of earthquake peak ground acceleration in europe. Earthquake Engineering and Structural Dynamics, 1995. 24(4): p. 467-490.

[22] Abrahamson, N. and W. Silva, Summary of the Abrahamson & Silva NGA Ground-Motion Relations. Earthquake spectra, 2008. 24(1): p. 67-97.

[23] BSSC, NEHRP recommended provisions for seismic regulations for new buildings and other structures. 1998: FEMA.

[24] Boore, D.M. and G.M. Atkinson, Ground-motion prediction equations for the average horizontal component of PGA, PGV, and 5%-damped PSA at spectral periods between 0.01 s and 10.0 s. Earthquake Spectra, 2008. 24(1): p. 99-138.

[25] Campbell, K. and Y. Bozorgnia. Empirical ground motion model for shallow crustal earthquakes in active tectonic environments developed for the NGA project. in Proceedings of fourteenth world conference on earthquake engineering. 2008.

[26] Esteva, L. and E. Rosenblueth, Espectros de temblores a distancias moderadas y grandes. Boletin Sociedad Mexicana de Ingenieria Sesmica, 1964. 2(1): p. 1-18.

[27] Abrahamson, N.A., W.J. Silva, and R. Kamai, Summary of the ASK14 ground motion relation for active crustal regions. Earthquake Spectra, 2014. 30(3): p. 1025-1055.

[28] Douglas, J., Ground motion prediction equations 1964–2014. PEER Report 2011, 2014. 102.

[29] Bommer, J.J., et al., On the selection of ground-motion prediction equations for seismic hazard analysis. Seismological Research Letters, 2010. 81(5): p. 783-793.

[30] Esteva, L., Seismic Risk And Seismic Design Decisions. 1970, Massachusetts Inst. of Tech., Cambridge. Univ. of Mexico, Mexico City.

[31] Campbell, K. and N.Y. BOZORG. Near-source attenuation of peak horizontal acceleration from worldwide accelerograms recorded from 1957 to 1993. 1994. Processing Of US National Conference On Earthquake Engineering.

[32] Joyner, W.B. and D.M. Boore, Peak horizontal acceleration and velocity from strong-motion records including records from the 1979 Imperial Valley, California, earthquake. Bulletin of the seismological Society of America, 1981. 71(6): p. 2011-2038.

[33] Boore, D.M., W.B. Joyner, and T.E. Fumal, Equations for estimating horizontal response spectra and peak acceleration from western North American earthquakes: A summary of recent work. Seismological research letters, 1997. 68(1): p. 128-153.

[34] Bommer, J., et al., The Influence of Strong-Motion Duration on the Seismic Response of Masonry Structures. Bulletin of Earthquake Engineering, 2004. 2(1): p. 1-26.

[35] Ambraseys, N. and S. Sarma, The response of earth dams to strong earthquakes. Geotechnique, 1967. 17(3): p. 181-213.

[36] Page, R.A., Ground motion values for use in the seismic design of the trans-Alaska pipeline system. Vol. 672. 1972: US Geological Survey.

[37] Bolt, B.A. Duration of strong ground motion. in 5th World Conference on Earthquake Engineering. 1973.

[38] McGuire, R. and T. Barnhard. The usefulness of ground motion duration in prediction of severity of seismic shaking. in Proceedings, 2nd US National Conference on Earthquake Engineering, Stanford, Calif. 1979.

[39] Kawashima, K. and K. Aizawa, Bracketed and normalized durations of earthquake ground acceleration. Earthquake engineering & structural dynamics, 1989. 18(7): p. 1041-1051.

[40] Trifunac, M.D. and A.G. Brady, A study on the duration of strong earthquake ground motion. Bulletin of the Seismological Society of America, 1975. 65(3): p. 581-626.

[41] Arias, A., A Measure of Earthquake Intensity. Massachusetts Institute of. Technology, 1969.

[42] Harp, E.L. and R.C. Wilson, Shaking intensity thresholds for rock falls and slides: evidence from 1987 Whittier Narrows and Superstition Hills earthquake strong-motion records. Bulletin of the Seismological Society of America, 1995. 85(6): p. 1739-1757.

[43] Kayen, R.E. and J.K. Mitchell, Assessment of liquefaction potential during earthquakes by Arias intensity. Journal of Geotechnical and Geoenvironmental Engineering, 1997. 123(12): p. 1162-1174.

[44] Husid, R., Características de terremotos. Análisis general. Revista IDIEM, 1969. 8(1): p. 21-42.

[45] Somerville, P.G., et al., Modification of empirical strong ground motion attenuation relations to include the amplitude and duration effects of rupture directivity. Seismological Research Letters, 1997. 68(1): p. 199-222.

[46] Hammal, S., N. Bourahla, and N. Laouami, Seismological Parameters Influence on PGA Prediction by a Neural Network Approach in 16th European Conference on Earthquake Engineering. 2018.

[47] Boore, D.M. and E.M. Thompson, Path durations for use in the stochastic-method simulation of ground motions. Bulletin of the Seismological Society of America, 2014. 104(5): p. 2541-2552.

[48] Nolasco, L.A., et al., Neural estimation of strong ground motion duration. Geofísica internacional, 2014. 53(3): p. 221-239.

[49] Abrahamson , N. and W. Silva Empirical ground motion models. report Brookhaven National Laboratory, 1996. 144.

[50] Dobry, R., I. Idriss, and E. Ng, Duration characteristics of horizontal components of strong-motion earthquake records. Bulletin of the Seismological Society of America, 1978. 68(5): p. 1487-1520.

[51] Du, W., Empirical correlations of frequency-content parameters of ground motions with other intensity measures. Journal of Earthquake Engineering, 2019. 23(7): p. 1073-1091.

[52] FEMA, A., 440, Improvement of nonlinear static seismic analysis procedures. FEMA-440, Redwood City, 2005. 7(9): p. 11.

[53] Málaga-Chuquitaype, C., A. Elghazouli, and R. Bento, Rigid-plastic models for the seismic design and assessment of steel framed structures. Earthquake engineering & structural dynamics, 2009. 38(14): p. 1609-1630.

[54] Riddell, R., J.E. Garcia, and E. Garces, Inelastic deformation response of SDOF systems subjected to earthquakes. Earthquake engineering & structural dynamics, 2002. 31(3): p. 515-538.

[55] Mavroeidis, G., G. Dong, and A. Papageorgiou, Near-fault ground motions, and the response of elastic and inelastic single-degree-of-freedom (SDOF) systems. Earthquake Engineering & Structural Dynamics, 2004. 33(9): p. 1023-1049.

[56] Li, H.N., F. Wang, and Z.H. Lu. Estimation of Hysteretic Energy of MDOF structures based on equivalent SDOF Systems. in Key Engineering Materials. 2007. Trans Tech Publ.

[57] Wang, F. and T. Yi, A methodology for estimating seismic hysteretic energy of buildings, in Civil Engineering and Urban Planning 2012. 2012. p. 17-21.

[58] Committee, S.J.V.G.D., et al., Recommended Seismic Evaluation and Upgrade Criteria for Existing Welded Steel Moment-frame Buildings. Vol. 351. 2000: Federal Emergency Management Agency.

[59] Kilar, V. and D. Koren. Usage of simplified N2 method for analysis of base isolated structures. in The 14th world conference on earthquake engineering, Beijing, China. 2008.

[60] Kilar, V. and D. Koren, Simplified inelastic seismic analysis of base-isolated structures using the N2 method. Earthquake engineering & structural dynamics, 2010. 39(9): p. 967-989.

[61] Koren, D. and V. Kilar, The applicability of the N2 method to the estimation of torsional effects in asymmetric base-isolated buildings. Earthquake engineering & structural dynamics, 2011. 40(8): p. 867-886.

[62] Ruiz-García, J. and E. Miranda, Inelastic displacement ratios for evaluation of existing structures. Earthquake Engineering & Structural Dynamics, 2003. 32(8): p. 1237-1258.

[63] Chopra, A.K. and C. Chintanapakdee, Inelastic deformation ratios for design and evaluation of structures: single-degree-of-freedom bilinear systems. Journal of structural engineering, 2004. 130(9): p. 1309-1319.

[64] Ruiz-García, J. and E. Miranda, Inelastic displacement ratios for design of structures on soft soils sites. Journal of Structural Engineering, 2004. 130(12): p. 2051-2061.

[65] Bozorgnia, Y., M.M. Hachem, and K.W. Campbell, Deterministic and probabilistic predictions of yield strength and inelastic displacement spectra. Earthquake Spectra, 2010. 26(1): p. 25-40.

[66] ATC, S., evaluation and retrofit of concrete buildings. vol. 1, ATC-40 report. Redwood City (CA): Applied Technology Council, 1996.

[67] Rupakhety, R. and R. Sigbjörnsson, Ground-motion prediction equations (GMPEs) for inelastic displacement and ductility demands of constant-strength SDOF systems. Bulletin of Earthquake Engineering, 2009. 7(3): p. 661-679.

[68] Park, Y.-J. and A.H.-S. Ang, Mechanistic seismic damage model for reinforced concrete. Journal of structural engineering, 1985. 111(4): p. 722-739.

[69] Fajfar, P. and T. Vidic, Consistent inelastic design spectra: hysteretic and input energy. Earthquake Engineering & Structural Dynamics, 1994. 23(5): p. 523-537.

[70] López-Almansa, F., A.U. Yazgan, and A. Benavent-Climent, Design energy input spectra for high seismicity regions based on Turkish registers. Bulletin of Earthquake Engineering, 2013. 11(4): p. 885-912.

[71] Housner, G.W. Limit design of structures to resist earthquakes. in Proc. of 1st WCEE. 1956.

[72] Akiyama, H., Earthquake-resistant limit-state design for buildings. 1985: University of Tokyo Press.

[73] Uang, C.M. and V.V. Bertero, Evaluation of seismic energy in structures. Earthquake Engineering & Structural Dynamics, 1990. 19(1): p. 77-90.

[74] The building center of Japan, T., BSL. The building standard law of Japan. 2005.

[75] Donaire-Ávila, J., et al. Energy-based seismic design methodology: a preliminary approach. in Proceedings of the 16th World Conference on Earthquake Engineering, January. 2017.

[76] Gong, M.-s. and L.-l. Xie, Study on comparison between absolute and relative input energy spectra and effects of ductility factor. Acta Seismologica Sinica, 2005. 18(6): p. 717-726.

[77] Tselentis, G., L. Danciu, and E. Sokos, Probabilistic seismic hazard assessment in Greece-Part 2: Acceleration response spectra and elastic input energy spectra. Natural Hazards and Earth System Sciences, 2010. 10(1): p. 41.

[78] Cheng, Y., A. Lucchini, and F. Mollaioli, Correlation of elastic input energy equivalent velocity spectral values. Earthquake and Structures, 2015. 8(5): p. 957-976.

[79] Alıcı, F. and H. Sucuoğlu, Prediction of input energy spectrum: attenuation models and velocity spectrum scaling. Earthquake Engineering & Structural Dynamics, 2016. 45(13): p. 2137-2161.

[80] Gong, M.S., J. Sun, and L.L. Xie. Attenuation of Hysteretic Energy Spectra of Strong Ground Motion. in Applied Mechanics and Materials. 2012. Trans Tech Publ.

[81] Alreja, J., et al., Estimating hysteretic energy demand in steel moment resisting frames using multivariate adaptive regression spline and least square support vector machine. Ain Shams Engineering Journal, 2015. 6(2): p. 449-455.

[82] Zhai, C., et al., Hysteretic energy prediction method for mainshock-aftershock sequences. Earthquake Engineering and Engineering Vibration, 2018. 17(2): p. 277-291.

[83] Dindar, A.A., et al., Development of earthquake energy demand spectra. Earthquake Spectra, 2015. 31(3): p. 1667-1689.

[84] National Research Institute for Earth Science and Disaster Resilience and NIED K-NET, KiK-net, National Research Institute for Earth Science and Disaster Resilience. 2019.

[85] Derbal, I., et al., Neural network-based prediction of ground time history responses European Journal of Environmental and Civil Engineering, 2017: p. 1-18.

[86] Noura, H., A. Mebarki, and M. Abed, Post-quake structural damage evaluation by neural networks: theory and calibration. European Journal of Environmental Civil Engineering, 2017: p. 1-18.

[87] Tettamanzi, A. and M. Tomassini, Soft computing: integrating evolutionary, neural, and fuzzy systems. 2013: Springer Science & Business Media.

[88] Nissen, S., Implementation of a fast artificial neural network library (fann). Report, Department of Computer Science University of Copenhagen (DIKU), 2003. 31: p. 29.

[89] Haykin, S. and R. Lippmann, Neural networks, a comprehensive foundation. International journal of neural systems, 1994. 5(4): p. 363-364.

[90] Adeli, H. and C. Yeh, Perceptron learning in engineering design. Computer-Aided Civil and Infrastructure Engineering, 1989. 4(4): p. 247-256.

[91] Adeli, H. and H. Seon Park, Counterpropagation neural networks in structural engineering. Journal of Structural Engineering, 1995. 121(8): p. 1205-1212.

[92] Xu, Y., et al., Adaptive multilayer perceptron networks for detection of cracks in anisotropic laminated plates. International journal of solids and structures, 2001. 38(32-33): p. 5625-5645.

[93] Su, Z. and L. Ye, Lamb wave propagation-based damage identification for quasi-isotropic CF/EP composite laminates using artificial neural algorithm: Part I-methodology and database development. Journal of intelligent material systems and structures, 2005. 16(2): p. 97-111.

[94] MOHAN, G.G., A. Upadhyay, and S. Kaushik, Assessment of longitudinal shear strength parameters of composite slab by artificial neural network. 2006.

[95] Kumar, R., B. Mishra, and S. Jain, Vibration control of smart composite laminated spherical shell using neural network. Journal of intelligent material systems and structures, 2008. 19(8): p. 947-957.

[96] Tsompanakis, Y., N.D. Lagaros, and G.E. Stavroulakis, Soft computing techniques in parameter identification and probabilistic seismic analysis of structures. Advances in Engineering Software, 2008. 39(7): p. 612-624.

[97] Wu, X., J. Ghaboussi, and J. Garrett Jr, Use of neural networks in detection of structural damage. Computers & structures, 1992. 42(4): p. 649-659.

[98] González, M.P. and J.L. Zapico, Seismic damage identification in buildings using neural networks and modal data. Computers & structures, 2008. 86(3-5): p. 416-426.

[99] Adeli, H. and A. Panakkat, A probabilistic neural network for earthquake magnitude prediction. Neural networks, 2009. 22(7): p. 1018-1024.

[100] Calabrese, A. and C.G. Lai, Fragility functions of blockwork wharves using artificial neural networks. Soil Dynamics and Earthquake Engineering, 2013. 52: p. 88-102.

[101] Mitropoulou, C.C. and M. Papadrakakis, Developing fragility curves based on neural network IDA predictions. Engineering Structures, 2011. 33(12): p. 3409-3421.

[102] Wang, Z., et al., Seismic fragility analysis with artificial neural networks: Application to nuclear power plant equipment. Engineering Structures, 2018. 162: p. 213-225.

[103] Sirca Jr, G. and H. Adeli, System identification in structural engineering. Scientia Iranica, 2012. 19(6): p. 1355-1364.

[104] Facchini, L., M. Betti, and P. Biagini, Neural network based modal identification of structural systems through output-only measurement. Computers & Structures, 2014. 138: p. 183-194.

[105] Wang, Z., I. Zentner, and E. Zio, A Bayesian framework for estimating fragility curves based on seismic damage data and numerical simulations by adaptive neural networks. Nuclear Engineering and Design, 2018. 338: p. 232-246.

[106] Goh, A.T., Seismic liquefaction potential assessed by neural networks. Journal of Geotechnical engineering, 1994. 120(9): p. 1467-1480.

[107] Ghaboussi, J. and D. Sidarta, New nested adaptive neural networks (NANN) for constitutive modeling. Computers and Geotechnics, 1998. 22(1): p. 29-52.

[108] Basma, A.A. and N. Kallas, Modeling soil collapse by artificial neural networks. Geotechnical & Geological Engineering, 2004. 22(3): p. 427-438.

[109] Sakellariou, M. and M. Ferentinou, A study of slope stability prediction using neural networks. Geotechnical & Geological Engineering, 2005. 23(4): p. 419.

[110] Samui, P. and B. Kumar, Artificial neural network prediction of stability numbers for two-layered slopes with associated flow rule. The Electronic Journal of Geotechnical Engineering, 2006. 11: p. 1-44.

[111] Shangguan, Z., S. Li, and M. Luan, Intelligent forecasting method for slope stability estimation by using probabilistic neural networks. Electron. J. Geotech. Eng. Bundle, 2009. 13.

[112] Derras, B. and A. Bekkouche, Use of the artificial neural network for peak ground acceleration estimation. Lebanese Science Journal, 2011. 12(2): p. 101-115.

[113] Lee, S.C. and S.W. Han, Neural-network-based models for generating artificial earthquakes and response spectra. Computers & structures, 2002. 80 (20-21): p. 1627-1638.

[114] Derras, B., A. Bekkouche, and D. Zendagui, Neuronal approach and the use of kik-net network to generate response spectrum on the surface. Jordan Journal of Civil Engineering, 2010. 4(1).

[115] Jain, A.K., J. Mao, and K.M. Mohiuddin, Artificial neural networks: A tutorial. Computer, 1996. 29(3): p. 31-44.

[116] Güler, A., Seismic vulnerability assessment using artificial neural networks. 2005, Middle East Technical University.

[117] Sazlı, M.H., A brief review of feed-forward neural networks. 2006.

[118] Konar, A., et al. Dynamic Fuzzy Networks for Real-Time Applications. in Türkiye Artificial Intelligence & Neural Network Symposium, TAINN'99. 1999.

[119] Fausett, L., Artificial Neural Networks. dalam Fundamentals of Neural Networks Architectires, Algorithms, and Applications, Prentice Hall Eagle Wood Cliff, NJ, 1994: p. 3.

[120] Rummelhart, D.E., J.L. McClelland, and P.R. Group, Parallel distributed processing: Explorations in the microstructure of cognition. Vol. 1. Foundations. Cambridge, MA: MIT Press, 1986.

[121] Aslanargun, A., et al., Comparison of ARIMA, neural networks and hybrid models in time series: tourist arrival forecasting. Journal of Statistical Computation and Simulation, 2007. 77(1): p. 29-53.

[122] Wang, L., Y. Zeng, and T. Chen, Back propagation neural network with adaptive differential evolution algorithm for time series forecasting. Expert Systems with Applications, 2015. 42(2): p. 855-863.

[123] Günaydın, K. and A. Günaydın, Peak ground acceleration prediction by artificial neural networks for northwestern Turkey. Mathematical Problems in Engineering, 2008. 2008.

[124] Derras, B., et al., Adapting the neural network approach to PGA prediction: An example based on the KiK-net data. Bulletin of the Seismological Society of America, 2012. 102(4): p. 1446-1461.

[125] Beale, M.H., M.T. Hagan, and H.B. Demuth, Neural Network Toolbox™ User's Guide. The Mathworks Inc. 1992.

[126] Laouami, N., et al., Evidence for fault-related directionality and localized site effects from strong motion recordings of the 2003 Boumerdes (Algeria) earthquake : consequences on damage distribution and the Algerian seismic code. Soil dynamics and earthquake engineering, 2006. 26(11): p. 991-1003.

[127] Lee, J. Directionality of strong ground motion durations. in Proceedings of the 10th National Conference in Earthquake Engineering, Earthquake Engineering Research Institute. 2014.

[128] Boore, D.M., Orientation-independent, non-geometric-mean measures of seismic intensity from two horizontal components of motion. Bulletin of the Seismological Society of America, 2010. 100(4): p. 1830-1835.

[129] Kanno, T., et al., A new attenuation relation for strong ground motion in Japan based on recorded data. Bulletin of the Seismological Society of America, 2006. 96(3): p. 879-897.

[130] Cotton, F., et al., On the discrepancy of recent European ground-motion observations and predictions from empirical models: Analysis of KiK-net accelerometric data and point-sources

stochastic simulations. Bulletin of the Seismological Society of America, 2008. 98(5): p. 2244-2261.

[131] Derras, B., Adapting the Neural Network Approach to PGA Prediction: An Example Based on the KiK-net Data. Bulletin of the Seismological Society of America, 2012. 102: p. 16.

[132. Guo, G., D. Yang, and Y. Liu, Duration effect of near-fault pulse-like ground motions and identification of most suitable duration measure. Bulletin of Earthquake Engineering, 2018. 16(11): p. 5095-5119.

[133] Fairhurst, M., A. Bebamzadeh, and C.E. Ventura, Effect of Ground Motion Duration on Reinforced Concrete Shear Wall Buildings. Earthquake Spectra, 2019. 35(1): p. 311-331.

[134] Chandramohan, R., J.W. Baker, and G.G. Deierlein, Quantifying the Influence of Ground Motion Duration on Structural Collapse Capacity Using Spectrally Equivalent Records. Earthquake Spectra, 2016. 32(2): p. 927-950.

[135] Barbosa, A.R., F.L.A. Ribeiro, and L.A.C. Neves, Influence of earthquake ground-motion duration on damage estimation: application to steel moment resisting frames. Earthquake Engineering & Structural Dynamics, 2017. 46(1): p. 27-49.

[136] Pan, Y., C.E. Ventura, and W.D.L. Finn, Effects of Ground Motion Duration on the Seismic Performance and Collapse Rate of Light-Frame Wood Houses. Journal of Structural Engineering, 2018. 144(8): p. 04018112.

[137] Prasanth, T., S. Ghosh, and K.R. Collins, Estimation of hysteretic energy demand using concepts of modal pushover analysis. Earthquake Engineering and Structural Dynamics, 2008. 37(6): p. 975-990.

[138] Wen, Y., Method for random vibration of hysteretic systems. Journal of the engineering mechanics division, 1976. 102(2): p. 249-263.

[139] Li, H.-g. and G. Meng, Nonlinear dynamics of a SDOF oscillator with Bouc–Wen hysteresis. Chaos, Solitons and Fractals, 2007. 34(2): p. 337-343.

[140] Hammal, S., N. Bourahla, and N. Laouami, Neural-Network Based Prediction of Inelastic Response Spectra. Civil Engineering Journal, 2020. 6(6): p. 1124-1135.

[141] Sheela, K.G. and S.N. Deepa, Review on methods to fix number of hidden neurons in neural networks. Mathematical Problems in Engineering, 2013. 2013.

[142] Raghunandan, M. and A.B. Liel, Effect of ground motion duration on earthquake-induced structural collapse. Structural Safety, 2013. 41: p. 119-133.

[143] Decanini, L.D. and F. Mollaioli, An energy-based methodology for the assessment of seismic demand. Soil Dynamics and Earthquake Engineering, 2001. 21(2): p. 113-137.

PUBLISHED WORKS

Research paper

- Hammal, Sofiane, Nouredine Bourahla, and Nasser Laouami. "Neural-Network Based Prediction of Inelastic Response Spectra." *Civil Engineering Journal* 6.6 (2020): 1124-1135.

Conference papers:

- Sofiane, Hammal, Nouredine Bourahla, and Laouami Nasser. "*Significant duration prediction and evaluation of the effects of seismological parameters using neural networks.*" Conference: The 2017 World Congress on Advances in Structural and Engineering Mechanics ASEM17 At: Ilsan Seoul Korea
- Sofiane, Hammal, Nouredine Bourahla, and Laouami Nasser. "*Seismological parameters influence on PGA prediction by a neural network approach*." Conference: 16 European Conference on Earthquake Engineering At: Thessaloniki, Greece June 2018.
- Sofiane, Hammal, Nouredine Bourahla, and Laouami Nasser. "*Neural networks based prediction of mean period of ground motions (tm) and sensitivity analysis to seismological parameters*" Conference: 8ème Symposium International sur la construction en zone sismique (SICZS'2018) At: Chlef

APPENDIX

Appendix. A Synaptic weight matrices and bias vectors for the ANN model.

w_1: the matrix of synaptic weights, its dimensions are Nh×N the input parameters and the hidden layer.

w_2: the vector of size Nh that contains the synaptic weights.

b_1, b_2: The bias vectors of the hidden layer and output layer.

PGA Model:

w_1=

1.1483	-1.6031	0.91218	0.048856	-0.56716	-0.64599
0.10273	0.42777	-0.36178	0.057407	-0.12529	-0.27508
-1.727	0.38588	2.0824	-0.486	0.1813	-0.48307
1.3525	-0.67121	0.92101	-1.5773	-0.016869	-1.4048
-0.59759	0.19538	1.0443	0.097137	0.085263	-1.6796
-1.206	-1.1835	1.5556	-0.70775	-0.67736	0.68444
-0.42559	-0.35528	0.24135	0.83902	0.2252	1.67
-0.37471	0.92767	-1.6935	-0.82764	0.61669	-0.98461
0.90866	0.21944	-0.8056	1.6722	0.45942	0.4847
0.40843	0.74955	-1.2999	-0.54665	0.74894	-0.74042

b_1=

[-1.9878;
-0.53903;
2.3438;
-0.37136;
-0.99748;
0.58767;
-0.59632;
1.2691;
1.4337;
2.3942]

w_2=

[-0.38069 2.3815 -0.58706 -0.41775 -0.30508 0.4202 -0.61476 -0.32847 0.0023957 -0.38659]

b_2=

[-0.79503]

Synaptic weight matrices and bias vectors SD 595 Model

w1						b1	w2	b2
1.388	1.095	1.206	-1.032	1.766	-0.003	-1.589	1.032	-0.185
0.174	0.424	0.180	0.591	-1.251	0.183	0.555	-1.111	
1.374	0.513	0.851	-0.181	0.878	0.065	-0.966	-1.322	
1.291	-0.889	-0.200	0.929	-1.412	0.181	-1.236	1.078	
0.213	-1.364	-0.872	0.595	-0.216	0.149	0.206	-0.968	
5.937	1.249	0.391	0.319	-0.347	0.042	2.370	-1.970	
-0.406	-0.994	-0.533	-1.534	-0.493	0.172	1.034	-0.274	
0.957	0.651	-1.495	0.145	-0.965	-0.049	-0.292	-0.355	
3.639	0.475	-0.155	1.102	-1.129	0.170	2.254	1.902	
-1.179	0.669	-1.326	0.669	1.653	-0.437	-2.649	-0.954	

Synaptic weight matrices and bias vectors SD 575 Model

w1						b1	w2	b2
2.100	0.982	0.823	-0.798	1.507	0.037	-1.294	0.887	-0.821
-0.365	0.211	-0.898	0.459	-0.991	0.270	1.458	-1.188	
2.343	0.346	0.821	-0.269	0.562	0.079	-1.585	-1.321	
1.688	-0.876	-0.347	0.637	-0.783	0.226	-1.076	1.132	
0.732	-0.895	-0.868	0.514	-0.395	0.193	-0.697	-1.136	
7.317	0.887	0.318	0.226	-0.108	0.035	3.379	-2.938	
-0.290	-1.302	-0.276	-1.053	-0.377	0.545	1.067	-0.038	
1.509	0.754	-1.277	-0.248	-0.604	0.136	-1.354	-0.239	
5.991	2.154	0.700	1.726	-1.326	0.253	3.807	2.886	
-1.119	0.857	-1.286	0.668	1.896	-0.508	-2.492	-0.632	

Synaptic weight matrices and bias vectors for Inelastic response spectra model

w1

-0.08273	7.784	6.06	0.93696	-6.2642
1.0767	0.11994	-0.31878	-2.5242	1.4537
0.075649	3.3268	4.7762	-5.396	-4.4799
-0.18466	-1.3965	11.6736	5.5936	7.0363
-0.23223	-7.6644	3.1154	1.5976	-4.143
0.042267	-2.9187	-6.8243	-9.4885	-6.0351
0.18276	-9.8872	-2.7308	-4.0899	0.86523
0.1035	-0.68123	-2.533	1.9296	4.5337
0.07839	-6.5307	-4.9244	-0.73972	6.7169
-0.42446	-1.1956	0.62353	-5.9804	1.7597

w2

-0.69497	1.2582	0.77342	0.0016248	-0.021422	0.00055935	0.0021854	-0.024154	-0.70027	-0.0022681
-0.69733	0.86513	1.2403	0.013469	-0.034106	0.012143	0.0031869	-0.042941	-0.69197	0.36583
-1.1977	0.91281	1.9885	0.023394	-0.043577	0.019466	0.0026424	-0.069414	-1.205	1.2067
-0.65189	0.45265	1.5371	0.0068614	-0.02991	0.0071722	-0.0014466	-0.069488	-0.647	1.2645
-0.7509	0.47741	1.2508	0.022784	-0.03719	0.023451	-0.021925	-0.062693	-0.72151	1.4402
-0.83841	0.26151	1.03	0.027707	-0.037612	0.031124	-0.03018	-0.062018	-0.80181	1.2971
-1.196	0.49005	1.4481	0.046532	-0.064452	0.053732	-0.044039	-0.12464	-1.136	1.5988
-1.0729	0.44047	0.89061	0.040776	-0.05067	0.044849	-0.035713	-0.083898	-1.0314	1.3869
-1.0936	0.26073	0.89589	0.039891	-0.045606	0.041438	-0.038445	-0.065939	-1.0535	1.6196
-1.3234	0.10961	0.97688	0.0541	-0.052664	0.059982	-0.052983	-0.069108	-1.2701	1.3794
-2.1844	0.39598	1.4031	0.083151	-0.076635	0.090104	-0.084084	-0.080215	-2.1072	1.3263
-2.2963	0.42051	1.2458	0.080693	-0.074154	0.084892	-0.086642	-0.067814	-2.2203	1.2239
-2.3437	0.31557	1.4189	0.094641	-0.088948	0.10172	-0.094376	-0.085297	-2.2537	1.3538
-2.4175	0.29894	1.3752	0.10258	-0.096166	0.10959	-0.097868	-0.10066	-2.321	1.2246
-2.2956	0.2035	1.0627	0.09809	-0.090498	0.10089	-0.087067	-0.098918	-2.2064	1.0843
-1.9691	0.25242	0.91327	0.091751	-0.090386	0.093216	-0.071693	-0.11333	-1.8898	1.0263
-1.8086	0.36762	0.8936	0.098733	-0.1023	0.10258	-0.070494	-0.14054	-1.7232	1.0054
-1.6493	0.57106	0.96845	0.10515	-0.10868	0.11292	-0.076605	-0.16067	-1.5543	0.9258
-1.3447	0.59052	0.8688	0.091351	-0.096803	0.098173	-0.06524	-0.14393	-1.2605	0.86493
-1.5417	0.72015	0.87311	0.10132	-0.10887	0.10759	-0.071355	-0.14891	-1.4501	0.97755
-1.5049	0.5505	0.82062	0.096973	-0.10752	0.10309	-0.070286	-0.13399	-1.4173	1.0786

b1
-11.53
-4.2793
-14.0707
0.27949
3.3898
-3.8287
6.1461
4.8577
10.0282
-7.856

b2
-11.53
-4.2793
-14.0707
0.27949
3.3898
-3.8287
6.1461
4.8577
10.0282
-7.856

Appendix B. Graphical user interfaces (GUIs) for attenuation relationship:

To make the use of the attenuation models more user-friendly a Graphical User Interface (GUI) MATLAB is developed for the proposed model. The input values of the models are as follow f0, Vs30, Mw, R, d, and Radial angle.

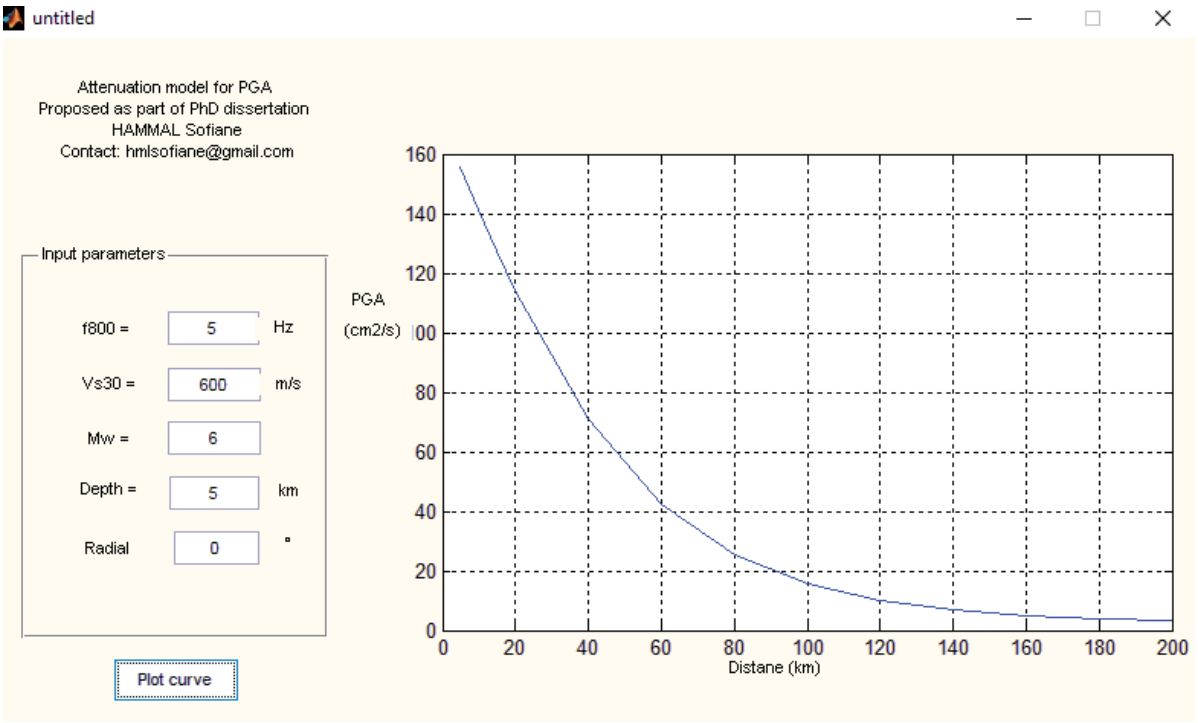

Appendix. C Ground Motion records list

Records name	Earthquake parameters						Intensity measures		
	Depht	Magn	R(km)	f800	Vs30 (m//s)	ɵ	Duration(s)	PGA(cm2/s)	Tm(s)
AICH049804222032.EW2	10	5.4	52.09	0.36	241.15	30.41	27.985	14.334	0.401
AICH049804222032.NS2	10	5.4	52.09	0.36	241.15	59.59	22.140	19.705	0.281
AICH079804222032.EW2	10	5.4	76.51	3.63	428.10	4.36	20.700	7.988	0.227
AICH079804222032.NS2	10	5.4	76.51	3.63	428.10	85.64	19.370	10.085	0.231
AICH089804222032.EW2	10	5.4	72.52	4.60	448.53	22.43	18.075	7.869	0.240
AICH089804222032.NS2	10	5.4	72.52	4.60	448.53	67.57	17.215	11.232	0.209
AICH099804222032.EW2	10	5.4	94.00	0.50	274.03	36.50	28.405	7.828	0.984
AICH099804222032.NS2	10	5.4	94.00	0.50	274.03	53.50	32.690	7.029	0.739
AICH119804222032.EW2	10	5.4	47.25	3.14	382.20	18.79	17.635	10.758	0.165
AICH119804222032.NS2	10	5.4	47.25	3.14	382.20	71.21	16.870	12.058	0.171
AKTH010307260713.EW2	12	6.2	164.83	2.01	475.09	72.17	29.870	8.803	1.167
AKTH010307260713.NS2	12	6.2	164.83	2.01	475.09	17.83	30.150	10.324	1.075
AKTH020307260713.EW2	12	6.2	149.14	3.35	620.40	69.93	39.780	8.345	0.625
AKTH020307260713.NS2	12	6.2	149.14	3.35	620.40	20.07	39.725	9.050	0.524
AKTH050307260713.EW2	12	6.2	104.64	7.42	829.46	45.38	39.990	9.251	0.278
AKTH050307260713.NS2	12	6.2	104.64	7.42	829.46	44.62	38.965	8.697	0.283
AKTH120307260713.EW2	12	6.2	186.78	2.03	389.24	64.35	40.900	8.763	0.863
AKTH120307260713.NS2	12	6.2	186.78	2.03	389.24	25.65	49.280	10.096	0.874
AKTH130307260713.EW2	12	6.2	187.25	5.08	535.72	69.69	10.795	39.847	0.245
AKTH130307260713.NS2	12	6.2	187.25	5.08	535.72	20.31	8.970	31.596	0.247
AKTH150307260713.EW2	12	6.2	157.16	4.64	498.05	65.47	37.385	4.678	0.424
AKTH150307260713.NS2	12	6.2	157.16	4.64	498.05	24.53	36.270	5.618	0.562
CHBH040410231756.EW2	13	6.8	195.52	2.93	369.11	57.85	66.820	19.897	0.874
CHBH040410231756.NS2	13	6.8	195.52	2.93	369.11	32.15	51.445	19.310	0.807
CHBH041103230712.EW2	8	6	158.61	2.93	369.11	64.16	95.380	6.876	0.314
CHBH041103230712.NS2	8	6	158.61	2.93	369.11	25.84	96.170	8.302	0.333
CHBH141103230712.EW2	8	6	150.01	0.91	200.74	88.76	97.610	1.946	0.410
CHBH141103230712.NS2	8	6	150.01	0.91	200.74	1.24	94.340	2.490	0.397
EHMH011604182042.EW2	9	5.8	126.66	7.15	743.40	3.07	24.210	3.275	0.124
EHMH011604182042.NS2	9	5.8	126.66	7.15	743.40	86.93	23.490	3.858	0.126
EHMH030010061330.EW2	11	7.3	154.05	5.46	500.58	79.48	20.990	21.990	0.520
EHMH030010061330.NS2	11	7.3	154.05	5.46	500.58	10.52	24.035	20.094	0.429
EHMH031610211407.EW2	11	6.6	163.93	5.46	500.58	83.36	19.460	7.256	0.362
EHMH031610211407.NS2	11	6.6	163.93	5.46	500.58	6.64	25.590	6.368	0.304
EHMH050010061330.EW2	11	7.3	181.15	2.98	362.14	73.94	35.925	8.077	0.565
EHMH050010061330.NS2	11	7.3	181.15	2.98	362.14	16.06	38.515	10.540	0.477
EHMH051604160711.EW2	6	5.4	139.49	2.98	362.14	20.98	26.440	0.372	0.195
EHMH051604160711.NS2	6	5.4	139.49	2.98	362.14	69.02	23.930	1.084	0.219
EHMH051604182042.EW2	9	5.8	168.65	2.98	362.14	28.32	31.150	1.227	0.190